REGENERATION OF CARBON AEROGEL EXHAUSTED IN WATER PURIFICATION

A Dissertation

by

SANJAY TEWARI

Submitted to the Office of Graduate Studies of
Texas A&M University
in partial fulfillment of the requirements for the degree of

DOCTOR OF PHILOSOPHY

December 2011

Major Subject: Civil Engineering

Regeneration of Carbon Aerogel Exhausted in Water Purification

REGENERATION OF CARBON AEROGEL EXHAUSTED IN WATER PURIFICATION

A Dissertation

by

SANJAY TEWARI

Submitted to the Office of Graduate Studies of
Texas A&M University
in partial fulfillment of the requirements for the degree of

DOCTOR OF PHILOSOPHY

Approved by:

Chair of Committee,	Bill Batchelor
Committee Members,	Bryan Boulanger
	Anthony Cahill
	Bill Harris
Head of Department,	John Niedzwecki

December 2011

Major Subject: Civil Engineering

ABSTRACT

Regeneration of Carbon Aerogel Exhausted in Water Purification. (December 2011)

Sanjay Tewari, B.E., Sardar Vallabhbhai National Institute of Technology, Surat, India;

M.Tech., Indian Institute of Technology, Roorkee, India

Chair of Advisory Committee: Dr. Bill Batchelor

Carbon has been used electrochemically in various forms for water treatment and the carbon aerogel is one of them. Carbon Aerogels (CA) are used as electrodes due to their high surface capacity and high electrical conductivity. They are also known as Carbon Nanofoams (CNF). CA electrodes attract oppositely charged ions that are nearby. This concept is known as Capacitive De-Ionization (CDI). The use of CA in CDI for water purification is well documented, but not much work has been done on regeneration of CA electrodes. Once saturated, these electrodes lose their ability to adsorb additional ions and it must be restored by regeneration. If they cannot be regenerated, they would need to be replaced, which would greatly increase the cost of the treatment they are expensive. The goal of this study is to obtain data to define optimal regeneration conditions and to develop predictive capability by examining desorption behavior of adsorbed ions on CA electrodes.

This study focuses on desorption of adsorbed ions and regeneration of CA. Various experiments were conducted to explore the effects on regeneration of CA of shorting of electrodes, change of polarity of electrodes, flow speed of water over CA

electrodes, and temperature of regeneration water. The optimal combination of experimental variables was identified and was used for remaining experiments that tested the effect of size, charge and mass of adsorbed ions on regeneration of CA. Also, the effect of thickness of CA and its pore size on regeneration of CA was studied.

Results indicated that application of reverse potential for the first few minutes of the total regeneration time provided the greatest regeneration. Longer application of reverse potential did not result in higher regeneration. The regeneration behavior when no potential applied with and without shorting was as expected. Application of reverse potential with variable temperature or variable flow speed of water over CA surfaces provided results that were different from the ones that were obtained with no potential being applied with or without shorting of electrodes.

This dissertation is dedicated to

my parents and wife.

ACKNOWLEDGEMENTS

I would like to express my gratitude to my advisor and committee chair, Dr. Bill Batchelor for his guidance, support, and patience throughout the course of this research. He always had time for me, listened to me with patience and in most cases understood me better than I did myself. I learned a lot from him. In addition, I would like to thank my committee members: Dr. Bryan Boulanger, Dr. Anthony Cahill, and Dr. Bill Harris, for their suggestions, availability, and commitment.

I offer my thanks and appreciation to the Department of Civil Engineering and the Texas Water Resources Institute for their financial support. I would like to thank and remember Dr. Tim Kramer who helped me in early phase of this work. Many thanks to Dr. Bob Bruner, Dr. Calvin Woods and Dr. Nasir Gharaibeh, for their support and help in cultivating my teaching interests.

I would like to acknowledge the support from Dr. Daniel Shantz and Microscopy and Imaging Center at Texas A&M University for their help in CA characterization experiments conducted at their facility.

I thank my friends and colleagues, as well as, the other faculty and staff for making my time at Texas A&M University a great experience. Thanks to my friends who already graduated from A&M and shared some great memories with me. Special thanks to Bhanu Prakash Vellanki, Xu Liu, and other members of the research group for their support, and encouragement.

Last but not the least; I would not have been able to finish my doctorate without the unconditional love, constant encouragement and support of my family (my mother, father, wife, brother and sisters). Also, I would like to acknowledge my daughter Trisha, who missed a lot of her play time with me so that I can complete my doctorate. Thank you all!

TABLE OF CONTENTS

CHAPTER Page

CHAPTER Page

LIST OF FIGURES

Page

Page

Page

Page

Page

Page

Page

Page

Page

LIST OF TABLES

Page

CHAPTER I

INTRODUCTION

1.1 Statement of Purpose

Carbon has been used in different forms for water treatment including electrochemical desalination. Some carbon forms that have been used are high surface area carbon-cloth or carbon-felt electrodes and recently carbon aerogels (CA). Electrically conductive carbon nanofoams (CNFs) are a type of CA and they were used in this study. These are a new type of material with many of the properties of traditional aerogels. They are synthetic, lightweight foams in which the solid matrix and pore spaces have nanometer-scale dimensions and are available in the form of monoliths, granules, powders and papers. Prepared by sol-gel methods, nanofoams typically have low density, continuous porosity, high surface area, and fine cell/pore sizes. The foams are also electrically conductive and have a high capacitance. Similarly an aerogel is a highly porous solid material with a continuous three-dimensional framework formed by replacement of liquid in a gel with a gas, so that there is little shrinkage.

One way of producing a CA is by the aqueous polycondensation of resorcinol (1,3 dihydroxybenzene) with formaldehyde. The reaction under alkaline conditions proceeds through a sol-gel transition and results in the formation of a highly crosslinked polymer that is a resorcinol-formaldehyde (RF) gel. This gel is a 3-dimensional tenuous

---

This dissertation follows the style of *Environmental Science and Technology*.

body, which typically contains water in the pores. If this water is simply evaporated from pores of the gel, large capillary forces are exerted and the gel structure is collapsed. This can be avoided if water is replaced with acetone by placing the gel in an acetone bath for a couple of days. Then the acetone is extracted by supercritical carbon dioxide. This process results in minimal shrinking and thereby preserves the gel skeleton. The nanoporous material that results from this operation is known as an aerogel. Once the gel has been dried under carbon dioxide supercritical conditions and all the solvent extracted, the CAs can be derived via the pyrolysis of the organic precursors. RF aerogels are formed by highly crosslinked aromatic polymers and they can be pyrolysed in an inert atmosphere to form vitreous carbon monoliths. The resultant porous material is black in color and known as a CA.

Fabrication of CNFs is similar to CAs in a way. CNFs are fabricated by infusing a RF gel into the voids of commercially available low density carbon-fiber paper. This material undergoes gelation, air (not supercritical) drying and pyrolysis to produce light weight, mechanically flexible and electrically conductive sheets of fiber-supported CNF. Due to their high surface areas and high electrical conductivities, they are used as electrodes for a range of energy storage applications e.g. electrochemical double-layer capacitors or supercapacitors.

Recent research has shown that CAs can be used effectively for water purification processes, such as removal of heavy metal ions and desalination of dilute solutions using electro-sorption. The idea behind electro-sorption is to force ions or ionic species towards oppositely charged electrodes with the help of an electric field. Under

this kind of environment, charged ions are held in the strong electrical field of the electrodes. These systems require electrodes with high electrical conductivity and high surface area. An electrical double layer is formed when charged surfaces come in contact with a liquid solution that contains ions of an opposite charge that are attracted to the charged surface. They form a layer adjacent to the surface in which the concentration of oppositely charged ions is higher than in the bulk solution.

Capacitive de-ionization (CDI) technology is based on electro-sorption. CDI is the process of removing ions using capacitive adsorption, which is a new way of removing salts and metals ions from liquid streams. When two oppositely charged electrodes are put very close to each other they act as a capacitor and create double layers of ions near the electrode surfaces. These capacitive electrodes are placed in the water to be treated. Oppositely charged ions are first trapped in the double layers and then they are adsorbed onto the porous carbon surface, producing relatively clean water. A DC voltage (1-2 Volts) is applied to the CNF electrodes which are placed very close to each other (about 1-2 mm). Once saturated with counter ions, these electrodes lose their adsorptive capacity and would need to be replaced. This increases the cost of the treatment process, because CAs are expensive. Regeneration and reuse of exhausted CAs will reduce this problem. The use of CAs in CDI for water purification is well documented, but very little work has been documented on regeneration of the aerogels and the proper methods of operation in order to maximize the quantity of clean water produced. Modeling of regeneration behavior of CA electrodes is not available. The goal of this study is to investigate the use of CNFs as electrode material in CDI technology

and to develop optimal regeneration procedures and the ability to predict performance by examining desorption behavior of adsorbed ions on CNF electrodes and developing a model to describe desorption behavior.

1.2 Hypotheses

In principle, regeneration of CNF depends on the extent of desorption and the rate of desorption, which is controlled by diffusion. Therefore, to control regeneration of CNF, diffusion of adsorbed ions back to the bulk solution must be maximized. Diffusion is controlled by concentration gradient. The greater the concentration gradient near the surface of CNF, the greater will be the rate of diffusion of ions. Also, diffusion is dependent on ion size as well as on pore size. This will be demonstrated with a combination of ions of various sizes and with CNF electrodes of varying pore size. Temperature also plays an important role in diffusion because the diffusion coefficient depends on temperature.

The major hypotheses are summarized as follows:

1) The rate of desorption is a diffusion-limited process.
2) Increasing concentration gradients increase the rate of diffusion, which results in increased rates of regeneration of CNF electrodes.
3) CNF pores trap ions during the adsorption process and during desorption these ions have to be released. Therefore, the pore size distribution of CNF is also important in determining rates of regeneration.

4) Physical sizes of ions being adsorbed and desorbed also play significant roles in rate of regeneration.
5) Higher temperature favors diffusion and thus hot feed water will increase extent of desorption.
6) The charges of ions play an important role in regeneration by desorption. Ions with more charge (multivalent ions) will behave differently than ions with less charge (monovalent ions) in terms of kinetic as well as equilibrium behavior.
7) The ions reaching the outer surface of CNF are assumed to penetrate further into the CNF by diffusing along the inner surfaces of micropores driven by the local concentration gradient of the adsorbate until ultimately adsorbed at the interior adsorption sites. The reverse of this should be true when it comes to desorption. Therefore, the thickness of the CNF will affect kinetics of sorption and desorption by requiring a longer path for ions to diffuse through before adsorbing. Thicker CNF would also provide more surface area for adsorption-desorption.

1.3 Objectives

The goal of this study is to identify optimal regeneration procedures and to develop the ability to predict desorption behavior of adsorbed ions on CNF electrodes by developing a model to describe desorption behavior. The kinetic as well as equilibrium behavior of CNF during regeneration is to be examined by varying parameters such as flow speed, pore size, ion size and thickness of CNF. The objectives are described as follows

Objective 1 - Study effect of potential applied to CNF electrodes on rate and extent of regeneration

Once ions are adsorbed onto CNF , they can be dislodged either by eliminating the force of attraction that holds these ions onto the CNF surface or by changing the polarity of electrodes so that adsorbed ions are dislodged by a repulsive force. The regeneration of CNF is studied by removing applied potential and then by applying the reverse potential across CNF electrodes.

Objective 2 - Study cumulative effect of flow speed, sonication and concentration of wash water on CNF regeneration kinetics and extent

Changing flow speed changes the thickness of the stagnant layer near the surface of the CNF, which changes the concentration gradient and results in increased transport rate through the film. Two things happen in series. First, ions desorb from the surface of the CNF and then they are transported through the film. If one of these steps is substantially slower than the other, it will control the overall rate of mass transport. Sonication may also affect the gradient and the rate. Both are expected to favor diffusion from the CNF surface and thus desorption. Measuring the effect of flow speed on desorption helps determine optimal conditions for efficient regeneration. Wash water of different concentration will be used to help create different concentration gradients.

Objective 3 - Study effect of pore size of CNF electrodes on CNF regeneration rate

Ions are adsorbed on numerous charged sites on the surface and in the micropores of CNFs, so the regeneration process must be able to release ions trapped in all of these locations. Small pore size would reduce the ability of ions to diffuse easily

and hinder regeneration. CNF with varying pore size distribution supplied by a commercial supplier will be evaluated. Further verification of pore size distribution will be done by gas adsorption porosimetry (typically using N_2, Ar or CO_2).

Objective 4 - Study effect of the physical size of adsorbed ions on CNF regeneration rate

Sizes of pores and ions play a very important role in regeneration. Small ions diffuse from these micro pores more easily than larger ions. Results from this study establish regeneration behavior of CNF as a function of physical ion size. This helps understand the suitability of CDI in the treatment of water with various ions. How the variation in ion size and type affects the regeneration process will be studied and will help to elucidate regeneration as a diffusion limited process.

Objective 5 - Examine thermal effects on rate and extent of desorption of ions from CNF electrodes

General thermal properties of desorption indicate that a rise in temperature increases diffusion and this property will be evaluated for its ability to enhance the regeneration of CNF electrodes. Hot feed water is used and how the temperature of feed water affects regeneration of CNF electrodes will be studied.

Objective 6 - Examine the effect of adsorbed multivalent and monovalent ions on rate and extent of regeneration of CNF electrodes

Ions are electrically adsorbed on CNF electrodes and thus their individual charge is a factor that affects regeneration of CNF electrodes. The effect of individual charge of adsorbed ions will be examined during regeneration of CNF electrodes.

Objective 7 - Effect of CNF thickness on extent of desorption

Micro-pores contribute significantly to the total surface area of CNF and they are interconnected. As the thickness of CNF electrodes increases, the total surface area available for ions to adsorb/desorb increases. Different CNF thickness will be used and the effect of variation of thickness on desorption will be studied.

Objective 8 - Modeling the sorption-desorption rate and extent of CNF

Modeling of the regeneration process will be the final step and it will be based on results of all experiments for desorption of ions from the CNF surface. A new surface-pore-diffusion model will be prepared to describe desorption behavior during regeneration of CNF electrodes.

This study helps in understanding the regeneration of CNF exhausted in CDI applied to water purification and desalination. Desorption behavior of CNFs during regeneration can be modeled better now and a good model will help to identify optimal regeneration procedures and will provide a predictive capability.

CHAPTER II

BACKGROUND AND RELATED WORK

2.1 Carbon in Electro-chemical Applications

Carbon in various forms and arrangements has been used in the past for electro-chemical applications. Types of carbon used include granular activated carbon (GAC)[1], graphite,[2, 2b] graphitized carbon black (GCB),[3, 4, 5] activated carbon cloth (ACC),[6, 7,8] carbon-cloth or carbon-felt,[9, 10, 11, 12] reticulated vitreous carbon (RVC),[13] carbon aerogels (CA)[14, 15, 16, 17]. In some cases, the surface of carbon was modified chemically[7, 18] or layered with semi-permeable coating[19] to help the electro-sorption process.

All these different forms of carbon have different properties and characteristics and have been used in electrochemical applications accordingly. One characteristic is that some of them operate such that transport of compounds through them is diffusion-controlled. Graphite is one of the allotropes and softest form of carbon. It is a semimetal, electrical conductor and the most stable form of carbon under standard conditions. Graphite has a layered, planar structure. In each layer, the carbon atoms are arranged in a hexagonal lattice. Graphite can conduct electricity due to the vast electron delocalization within the carbon layers. These valence electrons are free to move, so they are able to conduct electricity. GCBs are similar to graphite. The term GCB refers to carbonization of precursors such as petroleum coke, oil, and coal-tar pitch that form soft carbons. In these materials, the formation of carbon proceeds through an intermediate liquid-like phase known as mesophase, which facilitates the three-dimensional ordering that is

necessary to create a graphite-like structure. GCBs exhibit hydrophobic surface characteristics, meaning that small, polar molecules such as water are not adsorbed. Graphite and GCB materials generally are non-porous. A distinct property of GCBs is the organized nature of their carbon sheets, which is a result of heating at temperatures above 2500 °C. GCB particles are generally non-porous and their entire surface is available at the exterior of the particle for interactions. Consequently, surface interactions depend solely on dispersion (London) forces. In contrast, activated carbons are highly porous and thus have high surface area as compared to graphite and GCB. Diffusion of the adsorbate is an important factor in activated carbons and other porous solids. The term "activated" in activated carbon refers to making carbon more porous. Activated carbon can be produced either by physical reactivation or chemical activation. In physical activation, the precursor (nutshells, peat, wood, lignite, coal and petroleum pitch) is pyrolyzed at temperatures in the range 600–900 °C, in absence of oxygen and then the carbonized material is exposed to oxidizing atmospheres (oxygen or steam) usually in the temperature range of 600–1200 °C. In chemical activation, the precursors are impregnated with certain chemicals (an acid or strong base) prior to carbonization. Then, the precursor is carbonized at lower temperatures (450–900 °C). Activated carbon can be either in the granular form (GAC) or powdered (PAC). GAC has a relatively larger particle size compared to PAC; thus, it presents a smaller external surface and a smaller surface to volume ratio. Carbon cloth/felt and ACC are available in knitted and woven form and generally offer the advantages of superior contact efficiency and higher adsorption capacity over GAC. They have large surface area due to microporous

structure and that is why transport of compounds through them is diffusion controlled. RVC is foam-like material that is similar to carbon aerogel and that is why material transport through it will be diffusion-controlled. It has low electrical resistance, large surface area, and a physically continuous structure. RVC has 97% open porosity. It has been used as flow through electrodes. The resistance to solution flow is low and flow rates up to 25 mL/min were easily attained.[20]

Diffusion-limited mass transport can be enhanced by using high-area, porous electrodes at which two-dimensional electrochemistry starts acting like "quasi-3-dimensional behavior" due to the large distributed area [9]. This suggests that the use of high surface electrodes would yield better results when it comes to removal of impurities present in water. Various forms of carbon with different surface areas have been used in the past for this purpose.

An important application of carbon is as an electrode. Arnold and Murphy[18] studied the electrochemistry of carbon and chemically-modified carbon surfaces in contact with sodium chloride solutions. They studied commercial graphite and found it to be cation-responsive. They showed that anion-responsive graphite electrodes could be prepared by first depositing colloidal graphite from aqueous solution onto 1/16 inch thick Dacron felt backing material, then drying it at 100º for two hours to break the dispersion of the colloids. They reported that the electrical potentials of carbon electrodes in aqueous solutions are determined by the nature of chemical groups forming the partly-oxidized surface, impurities, and electrochemically-active additives. They classified electrodes based on their responsiveness to cations and anions. A cation-

responsive electrode would be one that could reversibly adsorb cations, regardless of whether adsorption were complete or not. They defined the adsorptive properties of carbons in terms of the presence of functional groups on the surface. Carbon prepared in different ways from different sources may have different groups and some of them may be dominant. They adopted quinine-hydroquinone theory to explain effects of different functional groups. This theory describes how the electrode capacity is determined by the number of carbonyl and phenolic groups on its surface, i.e. by the extent of surface oxidation.

Carbon has also been used to construct flow-through, porous electrodes that remove ions from solution. Johnson and Newman[1] analyzed ionic adsorption on porous carbon. The electrode consisted of porous carbon particles with void spaces between the particles. The fluid moved between the particles, thus it was called a flow-through electrode. They showed that porous carbon materials can be used to desalt water. Bennion and Newman[21] worked on a device for concentrating electropositive cations using porous, fixed, flow-through, carbon electrodes and were able to reduce a feed of 667 mg/L copper solution to less than 1 mg/L copper solution. Inexpensive flakes and chips of carbon and graphite were used as the porous flow-through electrodes. Graphite was used in the form of a packed bed by Chu et al.[2a] for electrochemical extraction and cathodic deposition of copper ions from flowing dilute aqueous solutions onto the packed bed. Zee and Newman[22] used the same porous, fixed, flow-though electrodes as Bennion and Newman for electrochemical removal and reduction of silver ions from photographic solutions. Oren and Soffer[3] used “Carbopak B”, which is graphitized

carbon black, as high surface area porous carbon electrodes. The specific surface area was reported to be about 100 m^2/g. Oren and Soffer proposed an electrochemical parametric pumping (ECPP) concept in which water desalination was achieved by adsorption of ions at the electrical double layer of carbon electrodes that have high specific surface areas. Two such electrodes were assembled in a cell, electronic charge was cycled between them, and liquid was pumped through the cell in a periodic, synchronous way. This process was termed ECPP. Their ECPP column for separation of NaCl from water consisted of identical high surface area carbon electrodes separated by an inert spacer. Each ECPP cycle consisted of four consecutive operations: 1) adsorption, which was induced by changing the potential difference across the electrodes; 2) forward axial pumping of the solution to transfer ions onto electrodes; 3) desorption; and 4) backward axial pumping of the solution to remove ions and carry them away. Oren and Soffer[5] used ECPP for water desalting. Optimization considerations of the two adsorptive electrode batch unit of the ECPP was optimized and modified charge coordinates, desalting efficiencies and isopotentiograms (analogous to adsorption isotherms) were derived and analyzed on the basis of the properties of each separate electrode. Oren et al.[4] used electroadsorption with a porous electrode bed to remove bacteria from a solution that was pumped through it. *E. coli* have a negatively charged cell wall that caused them to be adsorbed onto the positively-charged porous carbon electrode by electroadsorption. Matlosz and Newman[13] used flow-through porous electrodes made of reticulated vitreous carbon for removal of mercury from

contaminated brine solutions. Concentrations were reduced by as much as a factor of 5000 in a single pass through the electrode.

Ayranci and Conway[10] successfully used high surface area carbon-felt electrodes for water purification. They studied inorganic, sulfur-containing anions and concluded that effectiveness of adsorption was related to factors such as charge, size and shape of ions, all of which play an important role in their hydration behavior. They also observed that polarization of carbon-felt surfaces caused an increase in the rate of adsorption of the ions. They also found that reversing the polarization for sufficiently long periods of time caused an initial desorption of ions due to discharging of the electrode, followed by the re-adsorption of oppositely charged ions.

Koresh and Soffer[11] used ultramicroporous carbon electrodes (TCM 128 carbon cloth and TGM 389) to study double layer capacitance and charging rate. The diameters of pores in their electrode were as low as 0.37 nm. Their work was limited to ultramicropores of dimensions from close to those of water molecules up to 0.6 nm. They concluded that the mobility of ions into ultramicropores is several orders of magnitude smaller than in the bulk solution outside the pores and that surface dipoles have a stronger effect on adsorption and mobility into ultramicroporous carbons than on a flat surface.

Activated carbon in granular form (GAC) has been used in flow-through porous carbon electrodes as well as in the form of activated carbon cloth (ACC). Jayson et al.[6] studied adsorption and electrosorption of mercury (II) acetate onto ACC from aqueous solution using shaking and flow-through techniques. Application of an electrical

potential to the ACC during flow-through experiments increased the uptake of mercury (II) and it was enhanced when the applied polarity was -1 volt with respect to a calomel reference electrode. Ryoo and Seo[7] modified ACC with titania. It was effective in decreasing physical adsorption of NaCl and increasing electric field adsorption resulting in significant improvement of CDI performance. Avraham et al.[23] used commercial ACC obtained by carbonization and activation of phenol-formaldehyde polymer. The cell design was flow-through and included both single electrode as well as full cells comprising two symmetric electrodes. The use of GAC as ACC has some problems, e.g. the difficulty in applying GAC as a uniform coating. Furthermore, some kind of glue is needed to provide strength to the coating. This glue sometimes is not able to hold GAC to the surface adequately and it can reduce the overall adsorption efficiency, because it reduces the surface area in contact with liquid.

Monolithic CAs that have high surface area and high electrical conductivity have been used in by Fischer et al.[17] and Saliger et al.[24] for supercapacitors. CAs can be applied in thin layers more easily than GAC. They have been found to have excellent characteristics for electro-sorption. Researchers have shown that CAs can be used effectively for demineralization of wastewater. Electro-sorption has been used for different kinds of water purification processes, including removal of heavy metal ions and desalination of dilute solutions. Capacitive deionization (CDI) technology is a very good example of where electro-sorption has been applied by various researchers to water treatment and desalination.

CDI technology has been used in a number of applications. Farmer et al.[14, 16] and Farmer et al.[15] used CDI and CA electrodes for removal of NaCl, $NaNO_3$, NH_4ClO_4, and hexavalent chromium in the form of $HCrO_4^-/CrO_4^{2-}/Cr_2O_7^{2-}$. Tran et al.[25] used electro-sorption with CA electrodes for remediation of ground water contaminated with low-level radioactive wastes following the principle of CDI. Pekala et al.[26] used it for electro-chemical applications. Ying et al.[27] used CDI and two types of CA composites of different surface area to provide a better understanding on the mechanisms of electro-sorption. Type A had a BET surface area of 412 m^2/g and type B had 602 m^2/g. Most of the pores were smaller than 20 nm and none of them were more than 100 nm for both types of CAs. Both types of CAs had a large portion of the pore sizes below 1 nm, where a strong electrical double layer was expected. Pore size distribution and differential surface area analysis showed that the difference in the surface area between these two types was mainly due to micropores (<2 nm). They reported strong specific adsorption of NO_3^- and Cu^{2+} ions with no significant adsorption of F^- ions. Although the surface areas were different, the capacities of the two types of CA for adsorbing ions were found to be very similar. This was believed to be caused by the electrical double-layers overlapping in the micropores. When a pore size is of the same order of magnitude as the electrical double layer thickness, the electrical double layers will overlap each other inside the pore and this will result in the loss of some capacity to contain ions. The net electric charge in the diffuse layer (measured over diffuse layer thickness) is equal in magnitude to net surface charge but has opposite polarity, thus there is electrical neutrality. The net electric charge in the diffuse layer divided by the surface area is

defined as the diffuse-layer charge density. It can be said that the surface charge density is the same as diffuse-layer charge density but with opposite sign. In micropores, a shallow potential distribution is observed due to double-layer overlapping. This behavior causes ion exclusion and leads to a slow mass transfer rate of ions. This effect of ion exclusion increases and mass transfer rate decreases quickly with decrease in pore width. At a specific pore width, known as the cutoff pore width, the electrical double layer ceases to exist. The cutoff pore width may vary from 0.5-5 nm depending on the diffuse-layer potential. It has been shown that counter ions cannot move in a pore with width less than the cutoff pore width and that the electrical double layer exists only for pores widths larger than the cutoff value[28]. Pores with widths smaller than the cutoff value do not contribute to the electrosorption of ions. Gabelich et al.[29] used CA and CDI for electro-sorption of various inorganic salts from aqueous solutions. Multisolute systems in which ions compete for limited surface area were studied. It was shown that although CA electrodes have been treated as electrical double-layers capacitors, ion sorption followed a Langmuir isotherm indicating monolayer adsorption. Monovalent ions with smaller hydrated radii were preferentially removed compared to multivalent ions when measured as the fraction removed. The capacity of CA was found to be about 1.0-2.0 x 10^{-4} equiv/g. The average pore size was about 4-9 nm, but not all of those pores contributed towards electrosorption, because some of them had pore widths below the cutoff pore width. The surface area covered by an individual ion (m^2) was calculated by dividing the two-dimensional specific surface area (m^2/g, based on the ionic radius) by the product of the molar sorption capacity (mole/g) and Avogadro's number ($mole^{-1}$), i.e.

m^2 = (m^2/g)/[(mole/g)(1/mole)]. Unhydrated and hydrated radii of ions were used for this calculation and that is why only about 14-42 m^2/g aerogel surface area was available for ion sorption. This was low as compared to the total surface area of 400 m^2/g determined by BET surface area analysis, or the Langmuir surface area of 540 m^2/g. Langmuir surface area was calculated by multiplying molar sorption capacities from Langmuir adsorption isotherm with Avogadro's number and the two-dimensional surface area of the compound being adsorbed. Gabelich et al.[29] argued that based on the median pore size (4 nm) of the CA used, the Langmuir surface area may be more appropriate for determining the actual surface area. Both BET and Langmuir surface areas were calculated using pressurized nitrogen and both of these surface areas may be misleading in terms of actual surface area available for ion sorption. It was also argued that when electric double-layer formation for various concentrations of electrolytes was considered, the actual surface area available for sorption may be much lower than indicated by BET analysis. Double layer at the carbon-electrolyte interface is primarily formed in the mesopore region (pore size > 3 nm), so if Langmuir (single layer) sorption is assumed the measured aerogel surface area (540 m^2/g aerogel) is increased as well as the level of porosity of available to sorption. Recently Park et al. [30] used CA as electrodes for a electro-chemical double-layer capacitor.

2.2 Capacitive Deionization Technology

The idea behind capacitive deionization is to force ions or ionic species present in aqueous solutions to be treated, towards oppositely charged electrodes by use of an

electric field. Under this kind of environment charged ions are held in the strong field on the electrodes, and once the electric field is removed the ions are quickly released. These systems require electrodes with high electrical conductivity and high surface area. An electrical double layer is formed when charged surfaces come in contact with a liquid solution that contains ions of an opposite charge that are attracted to the charged surface. They form a layer adjacent to the surface in which the concentration of oppositely charged ions is higher than in the bulk solution.

CDI is the process of removing ions using capacitive adsorption. Capacitive adsorption occurs when applied external potential creates an electric field on the surface of electrodes. In this electric field, ions immediately next to the electrode surface are attracted to opposite electrostatic charge on the surface of electrodes and a double layer forms next to the surface. This double layer traps ions from the bulk water, thereby producing deionized water. Helped by this force of electrostatic attraction, ions are further drawn in to pores and get adsorbed deeper into pores. Capacitive adsorption differs from regular adsorption, in which ions are adsorbed on to the surface without any help of electrostatic attraction created by an applied external potential. However, the efficiency of CDI strongly depends upon the surface properties of the electrodes, such as surface area and surface chemistry[26, 31]. A number of publications and patents show the use of porous electrodes for recovery of heavy metals from aqueous solutions[13, 22, 32]. In these studies electro-sorption of metallic ions were observed on cathodes with relatively low surface areas.

CAs were the first electrically conductive aerogels. Their high electrical conductivity, high surface area and ultra-fine (nanometer) pore size make them an ideal choice for electrodes in supercapacitors and capacitive deionization (CDI) processes. A supercapacitor can store energy using voltage-induced separation of charge at the electrolyte/solid interface. CDI uses a similar principle as supercapacitors. A voltage is applied to the carbon electrodes, which remove ionic impurities from a flowing aqueous stream.

The earliest studies on CDI were conducted at the University of Oklahoma in the early 1960s[18]. Johnson and Newman[1] conceived a comprehensive theoretical model for the capacitive charging of porous carbon electrodes and this analysis is still generally applicable to all CDI systems. Activated carbon was difficult to hold and form into thin conductive sheets for use as electrodes. Inert polymeric binders were used to hold the GAC particles together in thin sheets and this inert material was not helpful in the electro-sorption process. Durability of the electrodes was the main problem.

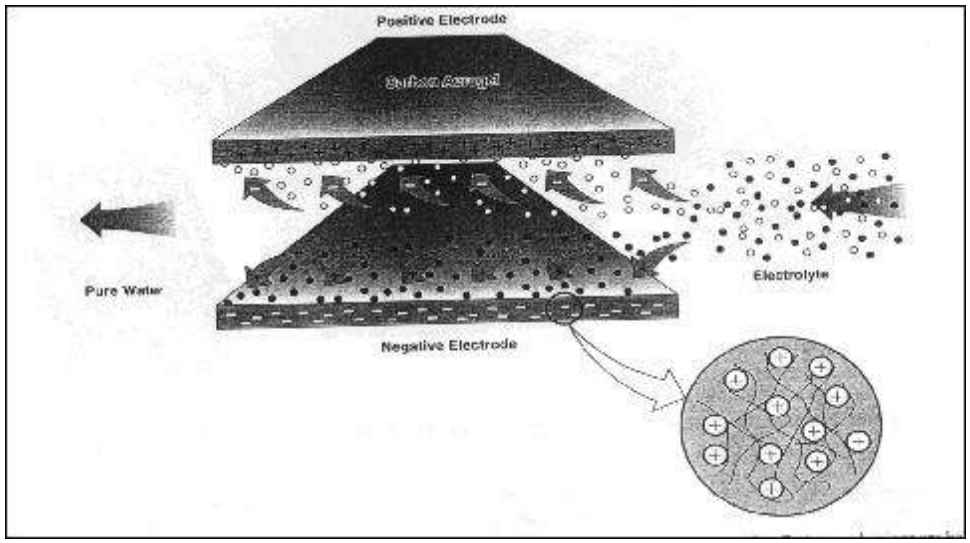

Figure II-1. Schematic diagram illustrating the principle of capacitive deionization with carbon aerogel electrodes. Cations and anions are held in the electric double layers formed at the cathode and anode, respectively. The high specific surface area of a carbon aerogel enables the process to remove a significant amount of dissolved ions from the water passing between the electrodes[16].

CAs have been used successfully and efficiently for electro-sorption of chromium ions as a means of treating ground water[15]; for capacitive deionization of NaCl and $NaNO_3$ solutions[14] and NH_4ClO_4 solutions[16]; for treating low-level radioactive waste[25]; for remediating contaminated ground water[25]; and for electro-sorption of inorganic salts from aqueous solution[12]. The basic principle of capacitive deionization is illustrated in Figure II-1. A voltage is applied to the carbon aerogel electrodes, which removes ionic impurities from a flowing aqueous stream by attracting ions to the oppositely charged electrode.

Framer et al.[15] examined the treatment of groundwater, contaminated with Cr(VI). During a feasibility study, it was observed that the level of hexavalent chromium in the groundwater could be lowered from 35 to 2 ppb, which is well below the

acceptable level of 11 ppb. A field test was also carried out successfully, in which three stacks of 48 double-sided carbon aerogel electrodes were polarized at 1.2 V and used to continuously remove Cr(VI) and Cr(III) from raw untreated ground water. Electro-sorption of chromium was favored over other anions at the part per million level even in the presence of 530 ppm of TDS.

Farmer et al.[14] carried out experiments on NaCl and $NaNO_3$ solutions. The solutions were passed through stacks of carbon of high specific surface area (400 to 1100 m^2/g) aerogel electrodes as shown in Figure II-2. After electrode polarization, non-reducible and non-oxidizable ions were removed from the electrolyte solution by the imposed electric fields and held in the electric double layers formed at the surfaces of the electrodes. Experiments were conducted over a broad range of solution conductivity and cell voltage. Conductivities ranged from 10 to 1000 μS/cm, and voltage levels were 0.0, 0.4, 0.6, 0.7, 0.8, 1.0, and 1.2 V. Four liters of electrolyte were recycled continuously in batch mode experiments at a flow rate of 1000 ml/min. Single-pass experiments were conducted by pumping 20 liters of electrolyte through the electrode stack at a flow of 25 ml/min. The ability of the electrodes to remove ions from water had a strong dependence on cell voltage. An imposed potential of 1.2 V gave best results and at 0.4 V performance was relatively poor. Salt removal of 95% from a 100 μS/cm feed stream was achieved until saturation of the carbon aerogel electrodes was reached. After operating for months (no information of exact number of months is given), a loss of 6 to 8 % of electrode capacity was observed.

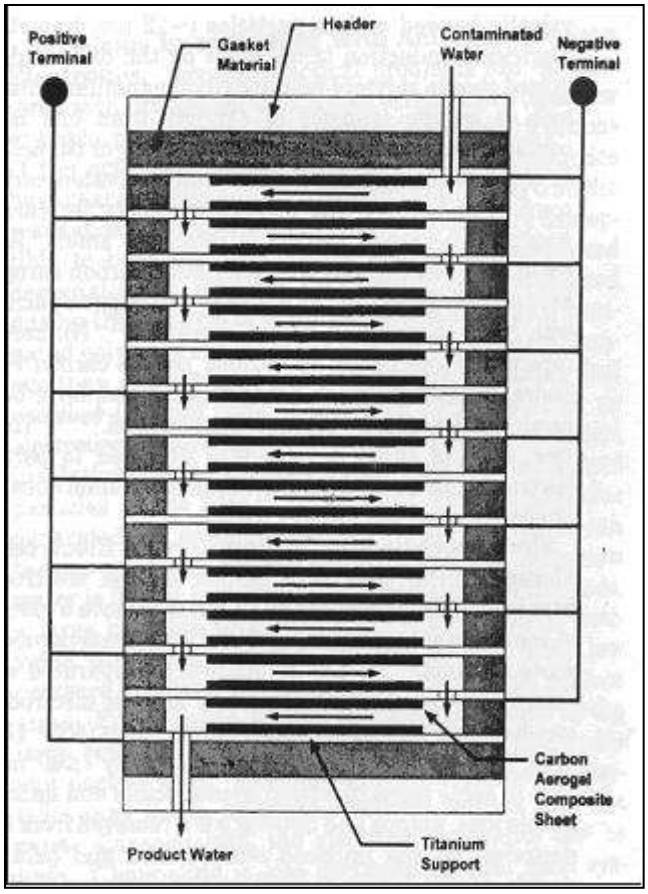

Figure II-2. Schematic representation of an electro-chemical cell similar to that used for experiments with 12 double-sided electrodes[15].

Farmer et al.[16] treated NH_4ClO_4 solutions following the same procedure as described above. The best salt removal voltage was found to be 1.2 V. For the single-pass experiments, 384 electrodes pairs were used in the system. Salt removal of 95% from a 100 μS/cm feed stream was achieved until saturation of the carbon aerogel electrodes was reached. The capacity of the carbon aerogel anode to electro-sorb ClO_4^- was found to be small, compared to the capacity of these electrodes to electro-sorb Cl^-

ions. This was also true in the case of NO_3^- ions. This study indicates a preference for smaller ions by the aerogel system.

Gabelich et al.[29] carried out extensive studies on the removal of various cations and anions by CAs. They determined that ion charge, ion size, and ion mass are the main variables affecting performance and electro-sorption capacity. Ca^{2+}, Na^+, Mg^{2+}, and Rb^+ cations and Cl^-, Br^-, NO_3^-, and SO_4^{2-} anions were selected for experiments because they can be found in natural water and are readily available as reagents. Experiments were carried out with 0.005 M solutions in a single-pass manner using CDI stacks as discussed before. The run time for these tests was 10 min at 1.4 V. No poisoning, scaling, or electrode degradation was observed under these operating conditions even after 36 experiments. Their data showed that carbon aerogel electrodes may reach saturation with respect to sorbing natural organic matter (NOM). Electrostatic attraction and physical enmeshment may be two possible mechanisms. It was thought that NOM sorbed due to enmeshment was not removed during regeneration, hence reducing the extent of regeneration of CA electrodes. Presence of NOM in source water reduced the inorganic sorption capacity of CA. Pretreatment for NOM removal was suggested to improve operational efficiency of CDI processes using CA. Removal of sodium from a natural water with 2.6 mg/L TOC was about 12 percent using an influent concentration of 3.2 M. Removal of potassium from the same water was 16 percent using an influent concentration of 0.2 M. These removals were high compared to those for calcium and magnesium, which were in the range of 5-8 percent for influent concentrations of 1-2 M. A similar pattern was observed for removal of anions. Removals of chloride (18 percent

for influent concentration of 2 M) and nitrates (22 percent for influent concentration of about 0.1 M) were highest and removal of SiO_2 (2-3 percent for influent concentration of about 0.2 M) was very low, while removal of sulfate was satisfactory (about 8 percent for influent concentration of about 2 M).

The total capacity of in an electro-sorption system depends mainly upon two factors. The first is the electrical double layer capacity due to the electrostatic attraction force between the ions and electrode. This is affected chiefly by the concentration of the ions in solution and the applied voltage. The other factor is the pseudo-capacity due to faradic reactions, which depend on the chemical characteristics of the solute and the functional groups on the electrode surface[27]. Yang et al.[28] proposed a model to understand the electro-sorption mechanisms on CAs from a microscopic view in order to describe total ion capacity. This model predicts electro-sorption of ions from aqueous solutions by carbon aerogel electrodes and is summarized in another section of this proposal (Past Models Describing Adsorption on CA Electrodes). Because of the porous nature of the electrodes, the total capacity of the system was obtained by summing the contributions of the individual pores. When a pore has a width smaller than a specific value (cutoff pore width), it does not contribute to the total capacity because of the effect of overlapping electrical double-layers. This effect greatly reduces the electro-sorption capacity for electrodes with significant area associated with micro-pores. The cutoff pore width was found to decrease with increasing concentration of the ion in solution and increasing applied voltage. Traditional approaches consider that the total surface area of the material is available for the electro-sorption, while Yang et al. (2001) showed that

pore size distribution of the material should also be considered. Therefore, total capacity should be calculated by integrating the capacity in each pore size category over the entire pore size distribution rather than using the total surface area.

2.3 Regeneration of CA Electrodes

The process of regenerating saturated CA electrodes involves release of captured ions and can occur via several methods. The basic technique is to simply backwash the cell with clean water. However, backwashing normally requires as much or more water for regeneration than the clean water produced, so additional techniques in combination with backwashing are required.

Gabelich et al.[29] short circuited the electrodes by removing the imposed potential while maintaining an electrical connection between them. The regeneration was carried out for approximately 20 min. by contacting the electrodes with the original test water. After each experiment the CDI unit was flushed with deionized water. Information about the amount of water required for regeneration was not given.

Farmer et al.[14] also short circuited the electrodes and aged electrodes were rejuvenated by voltage reversal. It was concluded that voltage reversal drives chemically bound ions from the surface of the carbon aerogel by imposing significant repulsive electrostatic force. Electro-sorption capacity of aged electrodes was restored to values that were approximately 80% to more than 95% of initial levels. The regeneration period was 32 min. They failed to mention how much water was required for this step. Farmer et al. carried out an experiment, with NH_4ClO_4 solutions in which regeneration was

complete after 30 min.[14] However, they did not mention the quantity of water used in the regeneration process.

Ryoo and Seo[7] defined adsorption of ions on to ACC electrodes without an electric field as physical adsorption and adsorption under an electric field as electric field adsorption. Polar groups of ACC work as adsorption sites for physical adsorption. It was noticed that physical adsorption took place initially when there was no applied electric field and once an electric field was applied there was even more adsorption (electric field adsorption) resulting in removal of more ions. Ions adsorbed because of electric field adsorption are more easily desorbed when either the electric field is removed or the electrodes are discharged than are ions adsorbed because of physical adsorption. A large electric potential is effective in promoting regeneration when electric field adsorption has removed the ions, while regeneration is difficult when physical adsorption is responsible for removal, because ions are not easily removed even after the electric field is removed.

Ayranci and Conway[10] evaluated high surface-area carbon-felt electrodes for water purification using adsorption and electro-sorption and discovered that partial desorption was achieved by discharging the electrodes. They suggested flushing the system with hot water, because the extent of desorption is expected to increase with temperature.

Kramer et al.[33] conducted an evaluation of a device using CAs for capacitive deionization. The device was called an Aquacell and was produced by Capacitive Deionization Technology Systems, Inc. This study concluded that successful

regeneration could be carried out for water with low TDS concentrations, but the amount of water used for regeneration was more than the amount of clean water produced. Deterioration of the CA was also noticed during experiments, which was believed to be due to short circuiting of water in the system.

CAs can be very useful in the purification of water, as there is very little loss of the aerogel material during regeneration. The power requirement for an operating a CDI unit is not large (requiring only 1.5 volts DC at 0.4 amps maximum). CAs are better candidates for electrodes than loosely bound activated carbons.

Basic information for studying electro-sorption of metals and other impurities are available and could be used to design experiments to study regeneration of CA that has been exhausted in desalination and purification of water contaminated with salts and metal ions. These treatment systems that use CA should have ionic selectivity, i.e., removals should depend on the size, charge, and extent of complexation of the ions being separated. It must be noted that very little work has been documented on regeneration of the aerogels and the proper methods of operating the regeneration process in order to maximize the quantity of clean water produced.

2.4 CA Preparation and Properties

Aerogels are derived from a gel in which the liquid component of the gel has been replaced with a gas. The result is an extremely low-density solid. They were first produced by Samuel Stephens Kistler[34] in 1931 from silicon dioxide. They were silicon-based porous solids with a sponge-like structure in which 99.8 percent of the volume

was air. They were prepared like gelatin, by mixing a liquid silicon compound and a fast-evaporating liquid solvent to form a gel that was then dried in an instrument similar to a pressure cooker. The mixture thickened while drying and then careful heating and depressurizing produced a glassy sponge of silicon.

Aerogels were initially thought to have no practical use. However, they are unique materials with ultra-fine pores (<100 nm), high surface area (> 400 m^2/g), extremely low density, and high electrical conductivity. Aerogels can be transparent, giving rise to the nickname "frozen smoke". Aerogels can be made from various compounds including silica, RF, melamine-formaldehyde (MF) and various metal oxides and thus can be divided in two categories as organic and inorganic aerogels. The term "organic aerogel" can refer to one of many different kinds of aerogels, each with properties arising from the polymer that makes up the framework of the aerogel. Organic aerogels have very different properties than inorganic aerogels. They are generally less friable and less fragile than inorganic aerogels. In the early 1990s, researchers developed aerogels that were made from pure carbon. One way of producing a CA is by the aqueous polycondensation of resorcinol (1, 3 dihydroxybenzene) with formaldehyde. The reaction under alkaline conditions proceeds through a sol-gel transition and results in the formation of a highly crosslinked polymer RF gel. This gel contains water, which is replaced with acetone by placing the gel in an acetone bath for a couple of days. The acetone is extracted by supercritical carbon dioxide with minimal shrinking and thereby preserves the gel skeleton and gives rise to a nanoporous material. Once the gel has been dried with supercritical carbon dioxide and all of the solvent extracted, the CAs can be

produced via the pyrolysis of the organic framework. RF aerogels are formed by highly crosslinked aromatic polymers and they can be pyrolyzed in an inert atmosphere to form vitreous carbon monoliths. The resultant porous material is black in color and known as a CA and can be transformed into the forms of monoliths, powders, microspheres, or thin film composites[14, 35]. Figure II-3 shows CA at 500,000 times magnification used by Gabelich et al.[29]

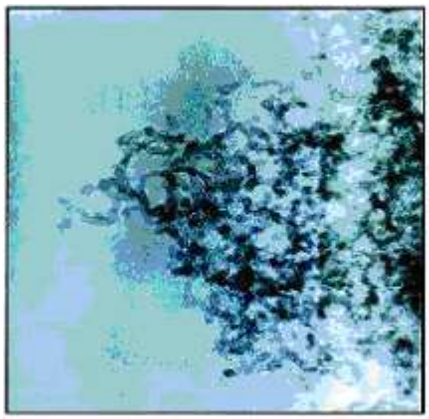

Figure II-3. Carbon aerogel microstructure: transmission electron micrograph at 500, 000 X magnification[29]

Fricke and Tillotson[36] discussed production, characterization, and applications of CAs in detail. Li and Guo[37] carried out some experiments for the preparation of low-density CAs from cresol/formaldehyde mixtures. In their experiments, a cresol mixture was first poly-condensed with formaldehyde and this reaction was catalyzed by NaOH. They concluded that a cresol mixture could be used as a raw material to prepare low-density, monolithic, crack-free aerogels and CAs[37]. Li et al.[38] attempted to make lower cost aerogels by using cresol. A mixture of cresol (C_m), resorcinol and formaldehyde has

been used as a more economical alternative route than the classical resorcinol-formaldehyde synthesis method. The porous structure of the mixed CAs (C_mRF) is similar to that of RF CAs.

The thermal properties of CAs do not play much of a role in water treatment processes, but heat/temperature treatment during their formation plays an important role in determining the structure of the CAs. It is known that the porosity of the carbon, measured by adsorptive methods, decreases with increasing heat treatment temperature[39]. Much work has been carried out to understand the thermal properties of CAs. Bock et al.[40], Gross and Fricke[41], and Hanzawa et al.[42] discussed the thermal behavior of CAs during their preparation. Wang et al.[43] studied morphological effects such as density and microstructure on electrical and electro-chemical properties of CAs and concluded that electrical conductivity increases with increase in both temperature and density of CA.

Reichenauer et al.[44] and Saliger et al.[45] conducted investigations concerning the micro-porosity of CAs. Reichenauer et al.[44] concluded that higher pyrolysis temperatures trigger formation and growth of 'encapsulated' micro-pores like those present in glassy carbon. Saliger et al.[45] observed in their experiments that a large amount of micro-porosity that is hidden in CAs could be made accessible without loss of uniformity by applying activation methods. Tamon et al.[46] studied the mesoporous structure of CAs and concluded that the mesopore radius of the RF can be controlled in the range of 2.5-9.2 nm by changing the mole ratio of resorcinol to Na_2CO_3 used as catalyst and the ratio of resorcinol to distilled water used as diluent. Shrinkage also plays a role in the control

of the mesopore radius. The pyrolysis temperature is also significant. As it increases, the mesopore volume becomes smaller, but the peak radius of the pore size distribution is maintained. The CAs prepared by pyrolysis at 1000 °C have the same adsorption characteristics for ethane and ethylene as activated carbons do.

2.5 Sonication

Ultrasonic waves have been used for various purposes, e.g. mixing and degassing of analytical samples, precision cleaning, and processing soil samples. The basic principle of any sonicator is transforming AC line power into ultrasound using a series of steps. First, the AC signal is converted by an ultrasonic electronic generator to produce a signal of 20 KHz or higher. This electrical signal drives a piezoelectric converter/transducer that produces mechanical vibrations. The vibrations are amplified and transmitted down the length of the horn/probe. The tip of the probe expands and contracts longitudinally. In liquids this motion causes cavitation, which is the formation and violent collapse of microscopic gas bubbles. Bursting of thousands of cavitation bubbles, releases tremendous energy in the cavitation field. This energy can be focused towards target objects or can be used in other ways, depending on the type of process. The effect of sonication on regeneration of exhausted CA electrodes will be studied in the proposed work.

2.6 Past Models Describing Adsorption on CA Electrodes

2.6.1 The Flow-through Electrode Model

Research[1, 3, 21-22, 32d, 47] has shown that flow-through porous electrodes can remove heavy metals from dilute streams. Trainham and Newman[32d] emphasized that more sophisticated models are required to help design better flow-through porous electrodes so that they can compete with other processes (e.g., foam fractionation, ion exchange, precipitation, and cementation). Trainham and Newman[32d] developed a one-dimensional model for flow-through porous electrodes operating above and below the limiting current of a metal deposition reaction. The model assumes that there is one primary reactant species in an excess of supporting electrolyte, and that a simultaneous side reaction may occur. Ohmic mass transfer and heterogeneous kinetic limitations were considered to predict a non-uniform reaction rate. According to Trainham and Newman[32d]:

Metal-ion removal from dilute streams using a flow-through porous electrode with parallel current can be described with the following restrictions

(i) The model is one dimensional;

(ii) The porous cathode is of length and has an isotropic porosity and specific surface area which remains constant in time;

(iii) The hydrodynamics are characterized by superficial speed and an average mass-transfer coefficient. Axial diffusion and dispersion account for deviations from plug flow;

(iv) There is one reactant species as well as a supportive electrolyte;

(v) A simultaneous side reaction may occur that is characterized by its rate at half-wave potential of the primary reaction. Also, if the side reaction involves generation of a gas, it is assumed that the gas will remain in the solution so that the speed profile will not be disturbed;

(vi) The conductivities of the matrix and pore solution phases are uniform.

Assumptions i-iii simplify the calculation procedure, and are necessary due to the lack of a better description of the complex porous geometry. The validity of the assumptions iv-vi rests on a small reactant concentration. As a consequence of assumptions iv and v, the current efficiency should be high, which further simplifies the model by removing the need to follow concentrations of any reactant species that participate in the side reaction. This approach emphasizes the salient features of the interaction between an unwanted side reaction and the metal deposition reaction.

Analysis and numerical solutions have been carried out in related publications. Trainham and Newman[32d] observed satisfactory agreement between model predictions and experimental data on over-all reactor performance and deposit distributions.

2.6.2 Electrical Double-layer Model[28]

An electrical double-layer (EDL) model has been proposed by Yang et al.[28] that includes the overlapping effect to describe the electro-sorption capacity of ions from aqueous solutions by carbon aerogel electrodes. The EDL model focuses on the formation of the electrical double layer and does not consider capacity. On the basis of

actual pore size distribution, the model describes the effects of applied voltage and ion solution concentration on the electro-sorption capacity and cutoff pore width.

The basis of this model is that the total capacity of electro-sorption on the CA electrodes is the sum of contributions from all of the individual pores inside the CA electrodes and hence, the total capacity can be obtained by integrating the electrical double-layer capacity of each pore over the entire pore size distribution. If a single pore with pore width w can be described as a slit formed by two planar plates with a separation distance w between them (as shown in the Figure II-4), then the electrical potential profile ψin a symmetric electrolyte solution between the two plates can be described by the planar Poisson-Boltzmann equation:

$$\frac{d^2\psi}{dx^2} = \frac{2zeN_0}{\in}\sinh\left(\frac{ze\psi}{kT}\right) \quad (1)$$

In this equation x is distance, ψ is electrical potential, e is the electrical charge of the electron, N_0 is the total number of ions in the bulk solution, $\in$is the dielectric constant of the medium, z is the valence of the ions, k is the Boltzmann constant and T is the absolute temperature.

Total Capacity of Electro-sorption: Calculations of the total capacity of electro-sorption are based on the work of Arnold and Murphy[18]. They systematically studied carbon electrode behavior for the purpose of water demineralization process development based on initial work by Blair and Murphy[48]. Blair and Murphy[48] compared their electrochemical method of saline water demineralization to electrodialysis as ions

were removed from solution by electrical transference. In order to achieve substantial salt removal in their system, the material in the anode must give up an electron which is transferred to the cathode. This increases the net positive charge on the anode, allowing it to attract more anions and decreases net positive charge allowing it to attract more cations. They further suggested that this mechanism ruled out the practical use of inert electrodes, but they stressed the need for stable and preferably thermodynamically reversible ones. They classified electrodes according to their ion responsiveness (complete or partial reversibility) to one general ion type (cation or anion). They used a pair of such electrodes (one cation responsive and one anion responsive) for demineralization. They focused their efforts towards development of graphite-type carbon electrodes of both types i.e. cation responsive and anion responsive. Arnold and Murphy[18] used a system that was similar to that used by Blair and Murphy[48] and they expressed the half-cell reaction of a cation-responsive electrode in a solution with sodium ions as:

$$C + Na^{+} + e^{-} = C^{-}Na^{+} \quad (2)$$

where C represents a site on the cation-responsive electrode. The half reaction of an anion-responsive electrode in solution containing chloride would be:

$$A + Cl^{-} = A^{+}Cl^{-} + e^{-} \quad (3)$$

where A represents a site on the anion-responsive electrode. Reduced C (C^{-}) and oxidized A (A^{+}) can act as ion-exchangers and passing current between A and C results in salt removal[18]. Arnold and Murphy followed quinine-hydroquinone theory for

interpretation of electrochemical and adsorptive properties of carbon and chemically modified carbon surfaces. They assumed that the cation-responsive character of graphite followed the following half-cell reaction:

$$\equiv C = 0 + Na^{+} + e^{-} \quad = \quad \equiv CO^{-}Na^{+} \tag{4}$$

where ≡C is an edge carbon atom in the graphite lattice. Organic molecules which undergo oxidation and reduction reactions, can be adsorbed on graphite to make anion-responsive electrodes. Capacities of the cathode and anode for electrosorption are termed the cation and anion capacity, respectively. The equivalents of cations removed must always equal the equivalents of anions removed because of the electro-neutrality constraint in aqueous solutions. Therefore, the total capacity is limited by either the cation capacity or the anion capacity, whichever is less. The CA material used by Yang et al.[28] was cation-responsive, so it would have a lower anion capacity than cation capacity and the anion capacity would control the total exchange capacity. This work will use a similar CA material, so the model will consider only the anion capacity resulting in positive ψ in Equation 1.

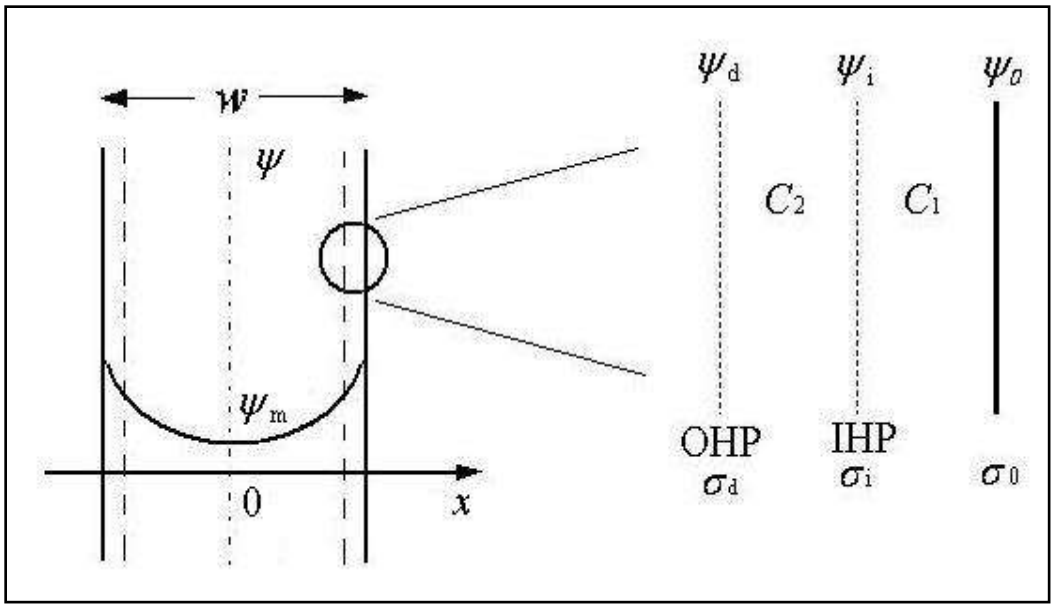

Figure II-4. Theoretical distribution of electrical potential inside a pore of width *w*; the dotted lines indicate the inner layer of the electrical double layer, which can be subdivided into the inner Helmholtz plane (IHP) and outer Helmholtz plane (OHP).

Boundary Conditions: Boundary conditions are established by placing the coordinate system such that the origin lies on the midplane of the pore space and x axis is perpendicular to this plane as shown in Figure II-4. The boundary conditions of equation 1 are described below

$$\frac{d\psi}{dx} = 0 \; and \; \psi = \psi_m \; at \; x = 0 \tag{5a}$$

$$\psi = \psi_d \; at \; x = \pm \frac{w}{2} \tag{5b}$$

The assumption is that the thickness of the inner layer (indicated by the dotted layer in Figure II-4) of the electrical double layer is small compared with the pore width *w* and it is reasonable to assume that the diffuse-layer boundaries are located at $x = w/2$

and - $x = w/2$. Here ψ_m is the electrical potential at the midplane and ψ_d is the diffuse layer potential. A constant-potential boundary condition (electrical potential on each side of the slit constant as the pore width w varies) is assumed to satisfy the boundary condition of equation 5b.

Inner Layer of Electrical Double Layer: The EDL model follows the Gouy-Chapman-Stern-Grahame model in respect to electrical double layers. The model states that the inner layers consist of two parts that are bounded by two planes: the inner Helmholtz plane (IHP) and outer Helmholtz (or diffuse-layer) plane (OHP) (Figure II-4). The locus of the centers of adsorbed ions is assumed to be the IHP and the OHP is the plane where the diffuse layer begins. Defining C_1 as the inner capacitance and C_2 as the outer capacitance, Yang et al.[28] obtained the following relationships between charge and potential:

$$\psi_0 - \psi_i = \int_0^{\sigma_0} \frac{d\sigma_0}{C_1(\sigma_0)} \tag{6a}$$

$$\psi_i - \psi_d = \int_0^{\sigma_d} \frac{d\sigma_d}{C_2(\sigma_d)} \tag{6b}$$

where $\psi_0$is the surface potential, ψ_i is the electrical potential at IHP, and surface and diffuse-layer charge densities are σ_0 and σ_d.

Applied Voltage and Surface Potential: Assuming anode and cathode are made of the same material and thus have the same electronegativity, the surface potential ψ_0 on the anode after an external voltage V is applied can be expressed as follows:

$$\psi_0 = \frac{V}{2} \quad \emptyset_{ecm} \tag{7}$$

where $\emptyset_{ecm}$ is the potential at the electrical capillary maximum and can be obtained from experiments as mentioned by Yang et al.[28]. The charge density at IHP(σ_i) becomes zero in the absence of specific adsorption and ψ_i and ψ_d in equations 6a and 6b become identical. The EDL model considers C_1 constant over the low voltage range. Integrating equation 6a after combining it with equation 7, gives the diffuse-layer potential ψ_d as follows:

$$\psi_d = \frac{V}{2}\, \emptyset_{ecm} \frac{\sigma_0}{C_1} \tag{8}$$

Surface Charge Density: The EDL model calculates the electrical potential distribution ψ by integrating equation 1 using boundary conditions 5a and 5b. It further states that for a symmetric potential distribution, the diffuse-layer charge density σ_d can be obtained by differentiating the electrical potential at the diffuse-layer boundary. This model assumes electroneutrality, thus surface charge density is the same as diffuse-layer charge density but with opposite sign and as this model was derived using NaF which is a 1:1 electrolyte, the surface charge density is derived as

$$\sigma_0 = \sqrt{4 \in RTI}\left[\cosh\left(\frac{e\psi_d}{kT}\right) - \cosh\left(\frac{e\psi_m}{kT}\right)\right]^{1/2} \tag{9}$$

where *I* is ionic strength and *R* is the gas constant.

Low potential Simplification: For low potential conditions, the P-B equation (equation 1) can be solved analytically for a single plane immersed in a solution of 1:1 electrolyte and the solution is shown below[49]

$$\frac{\exp(e\psi/2kT) - 1}{\exp(e\psi/2kT) + 1} = \left[\frac{\exp(e\psi_d/2kT) - 1}{\exp(e\psi_d/2kT) + 1}\right]\exp(-\kappa x) \tag{10}$$

where κ is the Debye-Hückel parameter, and is given for a 1:1 symmetrical electrolyte as

$$\kappa = \left(\frac{2N_A I e^2}{\in kT}\right)^{1/2} \tag{11}$$

where $N_A$is Avogadro's number. If we put *x* = *w*/2 in equation 10, we can get the expression for ψ_m, putting that expression into equation 9, the surface charge density can be expressed as follows:

$$\sigma_0 = \sqrt{4 \in RTI}\left[\cosh\left(\frac{e\psi_d}{kT}\right)\cosh\left\{8\left[\frac{\exp(e\psi_d/2kT) - 1}{\exp(e\psi_d/2kT) + 1}\right]\exp\left(-\frac{\kappa w}{2}\right)\right\}z\right]^{1/2} \tag{12}$$

When the product of the Debye-Hückel parameter (κ) and the pore width (w) is large, the exponential term containing the product becomes very small and thus cosh of second term approaches unity. Under this condition, the surface charge density can be expressed as follows

$$\sigma_0 = \sqrt{8 \in RTI}\sinh\left(\frac{e\psi_d}{kT}\right) \tag{13}$$

The charge density expressed in equation 13 is ideal charge density, when no electrical double-layer overlapping occurs. Equation 12 shows that surface charge

density (σ_0) decreases with decrease in pore width (w) and in some cases the bracketed expression may even be negative. There is a specific width (w_m) at which the value of the bracketed expression approaches zero and thus surface charge density approaches zero as well. The conclusion drawn is that electrical double layer exists only for pore width larger than w_m because the counter ions cannot be allowed to move in a pore of width smaller than w_m. The cut-off pore width is calculated by putting the right hand side of the equation 12 equal to zero and by doing so w_m is obtained as below:

$$w_m = \frac{2}{-\kappa} ln \left\{ \frac{e\psi_d [exp(e\psi_d/2kT) + 1]}{8kT[exp(e\psi_d/2kT) - 1]} \right\} \quad (14)$$

The EDL model discussed here is for background information. It is attractive from a theoretical perspective, but would not be as simple to apply to systems with mixed ions as the Langmuir isotherm. Therefore a competitive Langmuir isotherm will be applied to describe equilibrium in solutions of mixed ions in this work. If this approach is not successful, then the EDL approach will either be combined with the Langmuir model or used separately to describe equilibrium.

2.6.3 Homogeneous Surface Diffusion Model (HSDM)[50]

The HSDM was first presented by Notthakun et al.[51] and was adapted for the adsorption of arsenate on granular ferric hydroxide by Badruzzaman et al.[50], who stated that mass transport processes may be similar for porous metal oxides and activated carbon. They described the adsorption of arsenate on porous metal oxides as occurring in four steps: diffusion through bulk liquid, film diffusion, intraparticle diffusion and the

adsorption on the solid surface.[50] The diffusion through bulk liquid is rapid and thus not a rate limiting step. Film diffusion is directly proportional to the linear concentration gradient across the film and the film mass transfer coefficient (k_f) and it is affected by the packed-bed hydraulics and adsorbent particle size. Badruzzaman et al.[50] also noted that intraparticle diffusion may be caused by pore diffusion (i.e., with diffusion of ions in the pore space) or by surface diffusion (i.e., diffusion of ions on the surface of the pores) and that typically surface diffusion dominates over pore diffusion. Figure II-5 shows schematic of arsenate ion transport from solution onto porous metal oxide.

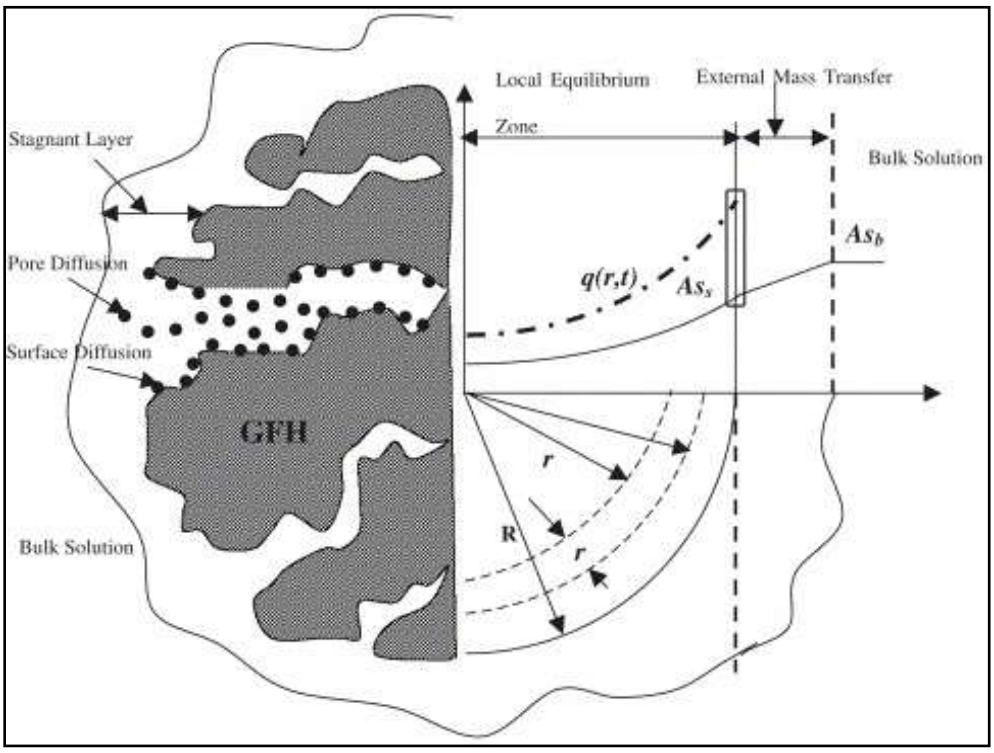

Figure II-5. Schematic of inorganic ion (arsenate) transport from the bulk solution onto porous metal oxides such as granular ferric hydroxide (GFH)[50].

Badruzzaman et al.[50] used the HSDM for describing a differential column batch reactor (DCBR). Root mean square difference between DCBR experimental data and HSDM output was minimized with a nonlinear least-squares optimization algorithm to obtain values of surface diffusivity (D_S) and film mass transfer coefficient (k_f). They summarized the HSDM model based on Fick's second law of diffusion, which is presented here in radial coordinates.

$$\frac{\partial q(r,t)}{\partial t} = D_S\left(\frac{1}{r^2}\frac{\partial}{\partial r}\left(r^2\frac{\partial q}{\partial r}\right)\right) \tag{15}$$

which is simplified as

$$\frac{\partial q(r,t)}{\partial t} = D_S\left(\frac{\partial^2 q(r,t)}{\partial r^2} + \frac{2\partial q(r,t)}{r\partial r}\right) \tag{16}$$

where q is defined as the solid-phase arsenate concentration that varies with time (t) and radial coordinate (r). It is assumed that at the particle surface (i.e., r is equal to R) there is an instantaneous equilibrium between liquid phase and solid phase arsenate concentrations. The solid phase concentration at the particle surface ($q(r = R, t)$) was calculated using the Freundlich isotherm.

$$q(r = R, t) = K\left(A_{S_s}\right)^{1/n} \tag{17}$$

where A_{S_s} is the liquid phase arsenic concentration at the external GFH surface and the isotherm parameters (K,1/n) can be obtained from batch isotherm experiments. HSDM requires one initial condition (equation 18) and two boundary conditions (equations 19

& 20) to obtain a unique solution. At t = 0 the following expression is true for a virgin GFH particle

$$q(r, t=0) = 0 \tag{18}$$

Also, the following expression is true, because there is no flux at the center of the particle.

$$\frac{\partial q(r=0,t)}{\partial r} = 0 \tag{19}$$

The external mass transfer flux and intraparticle diffusion flux must be equal at the solid-liquid interface to avoid accumulation of adsorbate at that point. Equating the fluxes and rearranging gives equation 20.

$$\frac{\partial q(r=R,t)}{\partial r} = \frac{k_f}{D_S \rho_p}\left[A_{S_b}(t) - A_{S_s}(t)\right] \tag{20}$$

where $A_{S_b}$is concentration of arsenic in the bulk solution and $\rho_p$is particle density. Badruzzaman et al.[50] summarized the HSDM model as discussed above but calculated bulk liquid arsenic concentration (A_{S_b}) as a function of time from equation 21

$$A_{S_b}(t) = A_{S_{b,0}} - \frac{m_{GFH}}{V} q_{avg}(t) \tag{21}$$

where

$$q_{avg}(t) = \frac{24}{d_p^3}\int_0^R q(r,t) r^2 dr \tag{22}$$

Equation 21 is derived from a material balance on arsenic over the liquid and solid phases (equation 23) using definition of q_{avg}, as shown in equation 22. The left side of equation 23 is the total amount of arsenic in the system at t=0. It assumes that there is no arsenic on the solid phase (equation 18). The right side is the total amount of arsenic in the system at any time t as shown by summation of remaining arsenic in the liquid phase and the adsorbed arsenic on GFH (solid phase). Equation 23 can be converted to equation 21 by solving for $A_{S_b}(t)$, which is the bulk liquid arsenic concentration at given time t.

$$V.A_{S_{b,0}} = V.A_{S_b}(t) + m_{GFH}.q_{avg}(t) \tag{23}$$

The relative importance of external mass transfer to intraparticle diffusion is expressed by the non-dimensional Biot number (B_i).

$$B_i = \frac{k_f d_p A_{S_0}}{2D_S \rho_p q_0} \tag{24}$$

The HSDM model discussed here is for spherical adsorbent particles, so it will not be applicable to the rectangular geometry of the CA electrode system used for this research. However, Fick's second law of diffusion can also be expressed in a Cartesian coordinate system, which could replace Equation 16.

2.6.4 Langmuir Adsorption Model[52]

The Langmuir model is the one of most commonly used isotherm models. It has been used to describe equilibrium adsorption of ions on various carbon forms. Gabelich

et al.[29] used Langmuir isotherm to describe equilibrium adsorption in electrochemical system (capacitive deionization) with CA. Other isotherms (Freundlich and BET) did not accurately modeled their data. They suggested that despite presence of electric double layer for modeling purposes, monolayer coverage of the CA surface may be used. At a given temperature, it is used to quantify the adsorbed amount of adsorbate on the surface of an adsorbent as a function of partial pressure or concentration. The adsorption process is considered to be a reaction where an empty site (*S*) on the adsorbent is covered by a molecule of adsorbate coming from a fluid (A_f) to give an adsorbed product (A_{ad}) as shown below.

$$A_f + S \rightleftharpoons A_{ad} \tag{25}$$

The following assumptions are made for a simple system with a single adsorbate adsorbing onto a series of equivalent sites on the surface of a solid.

1. The surface is homogeneous i.e. adsorbing sites are same in terms of their ability to adsorb compounds.
2. Only monolayer adsorption is possible i.e. each site only can hold at most one molecule of *A*.
3. There are no interactions among adsorbate molecules on adjacent sites.

A kinetic derivation of the Langmuir isotherm is discussed here and the adsorption reaction is written as an elementary chemical reaction that obeys mass-action kinetics. The fluid-phase concentration of A, $[A]$, has units of moles per volume or molecules per volume, [S] is the concentration of vacant sites in number/m^2 and $[A_{ad}]$ is the surface concentration of adsorbed molecules in number of molecules/m^2. The rate of

adsorption (r_{ad}) and rate of desorption (r_d) can be expressed using rate constantsk_{ad} and k_d as shown below.

$$r_{ad} = k_{ad}\,[A]\,[S] \tag{26}$$

$$r_d = k_d\,[A_{ad}] \tag{27}$$

The rate constants k_{ad} and k_d are assumed to be independent of the surface concentrations. This follows from the assumptions that the surface sites are all identical and that there are no interactions between adsorbed molecules. The rate of adsorption and desorption are equal at equilibrium.

$$r_{ad} = r_d \tag{28}$$

$$k_{ad}\,[A][S] = k_d\,[A_{ad}] \tag{29}$$

This can be rearranged to give the following expression, where K_{eq}^{A} is the equilibrium constant of the adsorption reaction.

$$\frac{[A_{ad}]}{[A]\,[S]} = \frac{k_{ad}}{k_d} = K_{eq}^{A} \tag{30}$$

The concentration of total sites $[S_0]$ is the sum of the concentration of unoccupied or available sites ($[S]$) and of occupied sites ($[A_{ad}]$).

$$[S_0] = [S] + [A_{ad}] \tag{31}$$

This equation can be combined with equation 30 to give the following.

$$[S_0] = \frac{[A_{ad}]}{[A]K_{eq}^{A}} + [A_{ad}] \tag{32}$$

$$[S_0] = \left(\frac{1 + [A]K_{eq}^{A}}{[A]\,K_{eq}^{A}}\right)[A_{ad}] \tag{33}$$

The fraction of the surface sites covered with *A* is represented as θ_A and is defined as shown

$$\theta_A = \frac{[A_{ad}]}{[S_0]} \tag{34}$$

Equations 33 and 34 are combined to give the Langmuir adsorption isotherm, as shown by equation 35.

$$\theta_A = \left(\frac{[A]K_{eq}^{A}}{1 + [A]K_{eq}^{A}}\right) \tag{35}$$

This Langmuir model for single sorbate can be further modified for systems with multiple adsorbates. Consider a system with two distinct adsorbate species *A* and *B*. These species are competing for the same adsorption sites. In addition to the previous assumptions, assume that each site can hold at most one molecule of *A* or one molecule of *B*, but not both at the same time. The equilibrium constant for adsorption of B is analogous to that for adsorption of A (equation 30).

$$\frac{[A_{ad}]}{[A]\,[\mathrm{S}]} = K_{eq}^{A} \tag{30}$$

$$\frac{[B_{ad}]}{[B]\,[\mathrm{S}]} = K_{eq}^{B} \tag{36}$$

The site balance equation 31 should be modified to reflect new system as shown below.

$$[S_0] = [S] + [A_{ad}] + [B_{ad}] \tag{37}$$

Following same steps that were taken to arrive at equation 34 for single adsorbate system i.e. inserting equilibrium equations into site balance equation shown above, we get competitive Langmuir adsorption isotherm model as shown below.

$$\theta_A = \left(\frac{[A]K_{eq}^{A}}{1 + [A]K_{eq}^{A} + [B]K_{eq}^{B}}\right) \tag{38}$$

$$\theta_B = \left(\frac{[B]K_{eq}^{B}}{1 + [A]K_{eq}^{A} + [B]K_{eq}^{B}}\right) \tag{39}$$

CHAPTER III

EXPERIMENTAL SYSTEM, METHODOLOGY AND EXPERIMENTS

This chapter is organized in three sections, i.e. experimental system, methodology and experiments. Experimental system used in this study is explained in detail including information about materials, equipment used and preparation of the capacitive de-ionization (CDI) cells. The second section describes the methodology that was adopted during experiments and the last section has information about experiments conducted as part of this study.

3.1 Experimental System

This section consists of information about the experimental system used in the study and it is divided into three parts. The first part is about materials used; the second part is about equipment; and the last part is about preparation of the CDI cells.

3.1.1 Materials

Materials used in this work are presented in two different groups based on their use. The first group contains materials needed for making CDI cells, while the second group contains chemicals needed to make various solutions that were used as feed water.

3.1.1.1 Materials used in CDI Cell

Four bench scale reactors were prepared and are called Capacitive Deionization (CDI) cells. Four different types of carbon aerogel (CA) were used in making these four CDI cells. Each CDI cell consists of two parallel carbon aerogel electrodes separated by a 1.50-1.53 mm gap for solution flow. The CA papers used in CDI cells were purchased from Marketech International, Port Townsend, WA. Figure III-1 shows CA used in this study.

Figure III-6. CA sheets used in making CDI cells.

The size of CA paper electrodes used to make CDI cells was 8.89 cm x 25.4 cm. Each carbon aerogel sheet weighed 2 g, with a total active surface area of approximately

8.16 x 10^6 cm^2. CAs with two different densities and two thicknesses were used as shown in Table III-1.

Table III-1. Characteristics of carbon aerogel sheets

Unit No.	Thickness (mils)	Density (g/ cm^3)
1	7	0.8
2	14	0.8
3	7	0.4-0.5
4	14	0.4-0.5

In addition of CA sheets, CDI cells also contained layers of aluminum foil (consumer grade), acrylic plastic, and glass, that were bound by nickel-filled, electrically conductive epoxy adhesive (40-3916 from Epoxies, Etc., Cranston, RI). This particular epoxy was chosen to provide a good balance of low cost and high conductivity. It is more resistant to corrosion than silver based epoxy systems, which are prone to corrosion when exposed to salt water. Consumer grade acrylic plastic sheets were used as spacers between two plates to get desired separation. All-purpose water-resistant glue (commercial name Quick Grip from Beacon Adhesives, Mt Vernon, NY) was used between acrylic plastics and glass plates. CDI cells were sealed using silicone based sealant (Silicone II from GE Sealants & Adhesives, Huntersville, NC). Epoxy-Patch® adhesive (Hysol®) from Loctite® was used to plug any leaks in the CDI cells. The glass plates were 6" x 12" and were procured from ACME Glass Products & Services, College Station, TX. A detailed description and related information about making a CDI cell is provided in the 'Preparation of CDI cell' section later in this chapter.

N_2 gas (ultra high purity, BOTCO, Bryan, TX) was used in experiments to determine surface area of CA.

3.1.1.2 Chemicals

All adsorption experiments were conducted with synthetic feed water prepared with various salts and deionized water. Potassium bromide (KBr), potassium chloride (KCl), potassium perchlorate ($KClO_4$), potassium nitrate (KNO_3), magnesium bromide 98% (MgBr), magnesium heptahydrate ($MgSO_4.7H_2O$), sodium bromide (NaBr), sodium chloride (NaCl), sodium nitrate 99% ($NaNO_3$) were purchased from Sigma-Aldrich Inc. All chemicals were at 99.5% or more pure unless otherwise noted and were used as received without further purification unless otherwise noted. Conductivity standard solutions were purchased from VWR and Corning Inc.

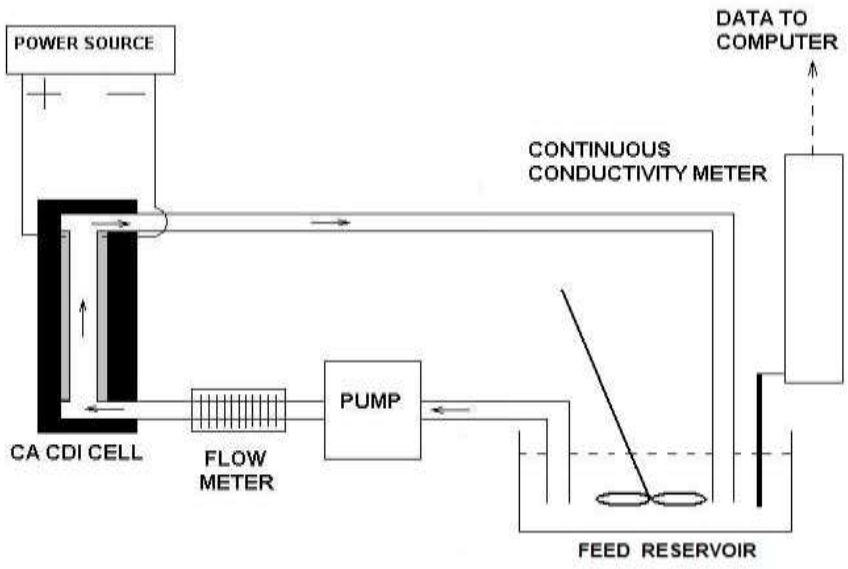

Figure III-7. Schematic diagram of experimental setup.

3.1.2 Equipment

Figure III-2 shows a schematic of the experimental system. A multi-output DC stabilized power supply unit (Kenwood PW18-1.8AQ) was used for applying a constant DC potential of 1.2 V across the CA electrodes as shown in the Figure III-2. A conductivity meter (Corning conductivity meter 441) was used in all experiments to measure conductivity of solutions. It was connected to a computer via COM1 port with a RS232 cable in order to record conductivity values with the help of RS232 Data Logger from Eltima Softwares. Values were saved for every other second in a CSV text file. Aqueous solutions were pumped using a peristaltic pump (MasterFlex Peristaltic pump model no. 7553-70) from Cole Parmer Instrument Co., Chicago, IL. A multimeter (Hewlett Packard multimeter 3468A) was used to verify that the applied potential across the CA electrodes was as indicated by the multi-output DC stabilized power supply unit (Kenwood PW18-1.8AQ). Also, a digital vernier caliper was used to measure thickness and separation distances. The BET surface area of CA samples was measured with a physisorption instrument (Accelerated Surface Area and Porosimetry (ASAP) Model 2000; Micromeritics, Norcross, GA) in the Microscopy and Imaging Center at Texas A&M University. Isotherms were measured at 77 K using nitrogen gas (ultra high purity, BOTCO, Bryan, TX). The standard mode of measurement was to apply a dose of nitrogen and then to measure the pressure above the sample. Stabilized pressure indicated that the sample was at equilibrium.

The feed solution was continuously mixed in the reservoir and pumped into the CDI cell from an inlet located at the bottom of the cell using the peristaltic pump. After

passing through a narrow space between two oppositely charged CA electrodes, the solution came out from the top of the cell outlet located diagonally opposite from inlet and carried back into the reservoir, where it was mixed continuously. Silicone tubing was used to carry water in all cases. Water flow was regulated by controlling the rotational speed of the peristaltic pump and the height of the feed reservoir.

3.1.3 Method of Preparation of CDI Cell

Glass plates were cleaned with regular dish washing detergent to remove all oil and dust from the surface. A hole was drilled into each plate for an inlet or an outlet depending on how it was to be used. A piece of plastic tubing with outer diameter that matched the diameter of the hole was inserted in to each hole and glued with an all-purpose water-resistant glue (Quick Grip, Beacon Adhesives, Mt Vernon, NY) and other epoxies making it leak proof.

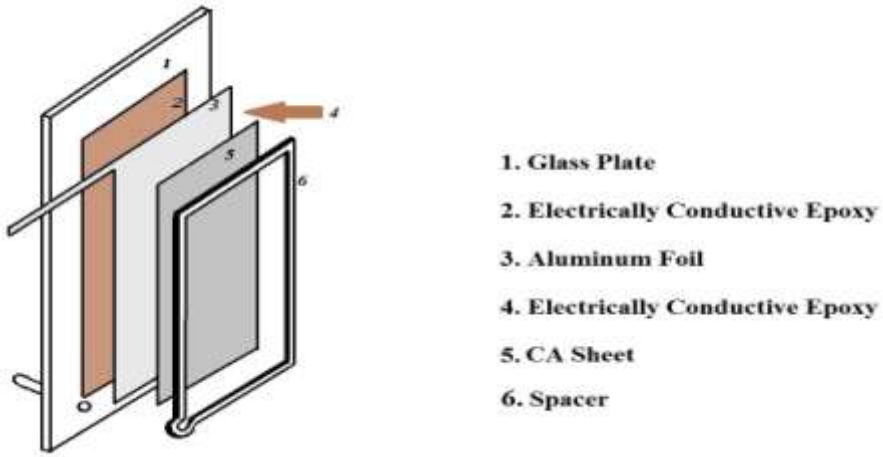

Figure III-8. Schematic of layered electrode that makes up half of a CDI cell.

A very thin and uniform layer of electrically conductive epoxy (layer 2 in Figure III-3) was applied with a brush. The thickness of epoxy in this layer was not considered to be import, because the sole purpose of this layer was to help the aluminum foil (layer 3 in Figure III-3) to stick to the glass plate. Care was taken to make sure that there was extra aluminum foil sticking out that could be used for electrical connections. A new layer of electrically conductive epoxy (layer 4 in Figure III-3) was applied on top of this aluminum foil and the CA sheet (layer 5 in Figure III-3) was placed on it gently. A heavy item with a clean and smooth surface was placed on the cell and allowed to stay there for 24 hours to allow the epoxy to cure. Once cured, these layers were well attached to each other. Figure III-3 shows the various layers used to construct the electrode as well as the spacer (layer 6 in Figure III-3) that fits between the two electrodes. The thickness of the spacer was chosen to insure a distance of 1.50-1.53 mm between the CA surfaces of adjacent electrodes. Four different strips were placed around the CA sheet to form the spacer and they were attached with glue that filled all joints. Special care was taken care around inlet and outlet openings. The space outside the spacers and between the glass plates was filled with a commercially available silicon-based sealant (Silicone II from GE Sealants & Adhesives, Huntersville, NC) making the CDI cell leak proof. Additional coatings of glue and sealant were applied whenever it was deemed necessary to fix any leaks. Various stages of a CDI cell construction are shown in Figure III-4.

Figure III-9. Various stages of a CDI cell construction.

3.2 Methodology

This study was focused on the regeneration of CA electrodes exhausted in capacitive deionization. Two types of experiments (adsorption and desorption) were conducted using four different CDI cells. CDI cells were used first for the adsorption phase and once electrodes were exhausted, the same cell was used for the desorption phase. The objective of these experiments was to collect data to show the extent of adsorption during the adsorption phase and the extent of regeneration of CA electrodes during the desorption phase.

Once the CDI cell and other instruments were put together as shown in Figure III-2, the system was flushed with deionized (DI) water to clean it before any experiments were conducted. After flushing for 2 hours, a recycled cleaning mode was begun by directing the outlet flow from the cell into the feed reservoir. The system was run in this initial cleaning mode for 1-2 days. The conductivity of water in the well mixed reservoir increased with time, which confirmed that some contaminants were present on the CA or were leaching from other parts of the CDI cells. DI water was replaced several times during this cleaning phase. Over a period of time, conductivities decreased and became constant with time, indicating that the contaminants were washed out of the system. Once there was no significant change in conductivity in DI water for an extended period and conductivity stayed very close to the fresh DI water used in flushing, CDI cells were ready for experiments.

3.2.1 Calibration of Conductivity Meter, Peristaltic Pump and Concentration versus Conductivity Curves

The conductivity meter was calibrated before every adsorption-desorption experiment. A two-point calibration method was used as suggested by the manufacturer of the instrument. The first calibration point was with the conductivity sensor being in air and second calibration point was with the conductivity sensor in a conductivity standard solution with conductivity of 83 µS/cm (8.3 mS/M). Conductivity of feed water varied between 300-175 µS/cm (30-17.5 mS/M) during adsorption experiments and between 0-50 µS/cm (0-5 mS/M) during desorption experiments.

Aqueous stock solutions of magnesium bromide ($MgBr_2$), magnesium sulfate ($MgSO_4$), potassium bromide (KBr), potassium chlorate ($KClO_4$), potassium chloride (KCl), potassium nitrate (KNO_3), sodium bromide (NaBr), sodium chloride (NaCl), sodium nitrate ($NaNO_3$) and sodium sulfate (Na_2SO_4) were prepared with DI water. These stock solutions were used to prepare solutions of various concentrations for each salt by dilution with DI water. Solutions were well mixed during and after dilution and conductivity measurements were taken of resulting solution. Three measurements were taken for each dilution. This process was repeated for 8-9 times in order to obtain data points over a wide range of concentrations. These data points were plotted as conductivity versus concentration curves for each salt and these curves were used to calculate concentrations of a particular salt from conductivity measurements. The range of concentrations used in the concentration versus conductivity curves was chosen based on the expected concentration range to be encountered in the experiments. The conductivity sensor was cleaned following recommended procedure after each experiment and re-calibrated before preparing a new calibration curve.

Calibrations of peristaltic pumps were done before every adsorption and desorption cycle in order to maintain a uniform volumetric flow of aqueous solution through the CDI cells. Silicon tubing was changed often and as needed when poor performance was observed.

3.2.2 Adsorption, Desorption and Cleaning Cycles

This section provides information of various modes of operation of CDI cells. Each CDI cell was operated in three modes, i.e. adsorption, desorption and cleaning. The adsorption mode was used for adsorption experiments and the desorption mode was used for regeneration experiments. Cleaning mode was used to clean the CDI cells after regeneration experiments in order to prepare them for adsorption experiments.

3.2.2.1 Adsorption Cycles

CDI cells were used for adsorption and desorption cycles followed by cleaning cycle before experiments were conducted with solutions of various salts. The initial concentration and volume of solutions needed to start an experiment was calculated to achieve a final concentration that could be easily measured. An initial estimate of adsorption capacity and mass of the CA was used to calculate the amount of salt expected to be removed by the CDI cells and this was added to the amount expected to not be removed (volume of solution times desired final concentration) to obtain the initial amount (volume times concentration). Adsorption experiments were conducted with 300 ml of 0.0015 M solution of NaCl (Phase 1 and 4) or as stated (Phase 2 and 3) at a temperature of 20 °C with an applied adsorption potential of 1.2 V and flow rate of 100 ml/min which resulted in a speed across the CA of 18.5 cm/min. Experiments were run for 12 hours for CA electrodes to have maximum adsorption and system to equilibrate. The conductivity sensor was placed in the reservoir. An initial conductivity reading was taken when no water was being pumped into the CDI cell. Conductivity measurements

were started the moment the pump and electronic timer were switched on. Conductivity values in the reservoir solution dropped with time indicating removal of ions due to adsorption on CA surfaces. An adsorption cycle was run until the CA was completely exhausted as indicated by no further drop of conductivity value measurements. Most runs lasted 12 to 13 hours. The concentrations were calculated using the conductivity versus concentration curve obtained for the salt being used in the experiment. No volume of the solution was lost and adsorption on CA surface inside CDI was assumed to be the only reason for the decrease in conductivity. Mass balance calculations were done based on initial and final concentrations to calculate amount of ions removed from solution.

The CDI was operated continuously in adsorption and desorption cycles without a cleaning cycle during hysteresis experiments (part of experiment 11). These experiments were started with 300 ml of 0.0015 M KBr solution applied at a flow speed of 18.5 cm/min) and applied adsorption voltage of 1.2 V across CA electrodes. Adsorption experiments were run for 12 hours so that equilibrium was achieved, as indicated conductivity being constant with time. Conductivity values were recorded over a period of time. A known quantity of DI water was added to the system to promote desorption and the system was allowed to react for 12 hours, so that it would reach a new equilibrium before measurement. An additional amount of DI water was added and the process was repeated. Adsorption was caused by adding small, known volume of a higher concentration KBr solution. This resulted in higher solution concentration and

the system was allowed to equilibrate again. This process was repeated multiple times, forcing the system to go through cycles of desorption, adsorption and finally desorption.

3.2.2.2 Desorption Cycles

Once the adsorption cycle was over, the pump was switched off, which stopped the flow through the system. The data logger was stopped and name of the CSV text file was changed from the default (COM1port) to a unique file name. Additional information was added to help identify the data and relate it to specific experiment. Before the desorption cycle was started, the old data in the COM1port CSV file was deleted so that new data could be saved in it. All of the solution that was present in the CDI cell and the tubing was pumped out. Extra care was taken to insure that water trapped in the tubes of the peristaltic pump and within the CDI cell was removed. Desorption cycles were started after addition of 300 ml of DI water, unless stated otherwise. The potential applied to the electrodes was not changed during the time water was drained and added to the system. After the data logger and timer were reset, the desorption cycle was started by simultaneously switching on the pump and the timer. Conductivity measurements were recorded as they were during the adsorption cycle. Conductivity values increased with time, indicating desorption of adsorbed ions. Initial and final conductivity measurements were used to calculate initial and final concentrations of the salt being used in the experiment. Mass balance calculations were made and the amount of salt desorbed was calculated. It was assumed that no volume of DI water was lost and that the increase of ions was the result of desorption from the CA.

3.2.2.3 Cleaning Cycles

The system was cleaned after each desorption cycle and before adsorption cycle in a manner similar to the initial cleaning. DI water was used for flushing the CDI cell and it was changed multiple times. Electrodes were shorted for first few hours and polarity was reversed multiple times for brief time intervals (5-10 minutes) to eliminate any residual charge on electrodes. Each cleaning cycle was run for about 48 hours. Conductivities increased slowly during this period, indicating desorption of remaining adsorbed ions. A cleaning cycle time of 48 hours and the required volume of DI water were determined during preliminary experiments. Conductivity measurements became constant towards the end of the 48-hour cycle, even when reservoir water was replaced DI water. Also, mass balance calculations were made to make sure all adsorbed ions were desorbed before another adsorption experiment was conducted.

3.3 Experiments

The experimental work was divided into four phases based on the research objectives that were defined in Chapter I. Phase 1 had 23 experiments at 9 sets of experimental conditions as shown in Table III-2. These experiments investigated the effect of the polarity of the electrodes on regeneration and how that effect was modified by changing temperature and water speed. Two different terms (“experiment” and series of experiments”) were used to describe Phase 1 experiments. The term “experiment” was used to describe a single set of condition while the term “series of experiments” term was used to describe a series of experimental conditions (e.g. variable time of

application of reverse potential, variable temperature and variable water flow speed over CA electrode surface). Different experiments were conducted within each series of experiments. Experiments with variable time of application of reverse potential were represented with an experiment number followed by a "-" and a number that shows the time of application of reverse potential in minutes. All experiments with reverse potential were conducted for total regeneration period of 12 hours. Lower case letters after a dash were used to describe experiments conducted at specific temperature, e.g. "a" is for 30°C and "b" is for 39°C. Roman numbers were used to describe different flow speeds, e.g. I is for 10.9 cm/min and II is for 32.2 ml/min. All experiments were conducted with a potential of 1.2 V applied across the CA electrodes during both the adsorption and desorption phases. Experiments were conducted with a flow speed of 18.5 cm/min and a temperature of 20 °C unless otherwise.

Experiments labeled 3-1, 3-2, 3-5, 3-14 and 3-32 were conducted with variable time of application of reverse potential, as indicated in Table III-2. After applying the reverse potential, the electrodes were shorted and desorption experiments were continued for about 12 hours.

Experiments 1 and 4 (4-a and 4-b) were conducted to evaluate the effect of temperature on regeneration when no potential was applied, while experiments 2 and 5 (5-a and 5-b) were conducted to evaluate the effect of temperature when the electrodes were shorted (i.e. connected externally with a conducting wire). Also, experiments 3 (3-1 and 3-5) and 6 (6-1-a, 6-5-a, 6-1-b and 6-5-b) were designed to show the effect of temperature on regeneration when a reverse potential was applied. Results of experiment

series 4, 5 and 6 can be compared in order to the effect of temperature on regeneration under different polarity conditions (potential applied, not applied, reversed). Similarly, results from experiment series 7, 8 and 9 can be compared to evaluate how the speed of water moving over the CA surface affects regeneration of CA under different conditions (no potential, shorting, and reverse potential). Adsorption experiments were conducted with 300 ml of 0.0015M NaCl solution at temperature of 20°C applied at a flow speed of 18.5 cm/min of 100 ml/min with a potential of 1.2 V applied across the electrodes. Adsorption experiments were run for 12 hours to allow the system to equilibrate. Desorption experiments were conducted with 300 ml of DI water of known starting conductivity and at temperature of 20°C (or as stated) using a flow speed of 18.5 cm/min (or as stated). The conditions of any applied potential during regeneration are as described in each sub-section. The solution was continuously well mixed in a reservoir and re-circulated to the system. Desorption experiments were also run for 12 hours to allow the system to equilibrate.

Table III-3 summarizes experiments that were part of phase 2. All experiments were done with a constant continuous water flow speed of 18.5 cm/min. Phase 2 experiments studied the effect of the mass of ions (experiments 1, 10 and 11) and their ionic radius (experiments 12 through 15) on regeneration of CA. Adsorption experiments were conducted with 300 ml of 0.0015 M solution of each salt that was applied at a flow speed of 18.5 cm/min at temperature of 20°C and potential of 1.2 V applied across the CA electrodes. Desorption experiments were conducted with 300 ml

of DI water applied at a flow speed of 18.5 cm/min with a temperature of 20°C and reverse potential of 1.2 V applied for the first 2 minutes of the 12-hr regeneration period.

Phase 3 experiments (16 through 19) are shown in Table III-4 and they were conducted to study the effect of charge of ions on regeneration of CA. Salts with cations and anions of varying charge were chosen accordingly.

Phase 4 experiments (1 and 20 through 22) are shown in Table III-5 and they were conducted to study the effects of the characteristics of CA on regeneration. Four different CDI units with two different thicknesses and two different densities were used in these experiments. Equilibrium adsorption experiments were conducted with 300 ml of 0.0015 M NaCl solution applied at a flow speed of 18.5 cm/min at a temperature of 20 °C with a potential of 1.2 V applied for the first 12 hours. Equilibrium desorption experiments were conducted with 300 ml of DI water applied at a flow speed of 18.5 cm/min at a temperature of 20°C and with a reverse potential of 1.2 V applied for the first 1 minute of the 12-hour regeneration period.

Table III-2. Phase 1 Experiments

Exp. #	Phase-1 Conditions
1†	No potential/shorting applied + backwash with DI water
2*	Shorting + backwash with DI water
3	Series of experiments with variable time of application of reverse potential
3-1*	Reverse potential applied (1 min)+ backwash with DI water
3-2*	Reverse potential applied (2 min)+ backwash with DI water
3-5*	Reverse potential applied (5 min)+ backwash with DI water
3-14*	Reverse potential applied (14 min)+ backwash with DI water
3-32*	Reverse potential applied (32 min)+ backwash with DI water
4	Series of experiments with no potential/shorting applied + backwash with hot DI water (varying temperature)
4-a*	No potential/shorting applied + backwash with hot DI water at 30°C
4-bΔ	No potential/shorting applied + backwash with hot DI water at 39°C
5	Series of experiments with shorting + backwash with hot DI water (varying temperature)
5-aΔ	Shorting + backwash with hot DI water at 30°C
5-bΔ	Shorting + backwash with hot DI water at 39°C
6	Series of experiments with reverse potential applied (variable time) + backwash with hot DI water (varying temperature)
6-1-a	Reverse potential applied (1 min) + backwash with hot DI water (30°C)
6-5-a	Reverse potential applied (5 min) + backwash with hot DI water (39°C)
6-1-b	Reverse potential applied (1 min) + backwash with hot DI water (30°C)
6-5-b	Reverse potential applied (5 min) + backwash with hot DI water (39°C)
7	Series of experiments with no potential/shorting applied + backwash with DI water (varying speed)
7-IΔ	No potential/shorting applied + backwash with DI water (10.9 cm/min)
7-IIΔ	No potential/shorting applied + backwash with DI water (32.2 cm/min)
8	Series of experiments with shorting + backwash with DI water (varying speed)
8-IΔ	Shorting + backwash with DI water (10.9 cm/min)
8-IIΔ	Shorting + backwash with DI water (32.2 cm/min)
9	Series of experiments with reverse potential applied (variable time) + backwash with DI water (varying speed)
9-1-I	Reverse potential applied (1 min) + backwash with DI water (10.9 cm/min)
9-1-II	Reverse potential applied (1 min) + backwash with DI water (32.2 cm/min)
9-5-I	Reverse potential applied (5 min) + backwash with DI water (10.9 cm/min)
9-5-II	Reverse potential applied (5 min) + backwash with DI water (32.2 cm/min)

† Experiment was repeated 5 times.

* Experiment was repeated 4 times.

Δ Experiment was repeated 3 times.

Table III-3. Phase 2 Experiments

Phase-2 (Effect of mass of ion on CA regeneration)		
Experiment #	Cation	Anion
1	Na^+	Cl^-
10	K^+	Cl^-
11	K^+	Br^-
Effect of ionic radius on regeneration		
12	Na^+	Br^-
13	Na^+	NO_3^-
14	K^+	Br^-
15	K^+	NO_3^-

Table III-4. Phase 3 Experiments

Phase-3 (Effect of charge of ion on regeneration)		
Experiment #	Cation	Anion
16	Na^+	Br^-
17	Na^+	SO_4^{2-}
18	Mg^{2+}	Br^-
19	Mg^{2+}	SO_4^{2-}

Table III-5. Phase 4 Experiments

Phase-4 (CA test electrode data)				
Experiment #	Unit	Aerogel sheet thickness (mils)	Density (g/cm^3)	Area (m^2/g)
1	1	7	0.8	400
20	2	14	0.8	400
21	3	7	0.4-0.5	600
22	4	14	0.4-0.6	600

CHAPTER IV

RESULTS AND DISCUSSION

This chapter presents results of previously listed experiments and they are grouped together and discussed accordingly. This chapter is divided in multiple sections. First section is about experiments and information that characterizes CA. A discussion on physical and surface properties is presented in this section. This section is followed by data and results of experiments done in phases I, II, III and IV. A discussion is presented wherever necessary. The results from one experiment are later compared with one or more experiments in order to get a better understanding of regeneration of CA.

4.1 Characterization of CA

The CA papers used in CDI cells were purchased from Marketech International, Port Townsend, WA. Material came with technical information that was used in this study. Some of the information was verified at the Microscopy and Imaging Center at Texas A&M University. SEM photographs (figures IV-1 through IV-4) of CA composite sheet show platelets of CA firmly attached to random carbon fibers, interspersed with macro porosity. These SEM photographs of a typical CA used in the study, were taken at 22 times, 100 times, 200 times and 1000 times magnification, respectively. SEM photographs show cracks on CA surface that may be the result of how CA was dried and pyrolyzed in manufacturing process. In addition, these cracks might be the result of how samples were prepared for SEM testing. One particular type of CA (density of 0.8 g/m^3,

thickness of 7 mil and areas of 400 m^2/g) was used in CDI unit 1 that was used for majority of experiments (all phase 1, 2 and 3 experiments) and many of them being repeated multiple times. No wear and tear was observed during experiments. The same should be true for other types of CA and they should be able to perform well during similar experimental conditions. This is consistent with the type of behavior that was observed in the past for adsorption studies by various scholars[14,16, 29, 33].

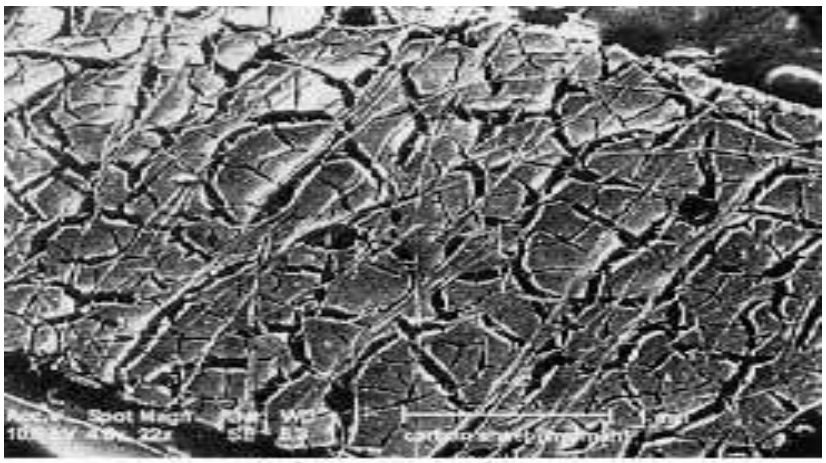

Figure IV-10. SEM image of CA taken at 22x magnification.

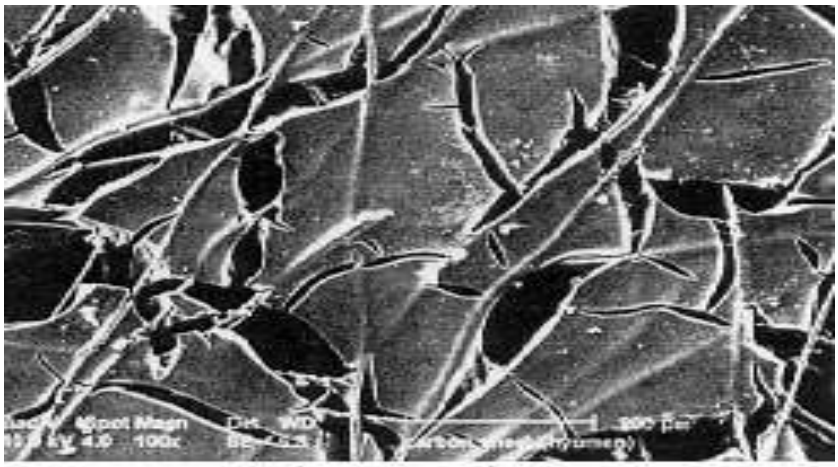

Figure IV-11. SEM image of CA taken at 100x magnification.

Figure IV-12. SEM image of CA taken at 200x magnification.

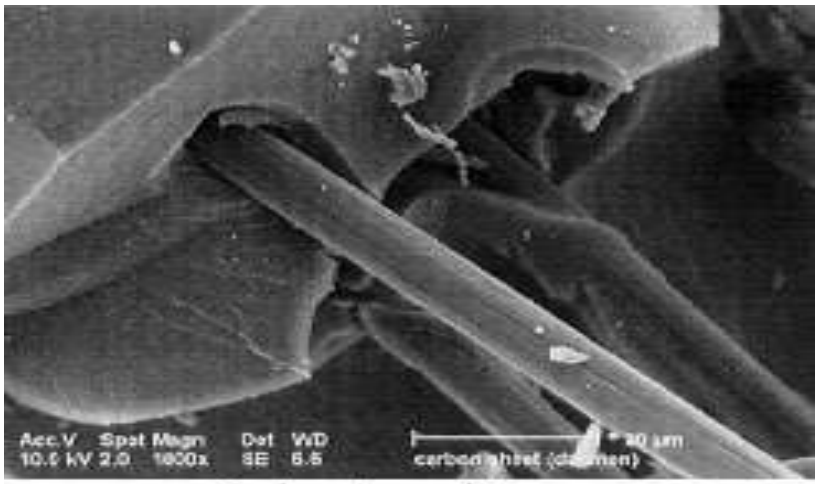

Figure IV-13. SEM image of CA taken at 1000x magnification.

The results of the BET analysis of CA sample #1 are shown in figures IV-5 to IV-7. Figure IV-5 shows data over the entire range of relative pressures, Figure IV-6 shows data only at low relative pressures, and Figure IV-7 shows the adsorption and desorption results. Data presented in these figures are at STP conditions and a conversion factor (0.0015468 (cm^3/g)/(cm^3/g-STP)) was used to arrive at the reported values of micropore volumes. Micropore volume was calculated by plotting a tangent at the lowest slope of BET curve and obtaining an y-intercept value. This value was multiplied with the conversion factor to arrive at the micropore pore volume. These results indicate that the material had a micropore volume between 0.1 - 0.14 cm^3/g. Measuring the micropore volume was difficult because it took a very long time to equilibrate at low nitrogen relative pressure (i.e. about 0.0001). BET surface area was found using linearized form of BET adsorption isotherm equation and finding the intercept and slope that provided the values for volume of monolayer coverage and the C

parameter. The total surface area of coverage was calculated using the known size of a nitrogen molecule and the volume of nitrogen absorbed to form a monolayer. The results of the BET analysis of CA sample #2 are shown in figures IV-8 and IV-9. The BET surface area was found to be about 400 m^2/g for CA sample #1 and sample #2, but this number is really meaningless because C parameter (a constant related to adsorption enthalpy) was quite negative (-100). There were some larger mesopores based on the jump in volume adsorbed at $p/p_o > 0.8$ suggesting that mesopore volume was on the order of 0.3-0.4 cm^3/g. There was very little increase in the volume adsorbed between 0.1-0.4 p/p_o. This low-slope region in the middle of the isotherm is where the first few multilayers of nitrogen adsorb onto the surface of meso and macropores before the onset of capillary condensation.

BET analysis of sample #1 and sample #2 of CA verified the information provided by the supplier that the surface areas of these samples were about 400 m^2/g. Both samples were similar in all aspects except for thickness. Once the reliability of the data provided by the supplier was established, no further BET tests were conducted on the other samples of CA. Sample #1 was from type 1 (thickness of 7 mil and density of 0.8 g/cm^3) and sample #2 from type 2 (thickness of 14 mil and density of 0.8 g/cm^3) of CA. They were used in CDI units #1 and #2, respectively as shown in Table III-1. Type 3 (thickness of 7 mil and density of 0.4-0.5g/cm^3) and Type 4 (thickness of 14 mil and density of 0.4-0.5g/cm^3) CA had surface areas of 600 m^2/g, as provided by the supplier.

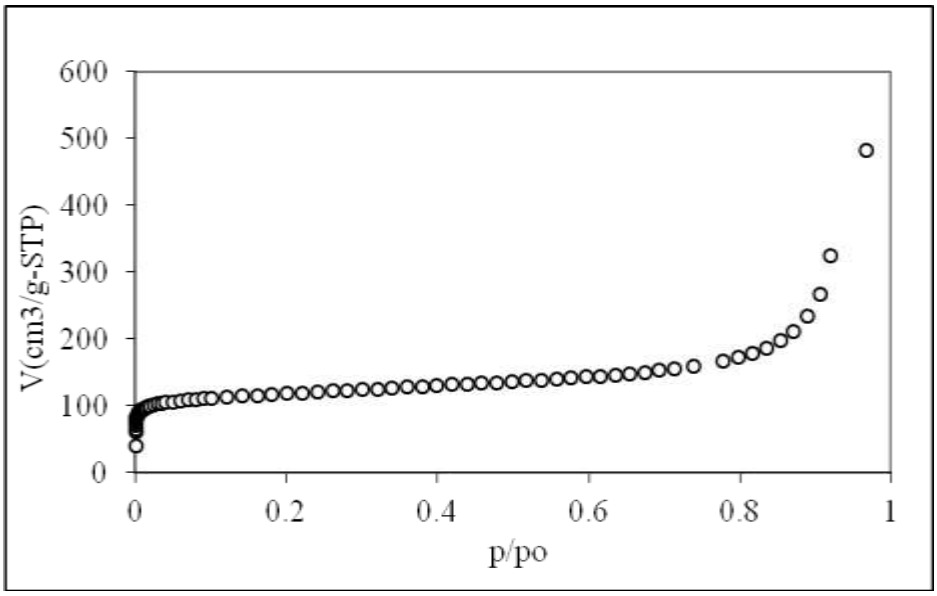

Figure IV-14. BET Adsorption plot, CA sample #1.

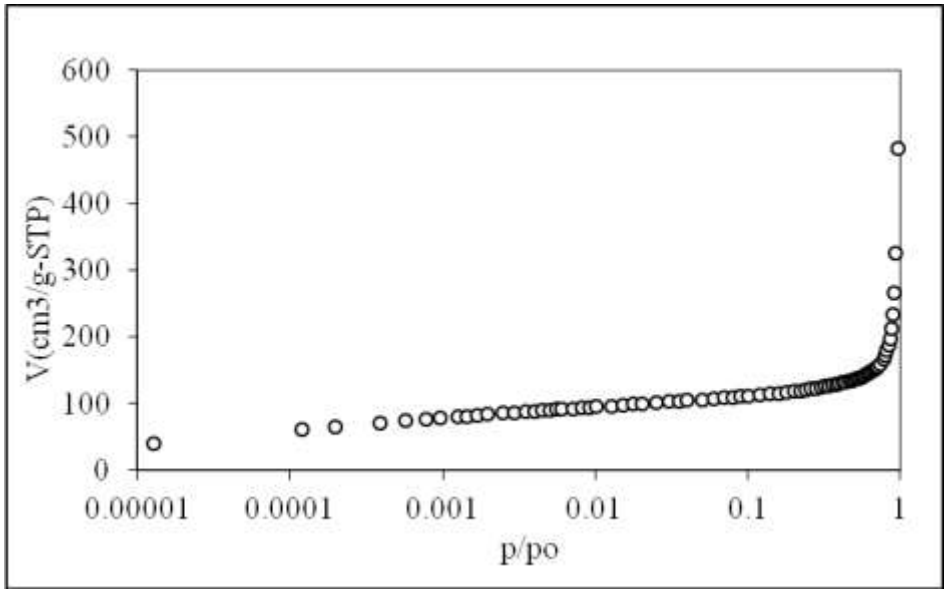

Figure IV-15. BET Adsorption plot, CA sample #1.

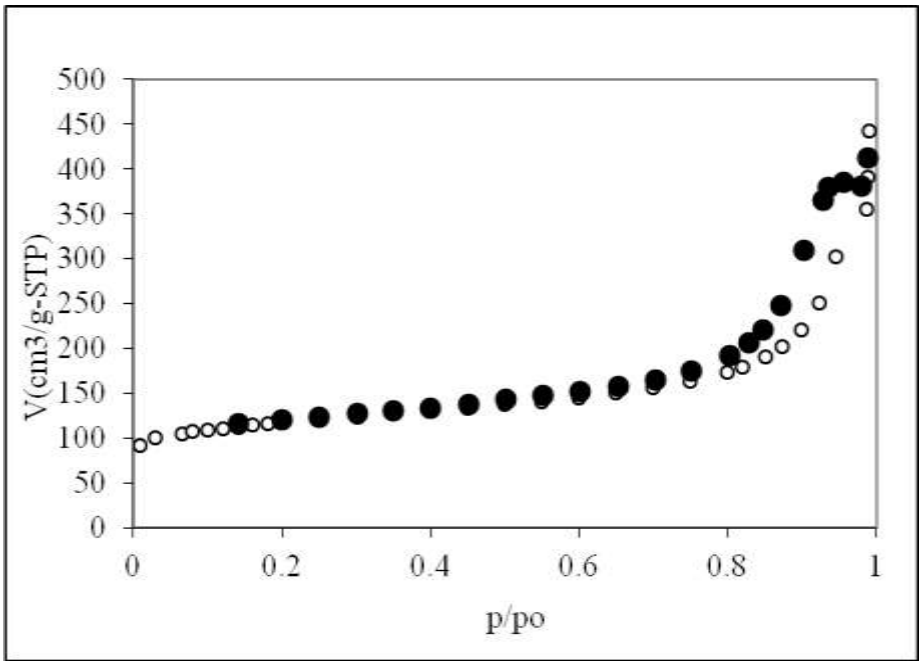

Figure IV-16. BET isotherm full plot, CA sample #1.

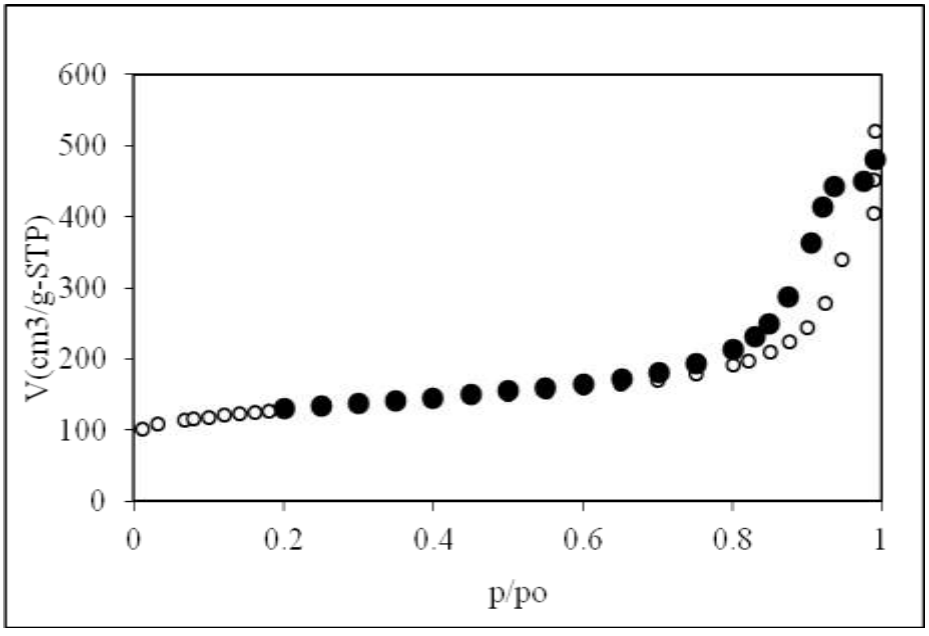

Figure IV-17. BET isotherm full plot, CA sample # 2.

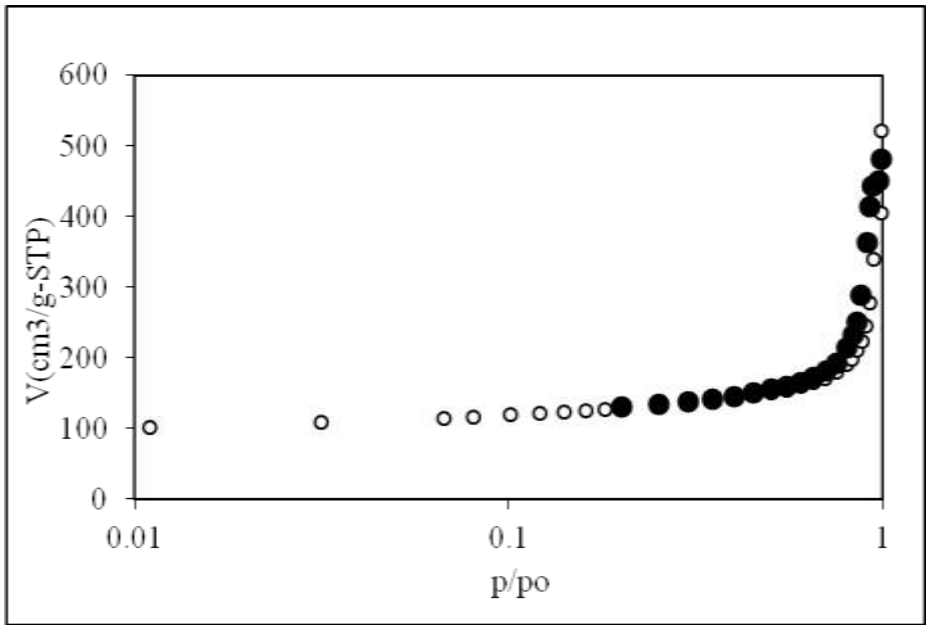

Figure IV-18. BET isotherm full plot, CA sample # 2.

4.2 Effect of Potential Applied to CA Electrodes on Regeneration

One of the focuses of the phase 1 experiments was to study the effect of application of potential across CA electrodes on their regeneration. These experiments were to address objective 1 that was stated in Chapter I. The conditions were used in these experiments: no potential, no potential along with shorting, and reverse potential. No potentials were applied across CA electrodes in experiment 1, 4 (4-a and 4-b) and 7 (7-I and 7-II). However, there was some residual charge on both electrodes, because they did receive a potential during the adsorption phase of the experiment. This residual charge could hold some ions on the surface of CA electrodes. Electrodes were shorted externally allowing discharge of residual charge in experiment 2, 5 (5-a and 5-b) and 8 (8-I and 8-II) and this resulted in release of ions that resulted in higher degrees of

regeneration. A reverse potential was applied across the CA electrodes during regeneration for first few minutes of the regeneration period in experiment series 3 (3-1, 3-2, 3-5, 3-14 and 3-32), 6 (6-1-a, 6-5-a, 6-1-b and 6-5-b) and 9 (9-1-I, 9-1-II, 9-5-I and 9-5-II).

The results of experiments on the effects of different ways of treating the electrodes on CA regeneration are presented in two sub-sections that follow. One compares the extent of CA regeneration when no potential was applied (no potential applied and no shorting; no potential applied with shorting) and when the electrodes were shorted. The other sub-section presents results of experiments when reverse potential was applied and includes experiments conducted where the time of application was varied.

4.2.1 Effect of No Shorting versus Shorting of Electrodes on Regeneration of CA

Results from experiments $1^{\dagger}$ and 2^{*}; 4-a^{*} and 5-a^{Δ}; 4-b^{Δ} and 5-b^{Δ}; 7-I^{Δ} and 8-I^{Δ}; and 7-II^{Δ} and 8-II^{Δ} are shown in Figure IV-10 through IV-14. These experiments compare the effect on regeneration on shorting or not shorting the CA electrodes after they had been exhausted in capacitive deionization. Superscripts †, * and Δ denote that experiments repeated 5, 4 and 3 times respectively. Statistical analysis was conducted to calculate 95% confidence intervals and results are shown in Table IV-1. Once CA electrodes were exhausted/saturated with adsorbed ions, mass balance calculations were conducted to quantify the amount of ions adsorbed on CA electrodes and the amount released during regeneration. The amount adsorbed was calculated as the difference

between the initial amount in solution (VC_0) and the amount remaining at the end of the adsorption phase of the experiment (VC_{final}). The amount desorbed was calculated as the amount in solution at the end of the regeneration phase, because the amount of ions in the solution at the start of a regeneration phase was zero. The percent regeneration was calculated as the amount of ions desorbed during the regeneration phase divided by the amount of ions adsorbed during the adsorption phase.

Table IV-6. Percent regeneration of CA and 95% confidence interval calculations.

	No Short.	Short.	No Short.	Short.	No Short.	Short.	No Short.	Short.	No Short.	Short.
Exp #	1	2	4-a	5-a	4-b	5-b	7-I	8-I	7-II	8-II
1st run	23.30	30.81	43.66	52.77	57.29	73.7	22.21	34.37	39.31	54.91
2nd run	17.30	22.15	52.95	59.1	57.54	67.66	24.19	34.48	40.12	52.14
3rd run	17.14	31.04	49.56	58.93	53.42	66.81	23.98	35.16	41.89	55.33
4th run	20.51	21.45	34.27	-	-	-	-	-	-	-
5th run	20.20	-	-	-	-	-	-	-	-	-
Mean	19.69	26.36	45.11	56.93	56.08	69.39	23.46	34.67	40.44	54.13
SD	2.56	5.28	8.18	3.61	2.31	3.76	1.09	0.43	1.32	1.73
α/2	0.025	0.025	0.025	0.025	0.025	0.025	0.025	0.025	0.025	0.025
n	5.00	4.00	4.00	3.00	3.00	3.00	3.00	3.00	3.00	3.00
df	4.00	3.00	3.00	2.00	2.00	2.00	2.00	2.00	2.00	2.00
t*	2.132	2.353	2.353	2.92	2.92	2.92	2.92	2.92	2.92	2.92
$SD/(n)^{\wedge 0.5}$	1.14	2.64	4.09	2.08	1.33	2.17	0.63	0.25	0.76	1.00
LCL	17.25	20.15	35.48	50.85	52.19	63.06	21.63	33.95	38.22	51.20
UCL	22.13	32.57	54.74	63.01	59.98	75.72	25.29	35.39	42.66	57.05

There was an increase in percent regeneration when electrodes were shorted as shown in Figure IV-10. This increase was probably due to the loss of residual charge when the CA electrodes were shorted. After residual charge was discharged more ions

were freed resulting in higher regeneration. The same effect was noticed in results of experiment 4-a (no shorting) and 5-a (shorting) that were conducted at 30°C (Figure IV-11) and in results of experiment 4-b (no shorting) and 5-b (shorting) that were conducted at 39°C (Figure IV-12). Similar behavior was noticed in results from experiment 7-I (no shorting) and 8-I (shorting) that were conducted at a flow speed of about 10 cm/min (Figure IV-13) and results from experiment 7-II (no shorting) and 8-II (shorting) at a flow speed of about 32 cm/min (Figure IV-14).

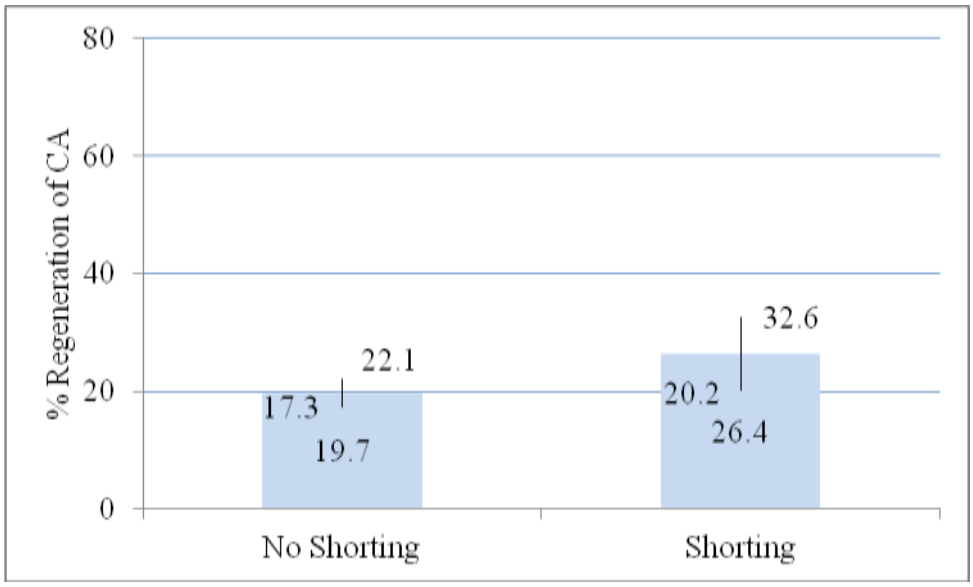

Figure IV-19. Effect of shorting electrodes with no applied potential on regeneration of CA at 20°C with a flow speedof 18.5 cm/min. Error bars are 95% confidence intervals. Data for no shorting are from experiment 1. Data for shorting are from experiment 2.

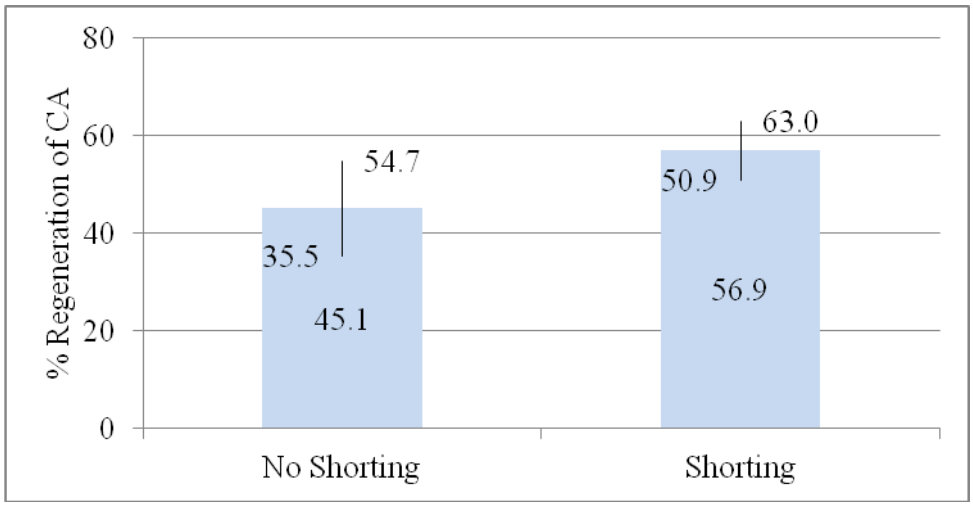

Figure IV-20. Effect of shorting electrodes with no applied potential on regeneration of CA at 30°C with a flow speed of 18.5 cm/min. Error bars are 95% confidence intervals. Data for no shorting are from experiment 4-a. Data for shorting are from experiment 5-a.

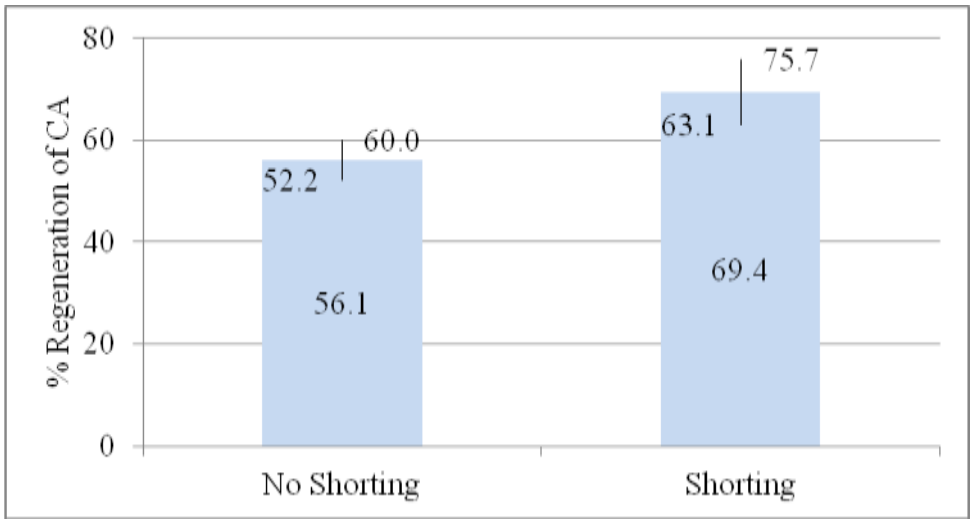

Figure IV-21. Effect of shorting electrodes with no applied potential on regeneration of CA at 39°C with a flow speed of 18.5 cm/min. Error bars are 95% confidence intervals. Data for no shorting are from experiment 4-b. Data for shorting are from experiment 5-b.

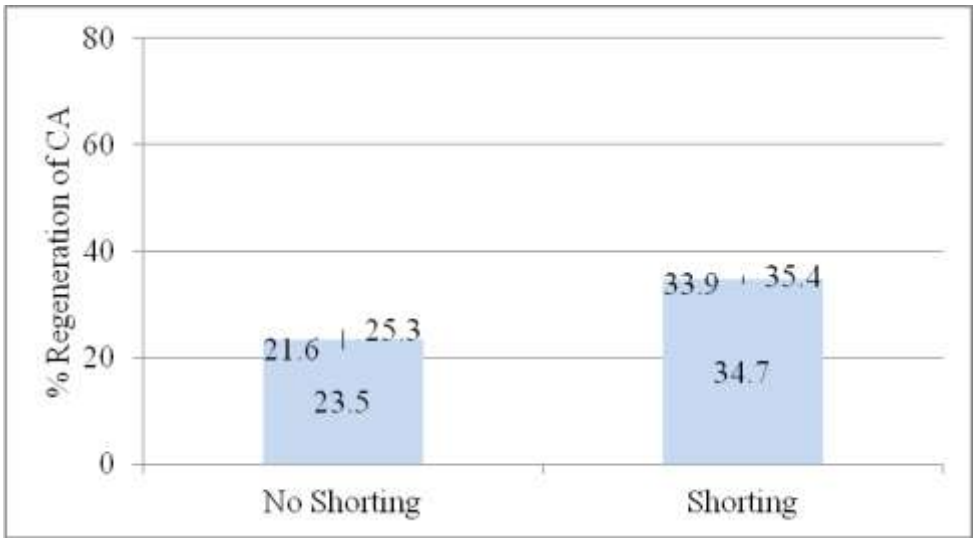

Figure IV-22. Effect of shorting with no potential applied on regeneration of CA at 20°C with a flow speed 10.9 cm/min. Error bars are 95% confidence intervals. Data for no shorting are from experiment 7-I. Data for shorting are from experiment 8-I.

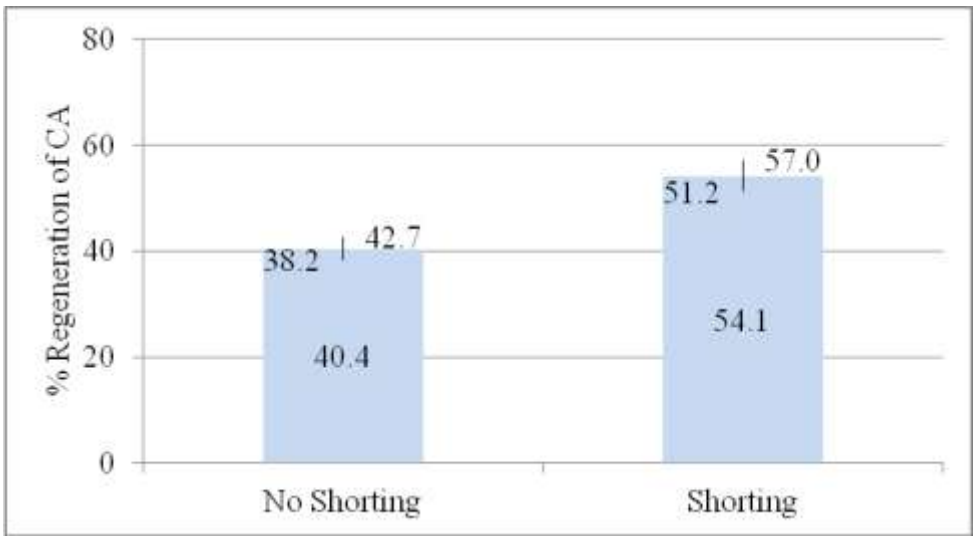

Figure IV-23. Effect of shorting electrodes with no applied potential on regeneration of CA at 20°C with a flow speed 32.2 cm/min. Error bars are 95% confidence intervals. Data for no shorting are from experiment 7-II. Data for shorting are from experiment 8-II.

4.2.2 Effect of Time of Application of Reverse Potential on Regeneration of CA

A series of regeneration experiments were conducted using a reverse potential of 1.2 V that was applied for variable time (phase 1, experiment series 3 in Table III-2). A reverse potential was applied for 1, 2, 5, 14 or 32 minutes during regeneration and then the electrodes were shorted for the remainder of the experiment (12 hr) to eliminate any residual charge. Each experiment was repeated 4 times.

Statistical analysis was conducted to calculate 95% confidence intervals and results are shown in Table IV-2. The mean percent regeneration of CA and the 95% confidence intervals are shown for various times that reverse potential was applied are presented in a condensed manner in Table IV-3. Mean percent regeneration values from Table IV-2 were plotted against time of application of reverse potential in Figure IV-15. Maximum regeneration achieved for these experimental conditions was 96.79%. There was a sharp increase in percent regeneration between 1 and 2 minutes of applying reverse potential and a sharp drop between 2 and 5 minutes. There was a gradual drop in percent regeneration for the remaining time of application of reverse potential (5 to 32 minutes). The initial increase in percent regeneration is believed due to the increased release of ions to the solution as the result of imposing the reverse potential. The later decrease in percent regeneration is believed due to the re-adsorption of ions onto the other electrode. Anions that had adsorbed to the electrode that was the anode would be released by the reverse potential, but then could adsorb on the electrode that was originally the cathode, but became an anode when reverse potential was applied. This process is not instantaneous because ions that were adsorbed on surfaces of inner pores

would need to diffuse through the pores to reach the solution. The time of application of reverse potential for maximum regeneration should be different for different CDI configurations. For example, the separation distance between electrode and different types of CA could affect the optimal time of application. Also, experimental conditions such as flow rate, temperature and magnitude of applied reverse potential could affect how extent of regeneration changes with time of application.

How conductivity changed over time during regeneration is shown in Figure IV-16. This data was collected during experiments that were conducted as part of experiment series 3. Reverse potential that was applied for 2 minutes gave fastest and greatest extent of regeneration during the first 200 minutes. Regeneration happened at a more rapid rate during the first 15-20 minutes of all five experiments. However, between 20 and 200 minutes the experiment with a 2-minute reversal time gave the fastest regeneration rate and the highest extent of regeneration. The rate of regeneration of CA was slowest when the reverse potential was applied for 32 minutes.

Table IV-7. Time of application of reverse potential and corresponding percent regeneration of CA and 95% confidence interval calculations.

Percent regeneration of CA electrodes at different times of application of reverse potential					
	1 min	2 min	5 min	14 min	32 min
1st run	84.25	97.98	73.97	71.00	64.92
2nd run	83.16	97.22	75.82	70.96	62.33
3rd run	83.94	96.97	74.79	70.71	63.88
4th run	82.96	94.97	75.48	71.82	64.01
Mean	83.58	96.79	75.02	71.12	63.79
SD (Std. Deviation)	0.62	1.28	0.82	0.48	1.07
alpha/2	0.025	0.025	0.025	0.025	0.025
n (no of sample)	4.00	4.00	4.00	4.00	4.00
df (degree of freedom)	3.00	3.00	3.00	3.00	3.00
t* critical value	2.353	2.353	2.353	2.353	2.353
SD/(n)^0.5	0.31	0.64	0.41	0.24	0.54

Table IV-8. Mean percent regeneration and 95% confidence intervals.

Time of application of reverse potential (min)	Mean % Regeneration (with 95% confidence)
1	83.58 (82.85, 84.30)
2	96.79 (95.27, 98.30)
5	75.02 (74.05, 75.98)
14	71.12 (70.55, 71.69)
32	63.79 (62.52, 65.05)

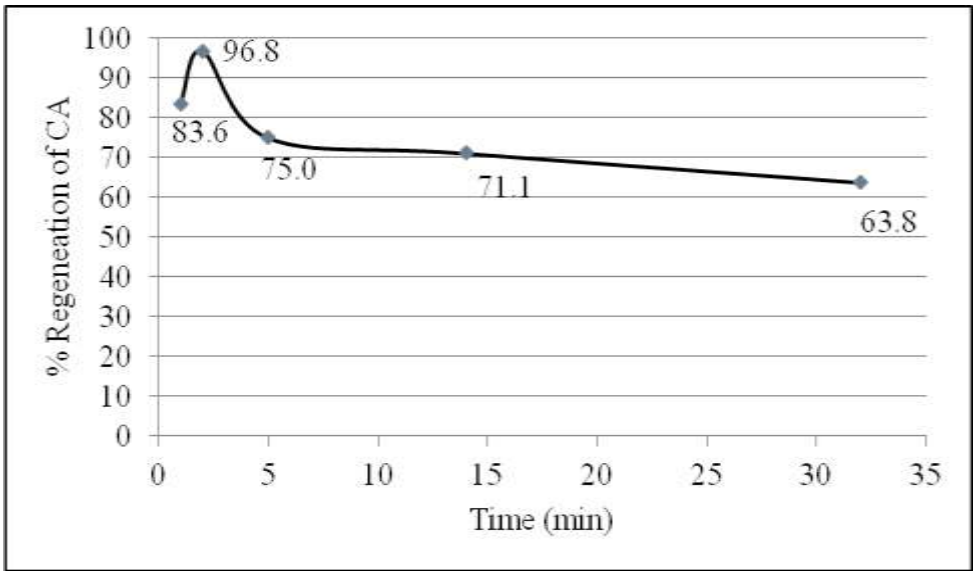

Figure IV-24. Effect of time of application of reverse potential on percent regeneration. Data are from experimental series 3.

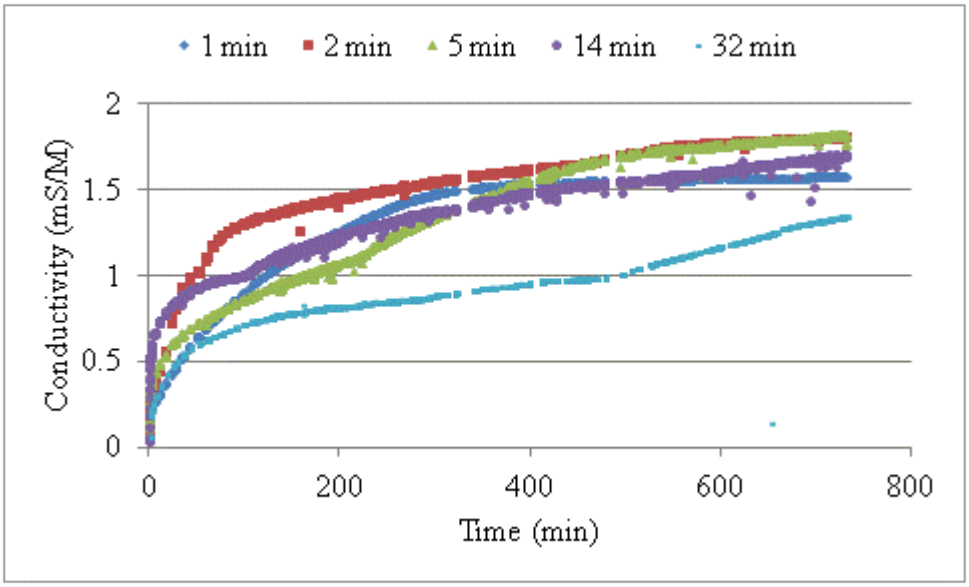

Figure IV-25. Effect of time on conductivity during regeneration after various times of application of reverse potential. Data are from experiment series 3.

4.3 Adsorption Isotherm and Effect of Temperature on Regeneration of CA

Regeneration was studied under three different temperatures (20°C, 30°C and 39°C). The range of temperature was kept in this range to simulate average weather conditions and also because of the limitations of the instruments used in the study. Various experiments at three different temperatures under different applied conditions were conducted. Data was collected to plot isotherms and to study how regeneration was affected by temperature.

4.3.1 Adsorption Isotherm

A series of equilibrium experiments (experiment 11) were conducted at 20°C and the data was used to plot linearized form of the Langmuir isotherm as shown in Figure IV-17. Gabelich et al had found that the Langmuir isotherm fit data on adsorption in a similar system. Additional adsorption and desorption experiments were conducted to see if there was a hysteresis effect, i.e. if the desorption isotherm differed from the adsorption isotherm. Figure IV-18 shows results of these experiments and indicates that hysteresis did occur.

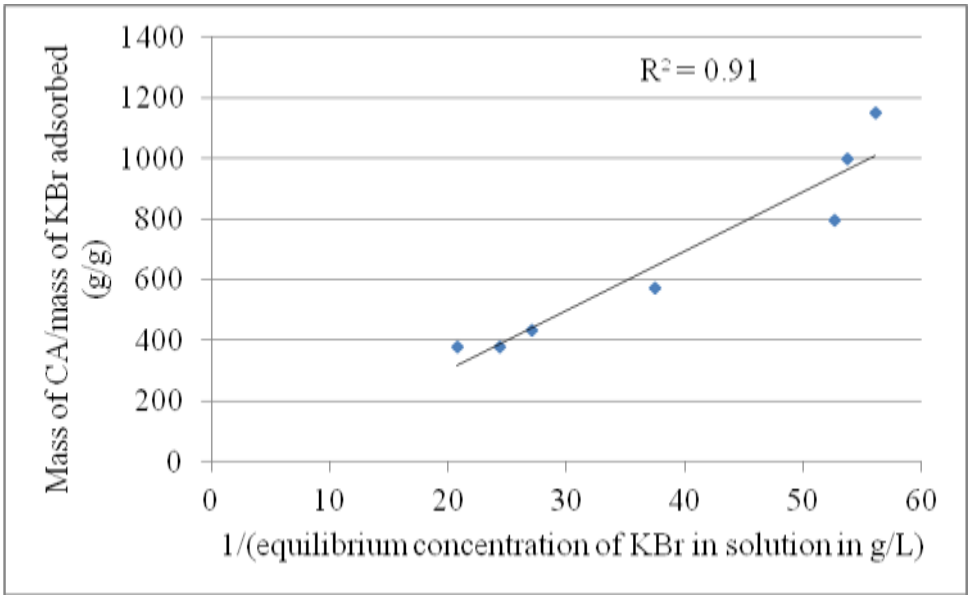

Figure IV-26. Langmuir Adsorption Isotherm for KBr sorption on CA. Data are from experiment 11.

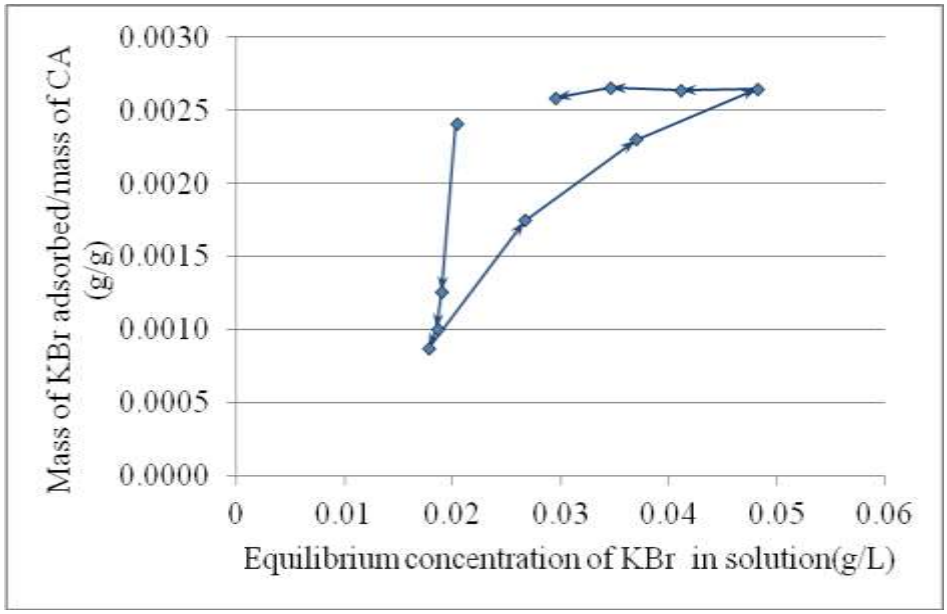

Figure IV-27. Hysteresis effect of KBr sorption on CA electrodes. Data are from experiment 11.

4.3.2 Effect of Temperature on CA Regeneration

Desorption experiments with and without shorting and with no applied potential were conducted at 20°C, 30°C and 39°C (experiment 1, 4-a and 4-b without shorting and experiment 2, 5-a and 5-b with shorting of electrodes). In addition, desorption experiments were conducted at the three temperatures with reverse potential of 1.2 V applied for 1 minute (experiment 3-1, 6-1-a and 6-1-b) and 5 minute (experiment 3-5, 6-5-a and 6-5-b). Percent regeneration with no potential applied and no shorting of electrodes are plotted in Figure IV-19 and Figure IV-20. It can be seen from Figure IV-19 that temperature definitely plays an important role in extent of regeneration of CA when no potential is applied and electrodes are not shorted, because higher percent regeneration was achieved at higher temperatures. Regeneration is direct result of desorption of adsorbed ions from the CA electrode surface. Most of the ions are adsorbed to surfaces of pores in the interior of CA. When the applied potential is removed at the start of a regeneration cycle, these ions desorb and need to diffuse along the pores to reach the exterior of the electrode. Because diffusion is temperature dependent, higher temperature results in faster diffusion and higher percent regeneration of CA measured at a specified time of regeneration.

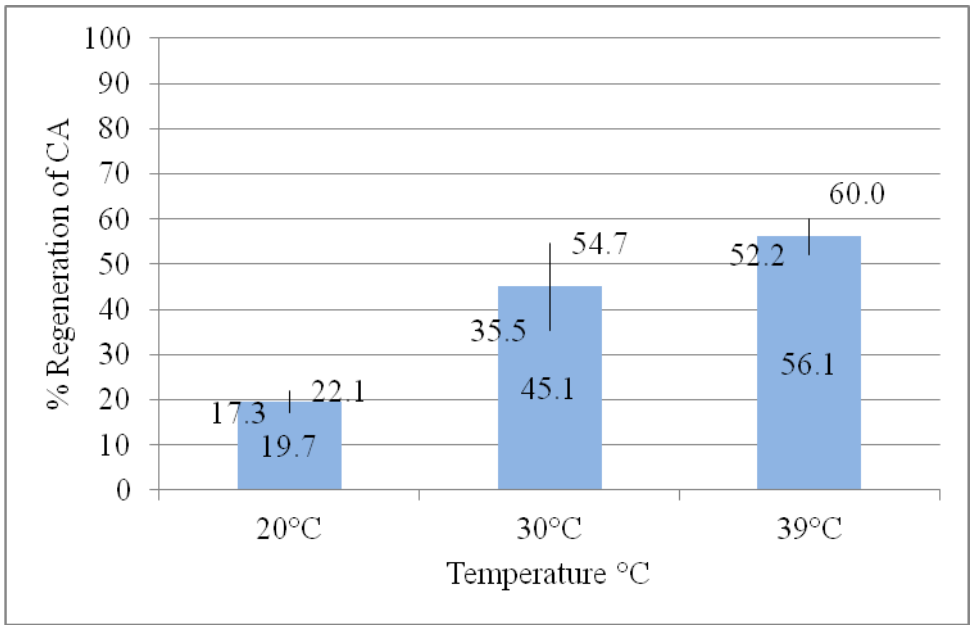

Figure IV-28. Effect of temperature on regeneration of CA with no applied potential and no shorting of electrodes. Error bars are 95% confidence limits. Data at 20°C are from experiment 1 and data at 30°C and 39°C are from experiment 4-a and 4-b respectively.

Conductivity measurements from experiments 1, 4-a and 4-b are plotted with respect to time in Figure IV-20 up to 12 hr. There is very little, if any, increase in conductivity with time after 12 hours in systems at 20°C and 30°C, but conductivity is still increasing with time even after 12 hours at 39°C. Also, there is a rapid increase in conductivity in the first few minutes at all temperatures, which is a result of flushing with DI water. It shows that when no potential is applied and the electrodes are not shorted most of the regeneration takes place during first few minutes. However at higher temperature, such as 39°C, the percent regeneration continues to increase with time and the extent of regeneration is higher than at 20°C and 30°C.

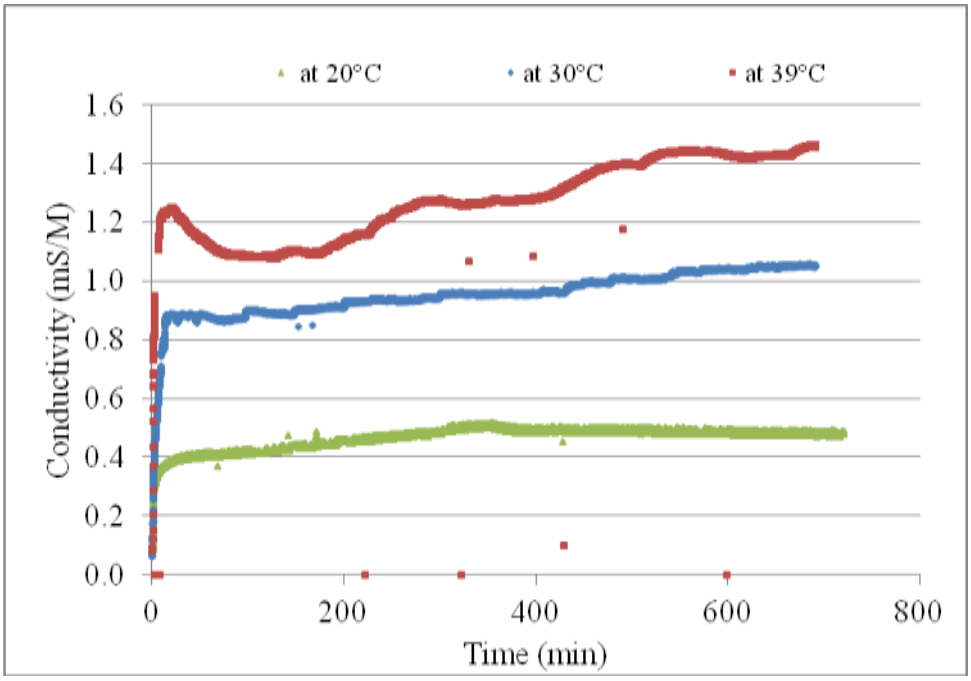

Figure IV-29. Effect of time on conductivity during regeneration at various temperature without shorting of electrodes. Data at 20°C are from experiment 1 and data at 30°C and 39°C are from experiment 4-a and 4-b respectively.

Results from experiments 2, 5-a and 5-b were plotted as shown in figures IV-21 and IV-22. Percent regeneration of CA increased with an increase in temperature. Figure IV-22 shows that there is very little increase in conductivity during regeneration after the first few minutes at 20°C and 30°C, but at 39°C conductivity kept increasing after the first few minutes until around 100 minutes. The initial increase in conductivity is greater at 39°C than at 20°C or 30°C. These results are the same as was seen in experiments that were conducted without shorting. One possible explanation may be that near 39°C, the conditions in CA pores are more conducive to diffusion, so ions diffuse down pores more effectively, resulting in the gradual increase in conductivity and higher extents of regeneration.

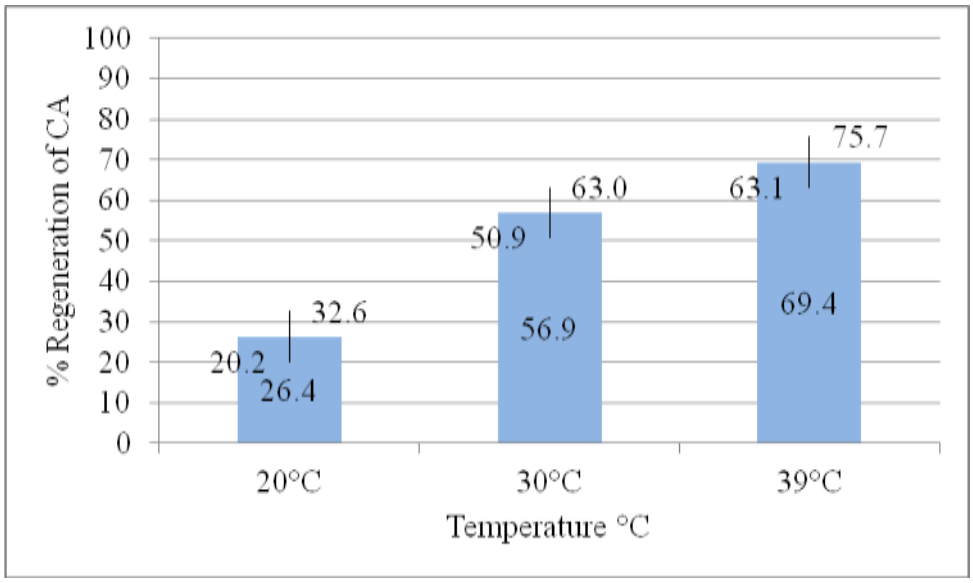

Figure IV-30. Effect of temperature on regeneration of CA with shorting of electrodes. Error bars are 95% confidence intervals. Data at 20°C are from experiment 2 and data at 30°C and 39°C are from experiment 5-a and 5-b respectively.

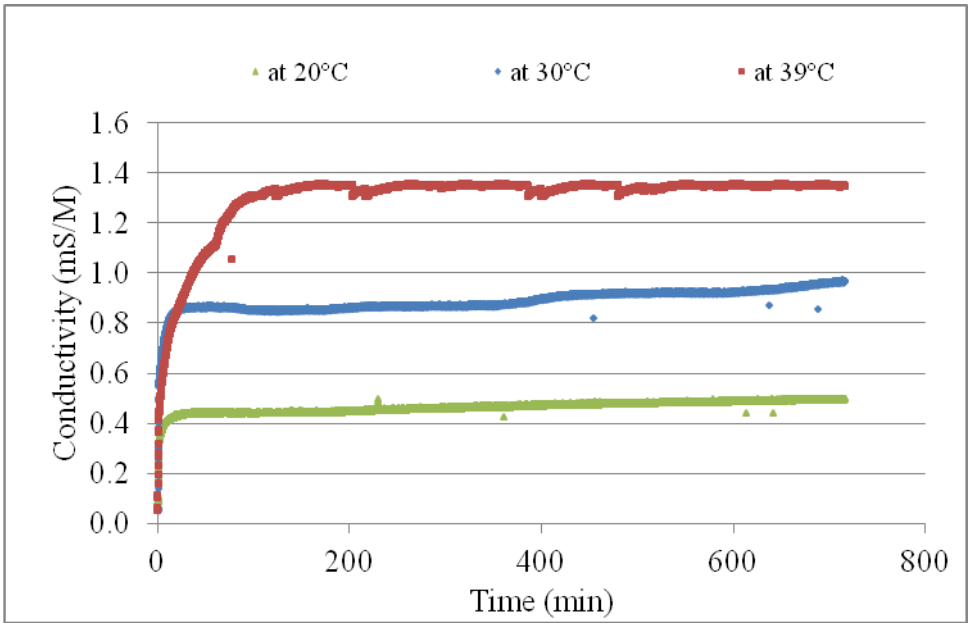

Figure IV-31. Effect of time on conductivity during regeneration at different temperature when electrodes are shorted. Data at 20°C are from experiment 2 and data at 30°C and 39°C are from experiment 5-a and 5-b respectively.

Same desorption experiments were conducted at the three temperatures but with a reverse potential applied for the first 1 minute (experiments 3-1, 6-1-a and 6-1-b) and 5 minutes (experiments 3-5, 6-5-a and 6-5-b) of the total regeneration period of 12 hours. Results are plotted in figures IV-23 through IV-26. Figure IV-23 shows that during the first 100 minutes after application of reverse potential for 1 minute, higher temperature resulted in higher extents of regeneration as indicated by higher solution conductivity. However, beyond 100 minutes there was no clear pattern. Figure IV-24 shows percent regeneration of the CA electrodes at the end of 12 hour desorption period. Figure IV-24 shows that the percent regeneration decreases with increasing temperature. The same kind of regeneration behavior was observed when desorption experiments were conducted with reverse potential applied for the first 5 minutes of desorption period, both in terms of regeneration kinetics and ultimate extent of regeneration (Figure IV-25 and Figure IV-26 respectively). Both measures of regeneration dropped with an increase in temperature from 20°C. However both measures increased a little as temperature increased from 30°C to 39°C.

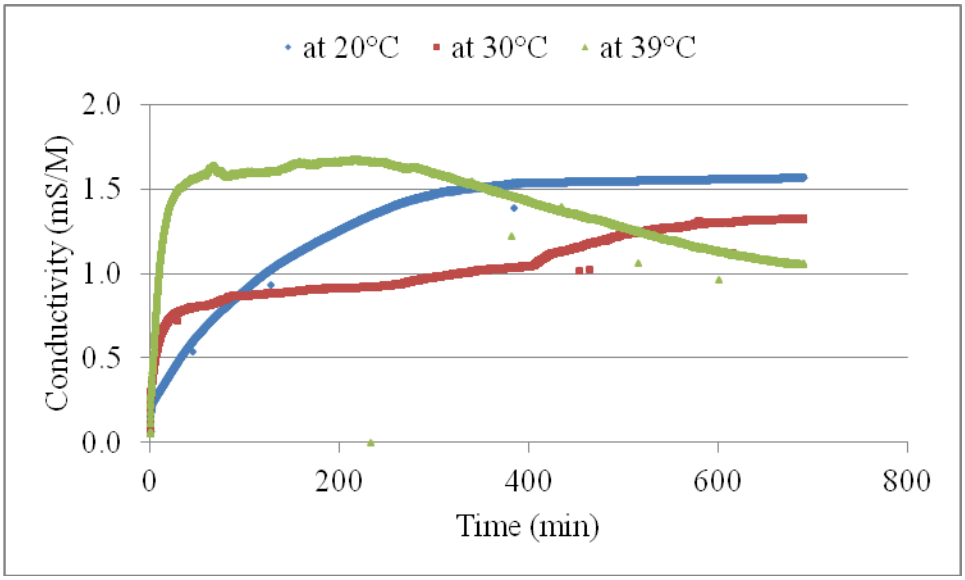

Figure IV-32. Effect of time on conductivity during regeneration at different temperature when reverse potential was applied for 1 minute. Data at 20°C are from experiment 3-1 and data at 30°C and 39°C are from experiment 6-1-a and 6-1-b respectively.

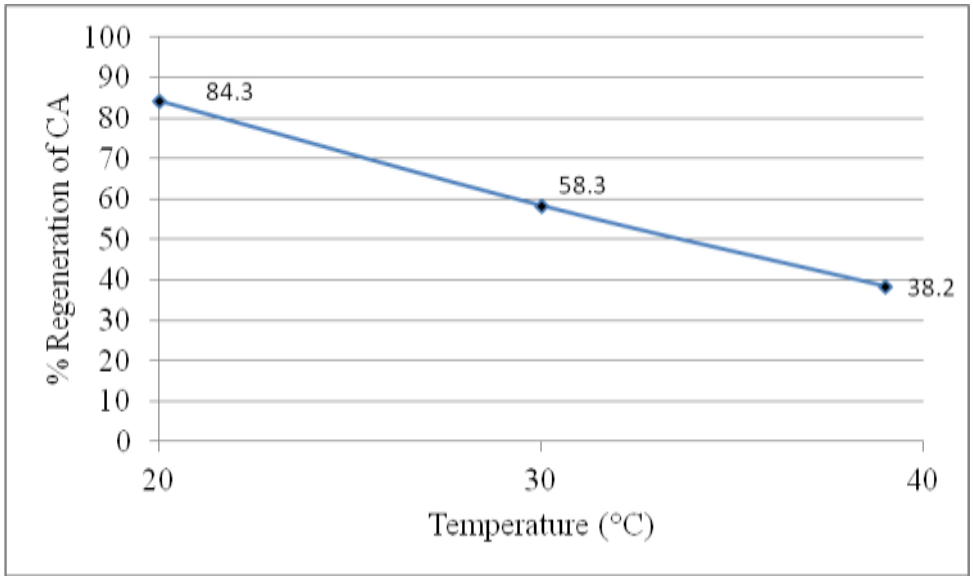

Figure IV-33. Effect of temperature on percent regeneration of CA when reverse potential was applied for 1 minute. Data at 20°C are from experiment 3-1 and data at 30°C and 39°C are from experiment 6-1-a and 6-1-b respectively.

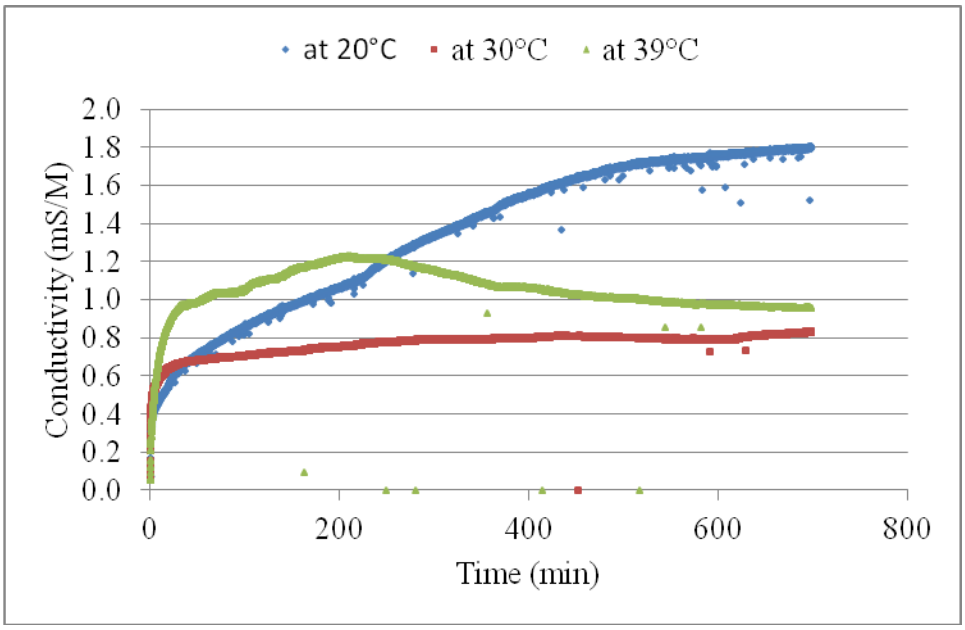

Figure IV-34. Effect of time on conductivity during regeneration of CA at different temperatures when reverse potential was applied for 5 minute. Data at 20°C are from experiment 3-5 and data at 30°C and 39°C are from experiment 6-5-a and 6-5-b respectively.

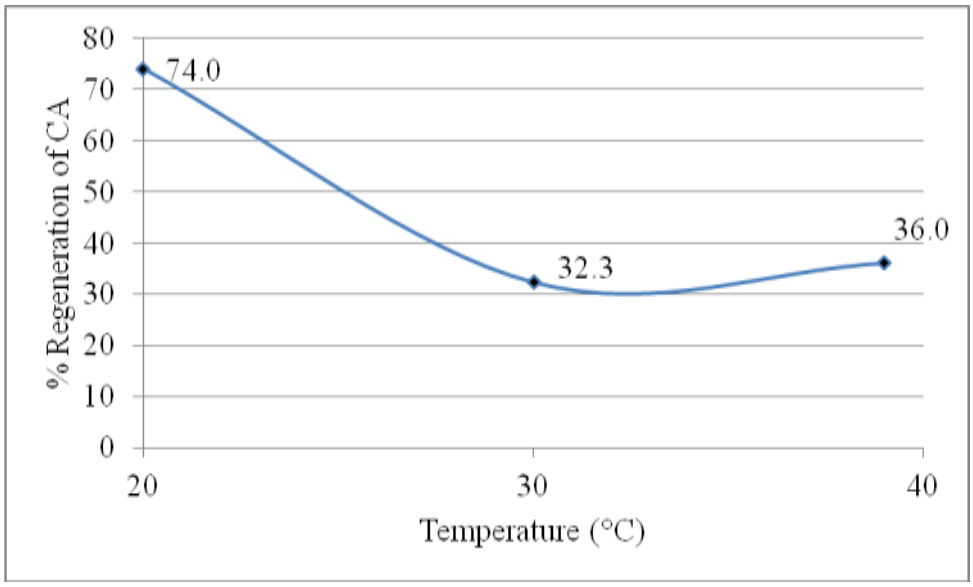

Figure IV-35. Effect of temperature on percent regeneration of CA when reverse potential was applied for 1 minute. Data at 20°C are from experiment 3-5 and data at 30°C and 39°C are from experiment 6-5-a and 6-5-b respectively.

4.4 Effect of Flow Speed on Regeneration of CA

Diffusion plays a major role in desorption and is controlled by the concentration gradient. An increase in concentration gradient increases the rate of diffusion, which in turn results in faster desorption and ultimately in higher regeneration. Higher flow rates through the cells during regeneration result in higher speeds of water flowing past the CA surface. Higher speeds will result in higher concentration gradients, because the increased water flow will remove ions that are diffusing out of pores at faster rate creating a lower concentration of ions near the CA surface as compared to concentration of ions in pores. Therefore, more extensive regeneration is expected with higher speeds. Experiments were conducted with three flow rates (59 ml/min, 100 ml/min, 174 ml/min) that resulted in three speeds (10.9 cm/min, 18.5 cm/min, 32.2 cm/min). These are the average speeds with which water will flow through the space between CA electrodes. The speeds were calculated by dividing flow rate by cross-sectional area of the open space within the CDI cell. Cross-sectional area was calculated by multiplying width of flow space (which was equal to the width of CA) with separation distance between the two electrodes.

The effect of flow speed of water across the CA surface on regeneration was studied without shorting, with shorting, and with reverse potential applied for 1 and 5 minutes. Results of these experiments are plotted in figures IV-27 through IV-34. Figures IV-27 and IV-28 show the effect of flow speed on CA regeneration when there was no shorting. The extents of regeneration were almost similar at 10.9 cm/min and 18.5 cm/min but at the higher speed of 32.2 cm/min the extent of regeneration was

significantly higher. The same experimental conditions were repeated, but with electrodes shorted, and the results are shown in figures IV-29 and IV-30. The regeneration behavior is similar in experiments with and without shorting.

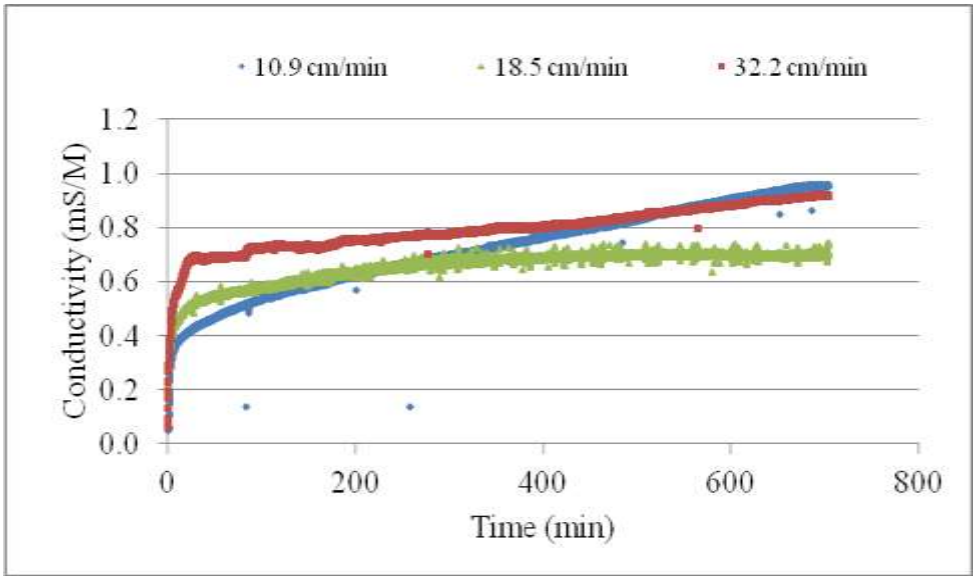

Figure IV-36. Effect of time on conductivity during regeneration with different flow speeds when electrodes were not shorted. Data at 18.5 cm/min are from experiment 1, and data at 10.9 cm/min and 32.2 cm/min are from experiment 7-I and 7-II respectively.

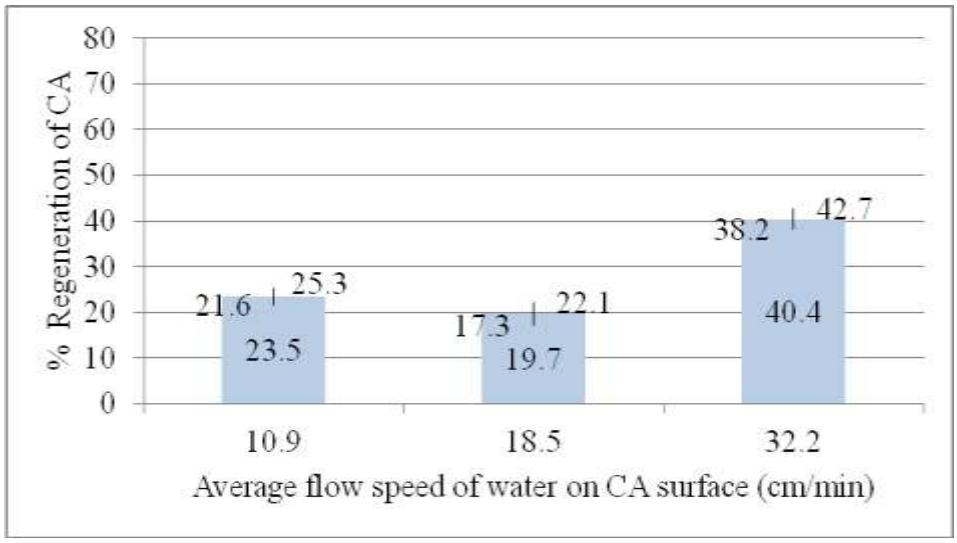

Figure IV-37. Effect of flow speed on percent regeneration when electrodes were not shorted. Data at 18.5 cm/min are from experiment 1, and data at 10.9 cm/min and 32.2 cm/min are from experiment 7-I and 7-II respectively.

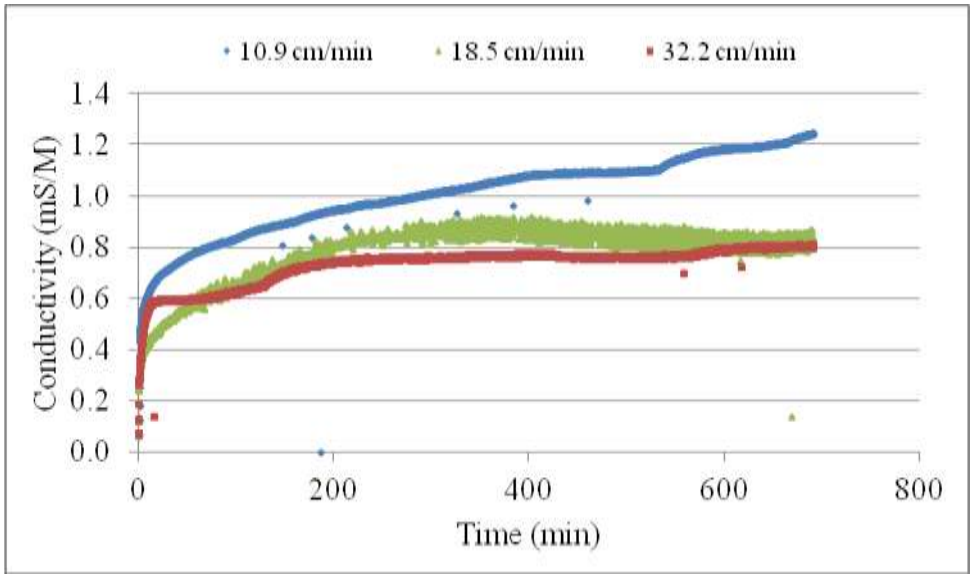

Figure IV-38. Effect of time on conductivity during regeneration at different flow speeds when electrodes are shorted. Data at 18.5 cm/min are from experiment 2, and data at 10.9 cm/min and 32.2 cm/min are from experiment 8-I and 8-II respectively.

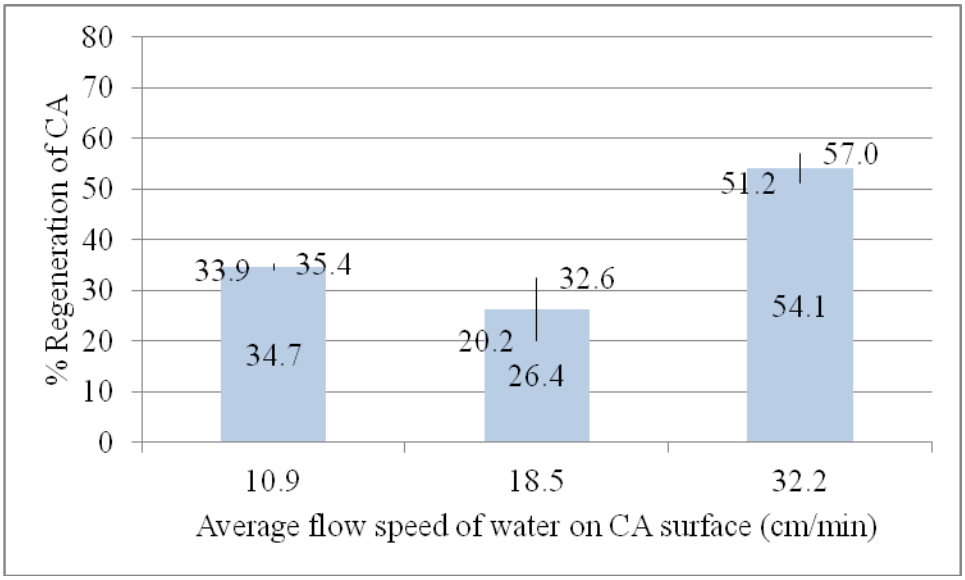

Figure IV-39. Effect of flow speed on percent regeneration when electrodes are shorted during regeneration. Data at 18.5 cm/min are from experiment 2, and data at 10.9 cm/min and 32.2 cm/min are from experiment 8-I and 8-II respectively.

The effect of flow of water was also studied in experiments where a reverse potential of 1.2 V was applied for 1 minute and the results are shown in figures IV-31 and IV-32. Figures IV-33 and IV-34 show results of experiments when the reverse potential was applied for a longer time (5 min). Again a maximum in the percent regeneration curve is observed at the middle speed. The regeneration behavior when reverse potential was applied is different from that when no potential was applied, whether shorting occurred or not. When the reverse potential was applied, a maximum in percent regeneration is observed at the middle speed (18.5 cm/min). When the reverse potential was not applied, a minimum in percent regeneration was observed at the middle speed (figures IV-25 and IV-28). It can be seen that regeneration behavior

because of water flow speed is similar in no potential/shorting applied and shorting applied across electrodes but it is different when reverse potential was applied.

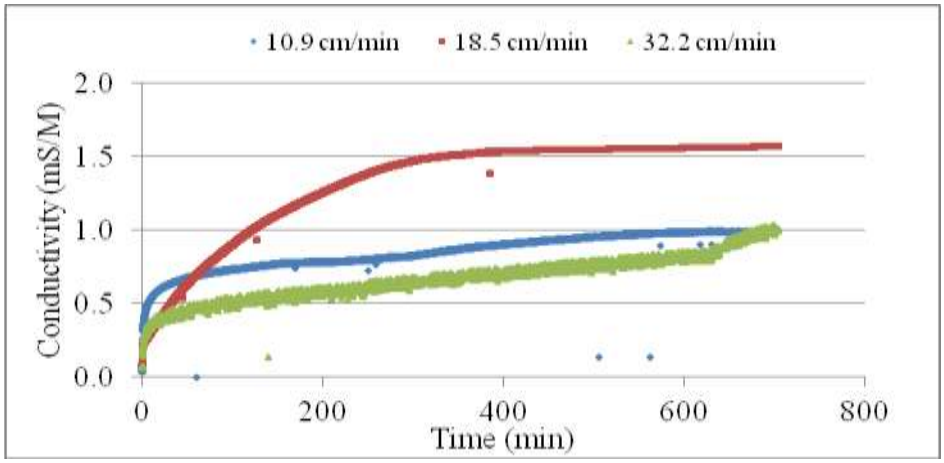

Figure IV-40. Effect of time on conductivity during regeneration with different flow speeds. A reverse potential of 1.2 volt was applied for the first 1 min during regeneration. Data at 18.5 cm/min are from experiment 3-1 and data at 10.9 cm/min and 32.2 cm/min are from experiments 9-1-I and 9-1-II respectively.

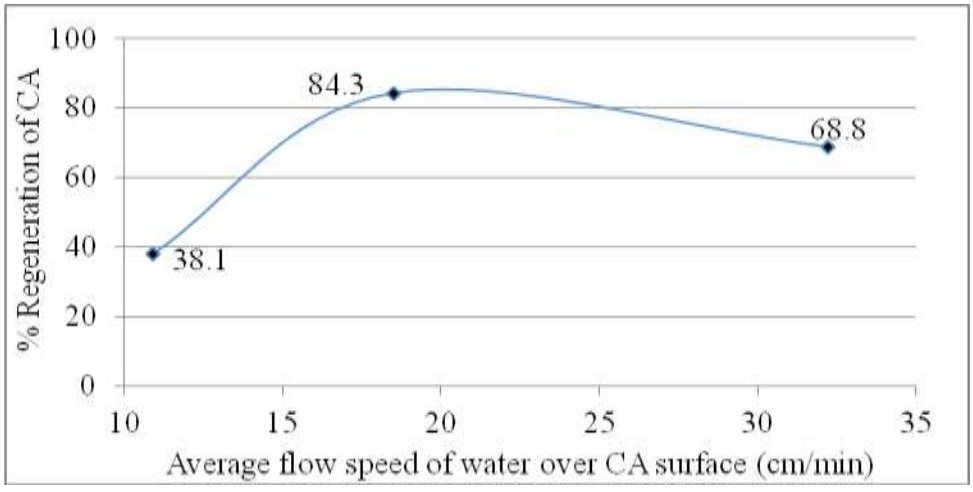

Figure IV-41. Effect of flow speed on percent regeneration when a reverse potential of 1.2 volt was applied for the first 1 min during regeneration. Data at 18.5 cm/min are from experiment 3-1 and data at 10.9 cm/min and 32.2 cm/min are from experiments 9-1-I and 9-1-II respectively.

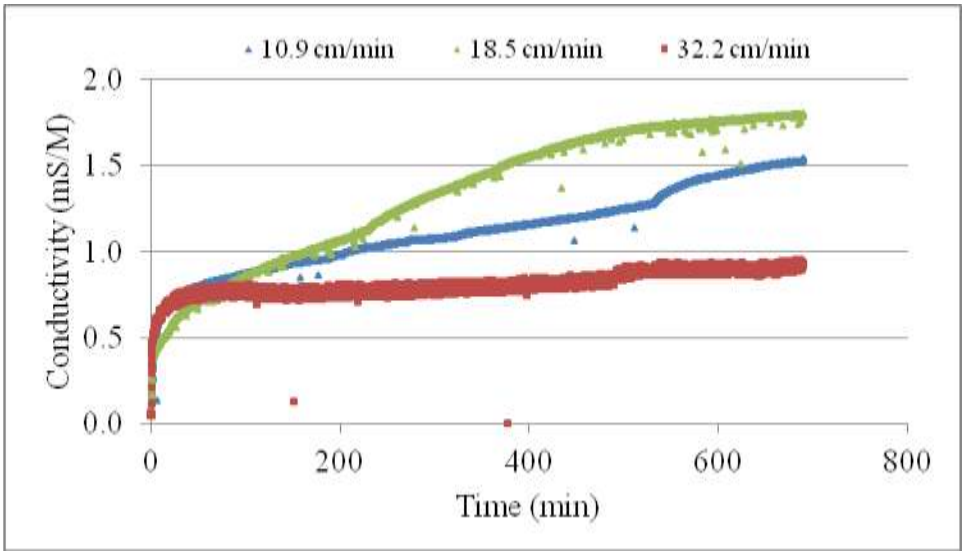

Figure IV-42. Effect of time on conductivity during regeneration with different flow speeds. A reverse potential of 1.2 volt was applied for first 5 minutes during regeneration. Data at 18.5 cm/min are from experiment 3-5 and data at 10.9 cm/min and 32.2 cm/min are from experiments 9-5-I and 9-5-II respectively.

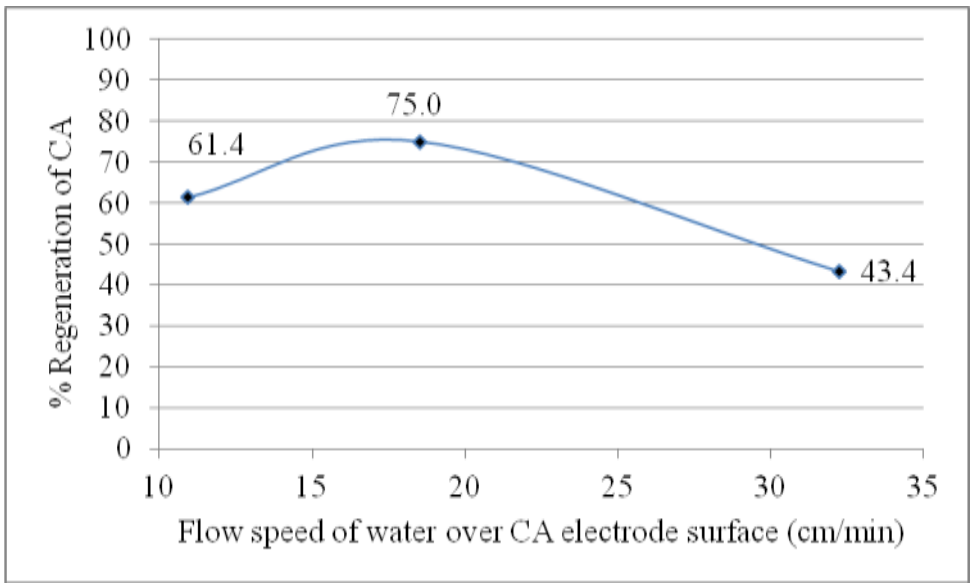

Figure IV-43. Effect of flow speed on percent regeneration when a reverse potential of 1.2 was applied for the first 5minutes during regeneration. Data at 18.5 cm/min are from experiment 3-5 and data at 10.9 cm/min and 32.2 cm/min are from experiments 9-5-I and 9-5-II respectively.

4.5 Effect of Mass and Size of Ion on CA Regeneration

4.5.1 Effect of Mass of Ion on CA Regeneration

Experiments were conducted in Phase-II to evaluate the effect of mass of ions on regeneration. Salts were chosen so that the valence charges of their ions were same and their hydrated radii were very close to being the same. Characteristics of the ions are shown in Table IV-4.

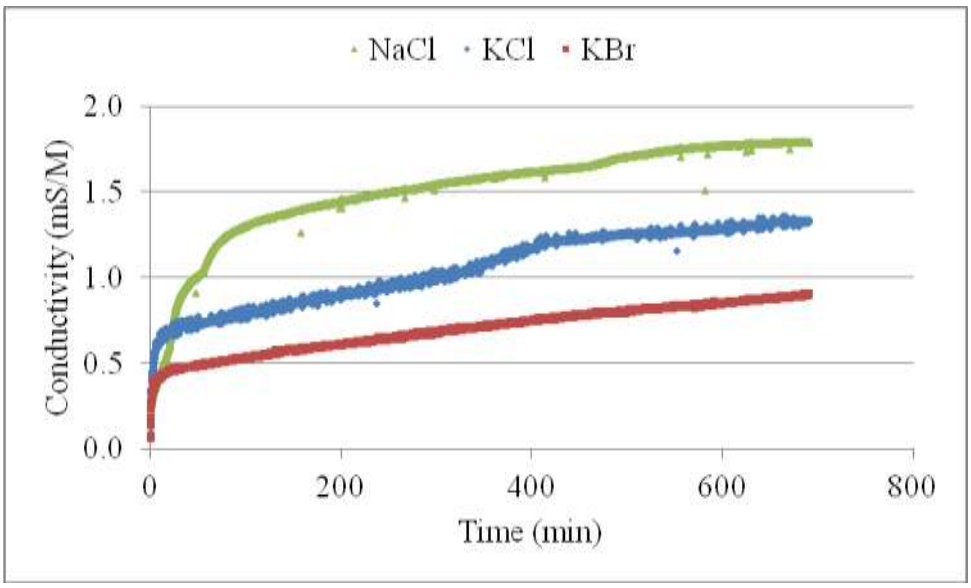

Figure IV-44. Effect of time on conductivity during regeneration of ions with different mass. Data for NaCl, KCl, and KBr are from experiments 3-2, 10 and 11 respectively.

Three salts NaCl, KCl and KBr were used in this study. Changes in conductivity with time for all three experiments are plotted in Figure IV-35. Conductivities of all three salt solutions seem to approach equilibrium slowly over 12 hours. The extents of regeneration at the end of the 12-hour regeneration period are plotted for all three salts in

Figure IV-36. Figure IV-36 shows that the percent regeneration decreases as the mass of ions increases. Gabelich et al. mentioned that the mass of ions had no observable effect on electrosorption behavior under condition used in that study. However, the same might not be true for the desorption experiments conducted in current study. Electrosorption experiments are usually conducted with some potential applied across CA electrodes throughout the adsorption period. However, in the regeneration experiments conducted in the current study a reverse potential was applied only for the first few minutes of a 12-hour regeneration period. Therefore, almost all of the regeneration occurred without any kind of potential being applied. Therefore, any behavior that was observed by Gabeich et al. may not have occurred in regeneration experiments presented here.

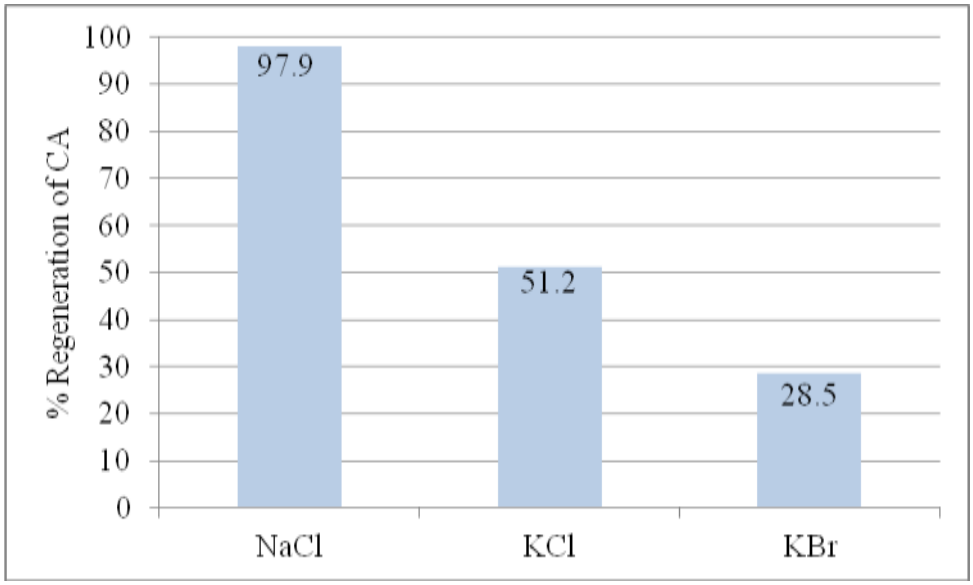

Figure IV-45. Effect of mass of ions on percent regeneration of CA. Data for NaCl, KCl, and KBr are from experiments 3-2, 10 and 11 respectively.

Table IV-9. Physical and chemical data of ions used in Phase-II

Ions	Mass (amu)	Charge	Ionic radius (x 10^{-12} M)	Hydrated radius (x 10^{-12} M)
sodium	22.990	+1	116	358
potassium	39.098	+1	152	331
magnesium	24.305	+2	86	428
chloride	35.453	-1	167	331
bromide	79.904	-1	182	330
nitrate	62.005	-1	165	335
sulfate	96.064	-2	244	379

4.5.2 Effect of Ionic Radius on CA Regeneration

Several experiments were conducted to study the effect of ionic radius of ions on regeneration of CA. Two monovalent cations (sodium, potassium) and two monovalent anions (bromide, nitrate) were used in these experiments, resulting in four different salts (NaBr, $NaNO_3$, KBr, KNO_3) being used. The hydrated radius of an ion is a function of the ratio of its charge to its ionic radius and this was taken in to account when comparing results. Gabelich et al. did not find any observable effect of ionic radius on adsorption under the experimental conditions that were used. However, this might not be the case for desorption in the current study. Results from experiments 12, 13, 14 and 15 are plotted in figures IV-37 and IV-38. If the sum of the hydrated radii of both ions (cation and anion) is used, the salts can be ranked according to size as shown below.

$$KBr < KNO_3 < NaBr < NaNO_3$$

This order is similar to the one observed in Figure IV-38. Percent regeneration of each salt followed approximately the same order, except that the positions of KNO_3 and

NaBr have been reversed. The reason behind this shift is not clear and more experiments are needed to explore this effect.

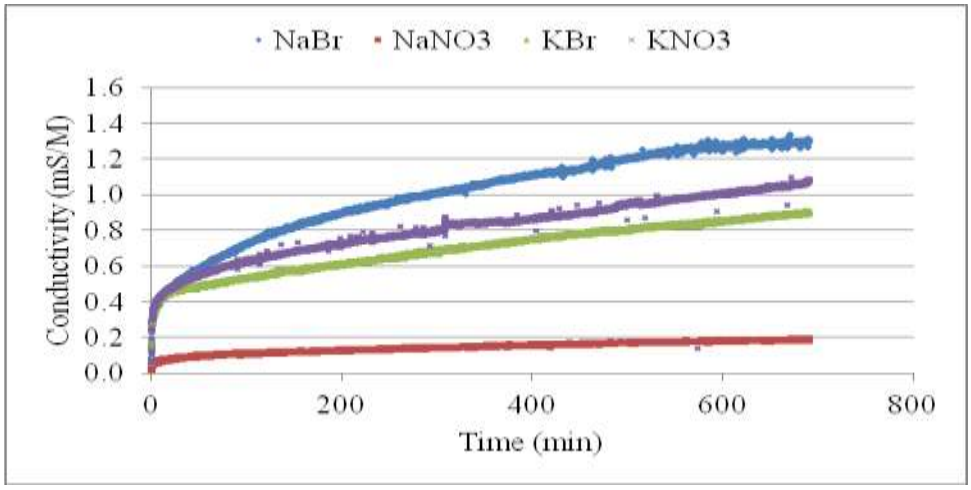

Figure IV-46. Effect of time on conductivity during regeneration using ions with different ionic radii. Data for NaBr, $NaNO_3$, KBr and KNO_3 are from experiments 12, 13, 14, and 15 respectively.

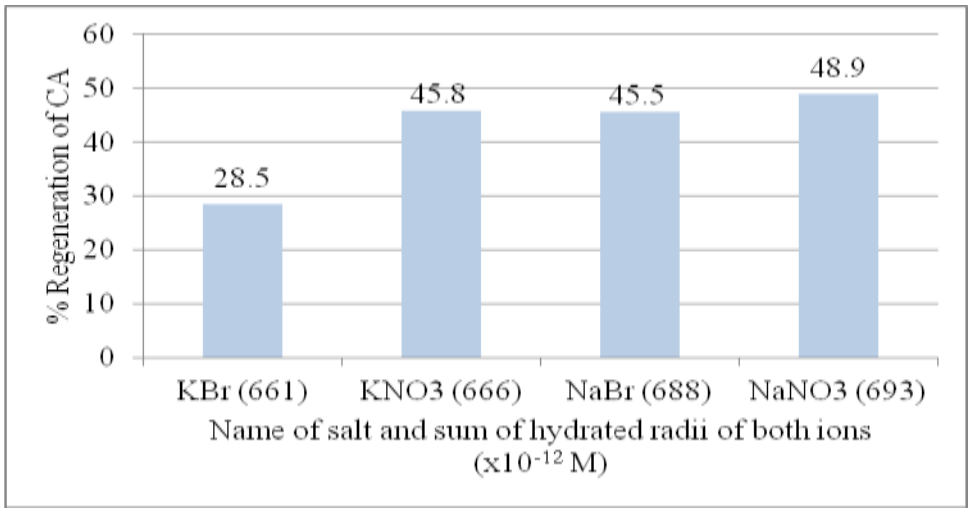

Figure IV-47. Effect of salts with different ionic radii on percent regeneration of CA. Data for NaBr, $NaNO_3$, KBr and KNO_3 are from experiments 12, 13, 14 and 15, respectively.

4.6 Effect of Ionic Charge on CA Regeneration

Experiments 18 through 21 of Phase-III were designed to investigate the effect on regeneration of the charge of ions in a salt (monovalent-monovalent, monovalent-divalent, divalent-divalent). Results from experiments 16 through 19 are plotted in Figure IV-39 and IV-40. Four different salts were used (NaBr in experiment 16, Na_2SO_4 in experiment 17, $MgBr_2$ in experiment 18, $MgSO_4$ in experiment 19). Percent regeneration was higher when cations and anions both were either monovalent (NaBr) or divalent ($MgSO_4$) as compared to having a monovalent cation and divalent anion (Na_2SO_4). This behavior is similar to that observed by Gabelich et al. for electro-sorption experiments except regeneration behavior of $MgBr_2$.

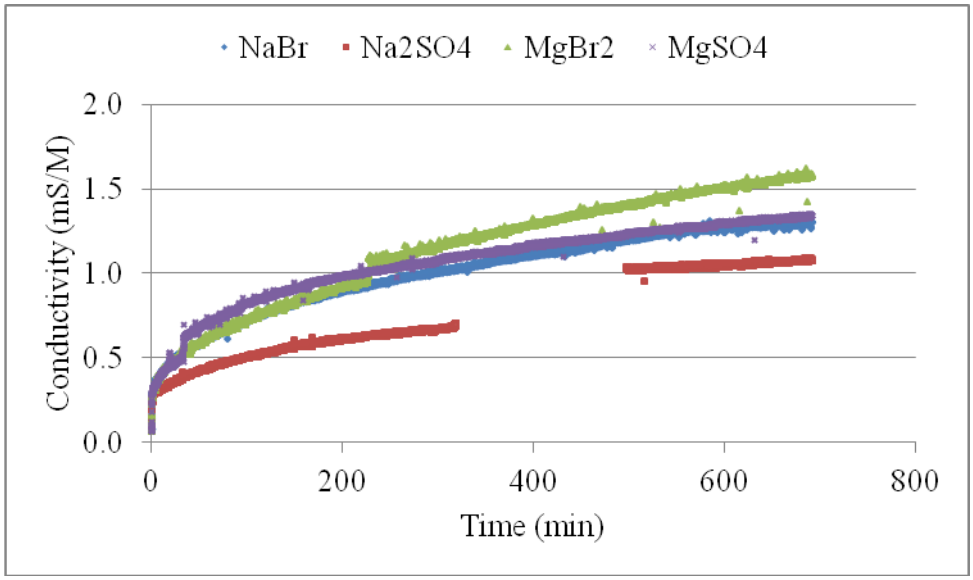

Figure IV-48. Effect of time on conductivity during regeneration of CA with ions of different charge. Data for NaBr, Na_2SO_4, MgBr and $MgSO_4$ are from experiments 16, 17, 18, and 19 respectively.

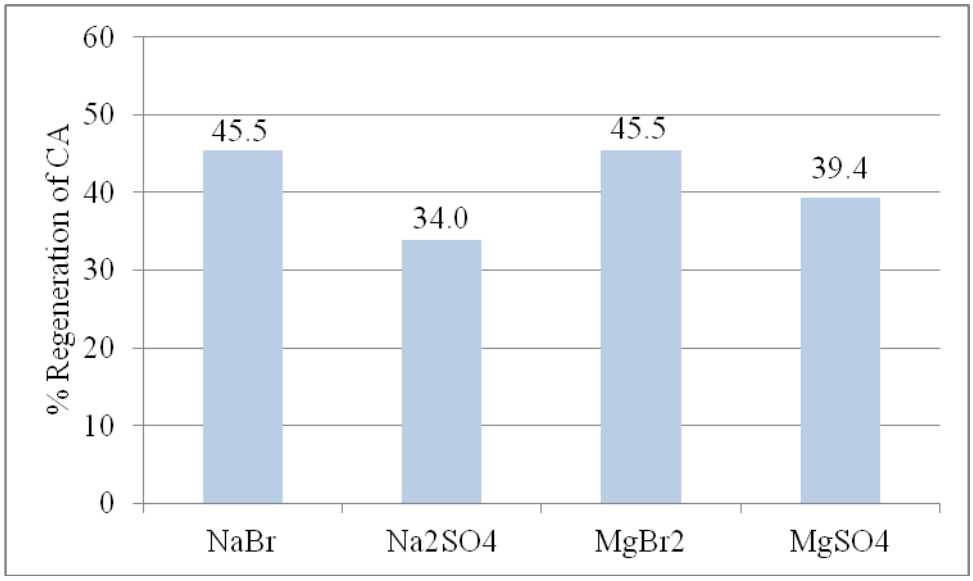

Figure IV-49. Effect of charge of ions on percent regeneration of CA. Data for NaBr, Na_2SO_4, MgBr and $MgSO_4$ are from experiments 16, 17, 18, and 19 respectively.

4.7 Effect CA Thickness and Density on Regeneration

The effects of various characteristics of the CA on regeneration were examined in a series of experiments that are described in Chapter III under "phase 4 experiments". Percent regenerations of four different CDI with four different types of CA are shown in the Figure IV-41. CDI unit # 1 (7 mil, 0.8 gm/cm^3) gave the highest percent regeneration. Higher percent regeneration doesn't mean higher adsorption capacity as CDI unit type 4 had the highest adsorption capacity but not the highest regeneration. Table IV-5 shows CDI units and CA used to make them.

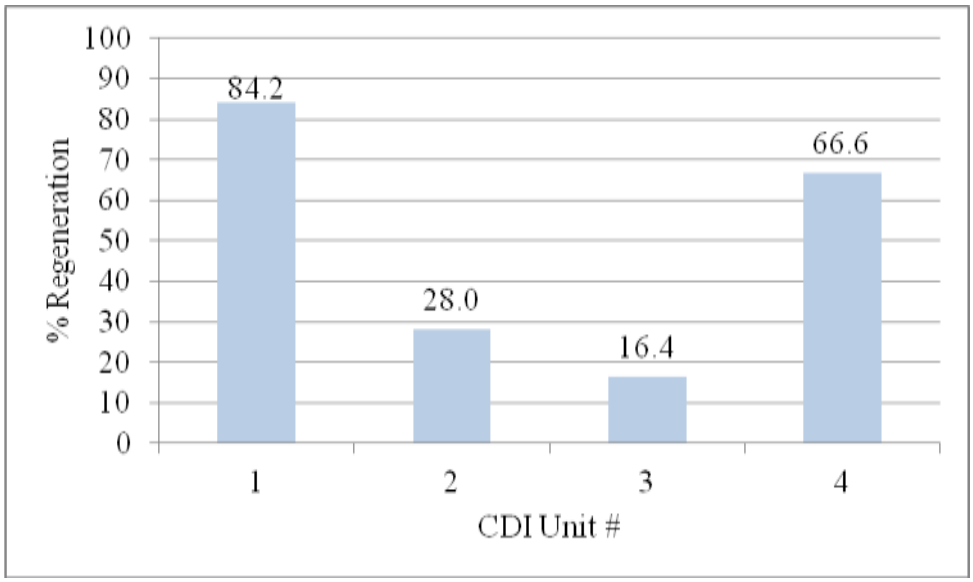

Figure IV-50. Effect of type of CA on percent regeneration. Data for CDI units 1, 2, 3, and 4 are from experiments 1, 20, 21 and 22, respectively.

Table IV-10. Four different types of CDI units.

CDI Unit	Thickness and density of CA electrodes
1	7 mil, 0.8g/cm^3
2	14 mil, 0.8g/ cm^3
3	7 mil, 0.4-0.5g/ cm^3
4	14 mil, 0.4-0.5g/ cm^3

CHAPTER V

CONCLUSIONS AND RECOMMENDATIONS

5.1 Conclusions

The results of this research demonstrate that CA that has been exhausted after capacitive deionization of water with various salts can be regenerated successfully. They also demonstrate the effect of various conditions on regeneration of CA. The results of this research: 1) provide basic knowledge about making a CDI cell with CA for deionization of water contaminated with various salts of metal ions, 2) provide basic information on procedures of operation of a CDI cell in deionization and regeneration mode, and 3) evaluate the effect of polarity of electrodes, application of reverse potential, temperature, flow speed of water on CA electrode surface, mass/size of ions and type of CA on regeneration of CA. This knowledge could be applied to other systems, including full-scale deionization systems.

The specific conclusions obtained from the research are as follows:

1) CA electrodes saturated with sodium and chloride ions were regenerated to the extent of 19.6% (mean value) with only DI water flushing at 20 °C using a flow speed of 18.5 cm/min when no potential and no shorting were applied during regeneration. Regeneration was rapid during the first few minutes and there was little increase in regeneration for rest of the 12-hour regeneration period.
2) Percent regeneration was increased to 26.3% (mean value) when electrodes were shorted and other conditions were similar to those described in (1). This increase

was probably due to loss of residual charge when CA electrodes were shorted. This jump in regeneration when electrodes were shorted was observed under various other conditions including temperature and flow speed of water over CA surface.

3) Application of reverse potential resulted in higher regeneration of CA. The extent of regeneration was dependent on the duration of application of reverse potential.
    a) There was a sharp increase in percent regeneration between 1 minute and 2 minutes and sharp drop in percent regeneration between 2 minutes and 5 minutes. The greatest extent and fastest regeneration of CA saturated with sodium and chloride ions was found to be about 97% when a reverse potential of 1.2 V was applied for 2 minutes at a temperature of 20°C with a water flow speed of 18.5 cm/min. This time of rapid increase in regeneration during application of reverse potential is a result of various factors such as type of CA used, configuration of CDI unit, separation between CA electrodes, method of water application (one-pass or re-circulated), temperature and flow speed of water across the CA surface.
    b) Results show that longer application of reverse potential will not result in higher regeneration. Also, regeneration happened at the lowest rate when the regeneration period was initiated with a reverse potential being applied for 32 minutes.
4) Regeneration increased with temperature. This trend was the same when no potential was applied and electrodes were shorted or not.

a) Without shorting, the mean percent regeneration was found to increase from 19.6% at 20°C to 45.1% at 30°C and to 59.9% at 39°C. The rate of regeneration did not increase with time after the first few minutes at 20°C and 30°C, but at 39°C it kept on increasing with time throughout the regeneration period.

b) Similar regeneration trends were noticed when electrodes were shorted. The mean percent regeneration increased from 26.3% at 20°C to 56.9% at 30°C and to 69.3% at 39°C. There was a rapid increase in conductivity during first few minutes at 20°C and 30°C but at 39°C it kept increasing until about 100 minutes and after that there was little increase in conductivity.

c) The extent of regeneration decreased with temperature (from 84.2% at 20°C to 58.2% at 30°C and to 38.2% at 39°C) when reverse potential was applied for 1 minute. The rate of regeneration increased with temperature for about 100 minutes.

d) Similar behavior was noticed when reverse potential was applied for 5 minutes. The extent of regeneration dropped from 73.9% at 20°C to 32.2% at 30°C but there was a slight increase to 36% at 39°C.

e) There was evidence of hysteresis because the desorption isotherm was different than the adsorption isotherm at 20°C. Also, the Langmuir isotherm was a good fit of the adsorption data as indicated by a R^2 value of 0.91 for the linear regression using the linearized Langmuir isotherm.

5) Regeneration behavior was studied for various flow speeds of water across the CA surface when no potential was applied without shorting as well as when no potential was applied with shorting. The extent of regeneration was similar at 10.9 cm/min and 18.5 cm/min, when 95 % of confidence intervals were considered. However, at higher speed of 32.2 cm/min, the extent of regeneration was significantly higher.
6) When regeneration was studied for various flow speeds of water with reverse potential applied for 1 minute and 5 minutes, the behavior that was observed was different than when the electrodes were shorted and when they were not shorted. There was increase in the extent of regeneration between 10.9 cm/min and 18.5 c/min and there was drop in extent of regeneration between 18.5 cm/min and 32.2 cm/min, when reverse potential was applied for 1 min as well as 5 minutes. Higher rates of regeneration were observed at 18.5 m/min than at 10.9 cm/min and at 32.2 cm/min.
7) The extent of regeneration of CA decreased with mass of ions. Percent regeneration decreased from 97.9% with NaCl, to 51.2% with KCl and to 28.4% with KBr. This suggests that at similar conditions (flow speed of 18.5 cm/min, reverse potential applied for 2 minutes at temperature of 20°C) ions with higher masses are harder to desorb and thus have lower extents of regeneration.
8) Regeneration of CA was found to increase with the size of ions when the order of sum of the hydrated radii of both ions (cation and anion) was used as a measure of size. Four salts used to study the effect of size can be arranged in order of sum

of the hydrated radii of both ions (cation and anion) as KBr < KNO_3 < NaBr <$NaNO_3$ and percent regeneration was found to be 28.4% (KBr), 45.7% (KNO_3), 45.5% (NaBr) and 48.92% ($NaNO_3$). One possible reason may be that ions with smaller hydrated radii adsorb more deeply into pores so that during regeneration ions with larger hydrated radii are released more easily, which results in higher extents of regeneration.

9) Percent regeneration was higher when a salt had ions that were either both monovalent (NaBr: 45.5%) or both divalent ($MgSO_4$: 45.5%) as compared to a salt having one monovalent ion and one divalent ion (Na_2SO_4 33.9%) although $MgBr_2$ did not follow the pattern (47.5 %). This general trend is similar to that observed in electro-sorption of these salts onto CA by previous scholars.
10) The percent regeneration was the greatest (84.2%) with CDI unit 1 among the four CDI units when reverse potential applied for 1 minute. CDI unit 1 had CA with a thickness of 7 mil, density of 0.8 g/cm^3 and surface area of 400 m^2/g. Regeneration was lowest (16.3%) with CDI unit 3 that had CA with a thickness of 7 mil, density of 0.4-0.5 g/cm^3 and area of 600 m^2/g.

5.2 Recommendations

The results described in this research leads to some relevant research topics for future work in similar experimental systems. The specific research topics for future research are as follows.

1) Determination of the effect of variation of the magnitude of reverse potential on regeneration of CA exhausted in capacitive deionization was not explored in this research and would be interesting to study.
2) Single salt solutions were used in this research. Solutions with various multiple salts should be used for future regeneration work. Also, the effect of various ions competing for available sites for electro-sorption has been studied by various scholars, but no work has been done to study their behavior during regeneration of CA exhausted in capacitive deionization.
3) Solutions were re-circulated in a multi-pass manner in CDIs used in this research. Multiple CDI cells arranged in a series and so that the solution would pass through the series of CDIs in a single-pass manner should give some interesting results.
4) Temperature range could be increased beyond the one used in this research (20°C to 39°C).
5) A wider speed range should be explored in the future to better determine the effect of this variable on regeneration.
6) More experiments are needed to better understand the effect of charge of ions on regeneration of CA. More experiments are needed to understand the behavior of salts of monovalent cations and divalent anions. In addition, in future studies, salts of various combinations of monovalent, divalent and trivalent ions should be used.

7) Not enough information was derived in this research about the effect of density, thickness and surface area of CA on regeneration. More experiments are needed to explore this effect.
8) Use of ultrasound was explored in early stages of this research as a mean to enhance desorption and ultimately increase regeneration. However, the CA was damaged by its use so further work was abandoned. In future work, careful use of ultrasound of various intensities is proposed.

REFERENCES

1. Johnson, A. M.; Newman, J., Desalting by Means of Porous Carbon Electrodes. *Journal of the Electrochemical Society* **1971,** *118* (3), 510-&.

2. (a) Chu, A. K. P.; Fleischm.M; Hills, G. J., Packed-Bed Electrodes.1. Electrochemical Extraction of Copper Ions from Dilute Aqueous-Solutions. *Journal of Applied Electrochemistry* **1974,** *4* (4), 323-330; (b) Bennion, D. N.; Newman, J., Electrochemical Removal of Copper Ions from Very Dilute Dolutions. *Journal of Applied Electrochemistry* **1972,** *2* (2), 10.

3. Oren, Y.; Soffer, A., Electrochemical Parametric Pumping. *Journal of the Electrochemical Society* **1978,** *125* (6), 869-875.

4. Oren, Y.; Tobias, H.; Soffer, A., Removal of Bacteria from Water by Electroadsorption on Porous Carbon Electrodes. *Bioelectrochemistry and Bioenergetics* **1983,** *11* (4-6), 347-351.

5. Oren, Y.; Soffer, A., Water Desalting by Means of Electrochemical Parametric Pumping. I. The Equilibrium Properties of a Batch Unit-Cell. *Journal of Applied Electrochemistry* **1983,** *13* (4), 473-487.

6. Jayson, G. G.; Sangster, J. A.; Thompson, G.; Wilkinson, M. C., Adsorption and Electrosorption of Mercury(II) Acetate onto Activated-Charcoal Cloth from Aqueous-Solution. *Carbon* **1987,** *25* (4), 523-531.

7. Ryoo, M. W.; Seo, G., Improvement in Capacitive Deionization Function of Activated Carbon Cloth by Titania Modification. *Water Research* **2003,** *37* (7), 1527-1534.

8. Avraham, E.; Bouhadana, Y.; Soffer, A.; Aurbach, D., Limitation of Charge Efficiency in Capacitive Deionization I. On the Behavior of Single Activated Carbon. *Journal of The Electrochemical Society* **2009,** *156* (6), 5.

9. Conway, B. E.; Ayranci, E.; Al-Maznai, H., Use of Quasi-3-dimensional Porous Electrodes for Adsorption and Electrocatalytic Removal of Impurities from Waste-waters. *Electrochimica Acta* **2001,** *47* (5), 705-718.

10. Ayranci, E.; Conway, B. E., Adsorption and Electrosorption at High-area Carbon-felt Electrodes for Waste-water Purification: Systems Evaluation with Inorganic, S-containing Anions. *Journal of Applied Electrochemistry* **2001,** *31* (3), 257-266.

11. Koresh, J.; Soffer, A., Double-Layer Capacitance and Charging Rate of Ultramicroporous Carbon Electrodes. *Journal of the Electrochemical Society* **1977,** *124* (9), 1379-1385.

12. Otowa, T.; Tomita, T.; Oda, H.; Andelman, M. D., *Novel Method to Remove Light Ions by Activated Carbon Electrodes*. Elsevier: Amsterdam, 1998; p 945-950.

13. Matlosz, M.; Newman, J., Experimental Investigation of a Porous Carbon Electrode for the Removal of Mercury from Contaminated Brine. *Journal of the Electrochemical Society* **1986,** *133* (9), 1850-1859.

14. Farmer, J. C.; Fix, D. V.; Mack, G. V.; Pekala, R. W.; Poco, J. F., Capacitive Deionization of NaCl and $NaNO_3$ Solutions with Carbon Aerogel Electrodes. *Journal of the Electrochemical Society* **1996,** *143* (1), 159-169.

15. Farmer, J. C.; Bahowick, S. M.; Harrar, J. E.; Fix, D. V.; Martinelli, R. E.; Vu, A. K.; Carroll, K. L., Electrosorption of Chromium Ions on Carbon Aerogel Electrodes as a Means of Remediating Ground Water. *Energy & Fuels* **1997,** *11* (2), 337-347.

16. Farmer, J. C.; Fix, D. V.; Mack, G. V.; Pekala, R. W.; Poco, J. F., Capacitive Deionization of NH_4ClO_4 Solutions with Carbon Aerogel Electrodes. *Journal of Applied Electrochemistry* **1996,** *26* (10), 1007-1018.

17. Fischer, U.; Saliger, R.; Bock, V.; Petricevic, R.; Fricke, J., Carbon Aerogels as Electrode Material in Supercapacitors. *Journal of Porous Materials* **1997,** *4*, 281-285.

18. Arnold, B. B.; Murphy, G. W., Studies on Electrochemistry of Carbon and Chemically Modified Carbon Surfaces. *Journal of Physical Chemistry* **1961,** *65* (1), 135-138.

19. Atlas, R., Purification of Brackish Water using Hybrid CDI-EDI Technology. In *14th Annual International Petroleum Environmental Conference*, Houston, TX, 2007.

20. Strohl, A. N.; Curran, D. J., Reticulated Vitreous Carbon Flow-Through Electrodes. *Analytical Chemistry* **1979,** *51* (3), 5.

21. Bennion, D. N.; J., N., Electrochemical removal of copper ions from very dilute solutions. *Journal of Applied Electrochemistry* **1972,** *2*, 10.

22. Vanzee, J.; Newman, J., Electrochemical Removal of Silver Ions from Photographic Fixing Solutions using a Porous Flow-through Electrode. *Journal of the Electrochemical Society* **1977,** *124* (5), 706-708.

23. Avraham, E.; Bouhadana, Y.; Soffer, A.; Aurbach, D., Limitation of Charge Efficiency in Capacitive Deionization I. On the Behavior of Single Activated Carbon. *Journal of the Electrochemical Society* **2009,** *156* (6), P95-P99.

24. Saliger, R.; Fischer, U.; Herta, C.; Fricke, J., High Surface Area Carbon Aerogels for Supercapacitors. *Journal of Non-Crystalline Solids* **1998,** *225* (1), 81-85.

25. Tran, T. D.; Farmer, J. C.; De Pruneda, J. H.; Richardson, J. H. In *Electrosorption on Carbon Aerogel Electrodes as a Means of Treating Low-level Radioactive Wastes and Remediating Contaminated Ground Water*, Proceedings of Sixth International Conference on Radioactive Waste Management and Environmental Remediation ICEM'97, Singapore, October 12-16, 1997; Baker, R.; Slate, S.; Benda, G., Eds. The American Society of Mechanical Engineers: Singapore, 1997; pp 547-553.

26. Pekala, R. W.; Farmer, J. C.; Alviso, C. T.; Tran, T. D.; Mayer, S. T.; Miller, J. M.; Dunn, B., Carbon Aerogels for Electrochemical Applications. *Journal of Non-Crystalline Solids* **1998,** *225* (1), 74-80.

27. Ying, T. Y.; Yang, K. L.; Yiacoumi, S.; Tsouris, C., Electrosorption of Ions from Aqueous Solutions by Nanostructured Carbon Aerogel. *Journal of Colloid and Interface Science* **2002,** *250* (1), 18-27.

28. Yang, K. L.; Ying, T. Y.; Yiacoumi, S.; Tsouris, C.; Vittoratos, E. S., Electrosorption of Ions from Aqueous Solutions by Carbon Aerogel: An Electrical Double-layer Model. *Langmuir* **2001,** *17* (6), 1961-1969.

29. Gabelich, C. J.; Tran, T. D.; Suffet, I. H., Electrosorption of Inorganic Salts from Aqueous Solution using Carbon Aerogels. *Environmental Science & Technology* **2002,** *36* (13), 3010-3019.

30. Park, S.; Liang, C.; Sheng, D.; Dudney, N.; DePaoli, E., Mesoporous Materials as Electrodes for Electrochemical Double-layer Capacitor. *Materials Research Society Symposia Proceedings* **2007,** *973*, 43-49.

31. Conway, B. E., *Electrochemical Supercapacitors: Scientific Fundamentals and Technological Applications*. Kluwer Academic / Plenum Publishers: New York, 1999; p 138-141.

32. (a) Blaedel, W. J.; Wang, J., Flow Electrolysis on a Reticulated Vitreous Carbon Electrode. *Analytical Chemistry* **1979,** *51* (7), 799-802; (b) Lessner, P.; Newman, J., Hydrodynamics and Mass-Transfer in a Porous-Wall Channel. *Journal of the Electrochemical Society* **1984,** *131* (8), 1828-1831; (c) Risch, T.; Newman, J., A Theoretical Comparison of Flow-through and Flow-by Porous-Electrodes at the Limiting Current. *Journal of the Electrochemical Society* **1984,** *131* (11), 2551-2556; (d)

Trainham, J. A.; Newman, J., Flow-through Porous-Electrode Model - Application to Metal-Ion Removal from Dilute Streams. *Journal of the Electrochemical Society* **1977,** *124* (10), 1528-1540.

33. Kramer, T. A.; Kim, J.; Kim, S. *Further Study of Desalination using Capacitive Deionization: As Evaluation of CDT Aqua Cell*; Texas Water Resources Institute: College Station, 2005.

34. Kistler, S. S., Coherent Expanded Aerogels and Jellies. *Nature* **1931,** *127* (3211).

35. (a) Lu, X. P.; Nilsson, O.; Fricke, J.; Pekala, R. W., Thermal and Electrical-Conductivity of Monolithic Carbon Aerogels. *Journal of Applied Physics* **1993,** *73* (2), 581-584; (b) Pekala, R. W., Organic Aerogels from the Polycondensation of Resorcinol with Formaldehyde. *Journal of Materials Science* **1989,** *24* (9), 3221-3227.

36. Fricke, J.; Tillotson, T., Aerogels: Production, Characterization, and Applications. *Thin Solid Films* **1997,** *297* (1-2), 212-223.

37. Li, W. C.; Guo, S. C., Preparation of Low-density Carbon Aerogels from a Cresol/formaldehyde Mixture. *Carbon* **2000,** *38* (10), 1520-1523.

38. Li, W. C.; Reichenauer, G.; Fricke, J., Carbon Aerogels Derived from Cresol-resorcinol-formaldehyde for Supercapacitors. *Carbon* **2002,** *40* (15), 2955-2959.

39. Marsh, H.; Wynne-Jones, W. F. K., The Surface Properties of Carbon - I The Effect of Activated Diffusion in the Determination of Surface Area. *Carbon* **1964,** *1* (3), 269-279.

40. Bock, V.; Nilsson, O.; Blumm, J.; Fricke, J., Thermal-Properties of Carbon Aerogels. *Journal of Non-Crystalline Solids* **1995,** *185* (3), 233-239.

41. Gross, J.; Fricke, J., Thermal Expansion of Carbon and Silica Aerogels above Room Temperature. *Journal of Non-Crystalline Solids* **1995,** *186*, 301-308.

42. Hanzawa, Y.; Hatori, H.; Yoshizawa, N.; Yamada, Y., Structural Changes in Carbon Aerogels with High Temperature Treatment. *Carbon* **2002,** *40* (4), 575-581.

43. Wang, J.; Zhang, S. Q.; Guo, Y. Z.; Shen, J.; Attia, S. M.; Zhou, B.; Zheng, G. Z.; Gui, Y. S., Morphological Effects on the Electrical and Electrochemical Properties of Carbon Aerogels. *Journal of Electrochemica Society* **2001,** *148* (6), D75-D77.

44. Reichenauer, G.; Emmerling, A.; Fricke, J.; Pekala, R. W., Microporosity in Carbon Aerogels. *Journal of Non-Crystalline Solids* **1998,** *225* (1), 210-214.

45. Saliger, R.; Reichenauer, G.; Fricke, J., Evolution of Microporosity upon CO_2-activation of Carbon Aerogels. In *Characterization of Porous Solids V*, 2000; Vol. 128, pp 381-390.

46. Tamon, H.; Ishizaka, H.; Araki, T.; Okazaki, M., Control of Mesoporous Structure of Organic and Carbon Aerogels. *Carbon* **1998,** *36* (9), 1257-1262.

47. Kuhn, A. T.; Houghton, R. W., Antimony Removal from Dilute-Solutions using a Restrained Bed Electrochemical Reactor. *Journal of Applied Electrochemistry* **1974,** *4* (1), 69-73.

48. Blair, W. J.; Murphy, W. G. In *Electrochemical Demineralization of Water with Porous Electrodes of Large Surface Area*, Saline Water Conversion, Cleveland, Ohio, April 1960 American Chemical Society Cleveland, Ohio, 1960; pp 206-223.

49. Hunter, R. J., In *Foundation of Colloid Science*, Oxford University Press: New York, 1992; Vol. I.

50. Badruzzaman, M.; Westerhoff, P.; Knappe, D. R. U., Intraparticle Diffusion and Adsorption of Arsenate onto Granular Ferric Hydroxide (GFH). *Water Research* **2004,** *38* (18), 4002-4012.

51. Notthakun, S.; Crittenden, J. C.; Hand, D. W.; El-behlil, A. M.; Arora, H.; Vaitheswaran, K. In *Prediction of Granular Activated Carbon Process Performance using Mass Transfer Models*, Proceedings of a Technology Transfer Conference: Design and Use of Granular Activated Carbon - Practical Aspects, Denver, CO, AWWA Research Foundation: Denver, CO, 1989.

52. Masel, R. I., *Principles of Adsorption and Reaction on Solid Surfaces*. Wiley Interscience: 1996.

APPENDIX

GRAPHS

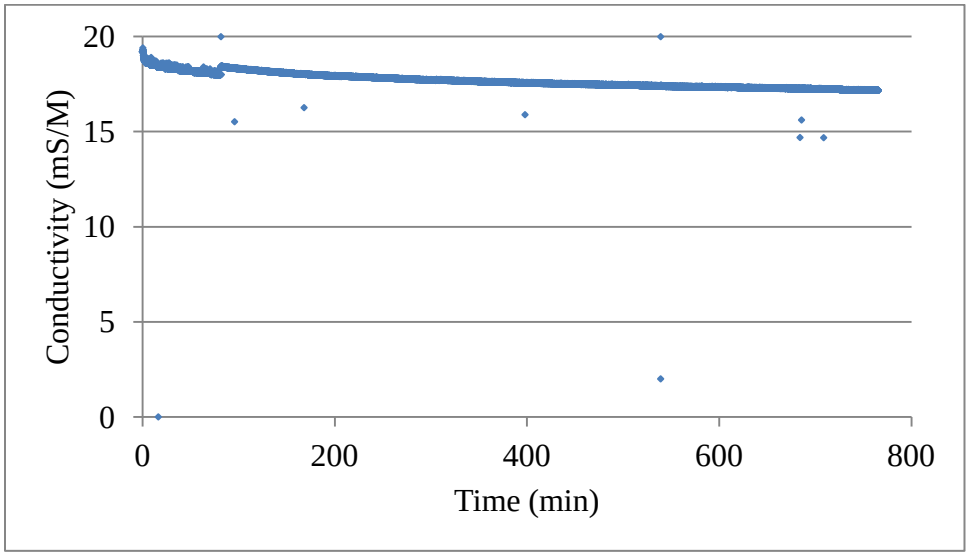

Figure A-51. Experiment 1 Adsorption.

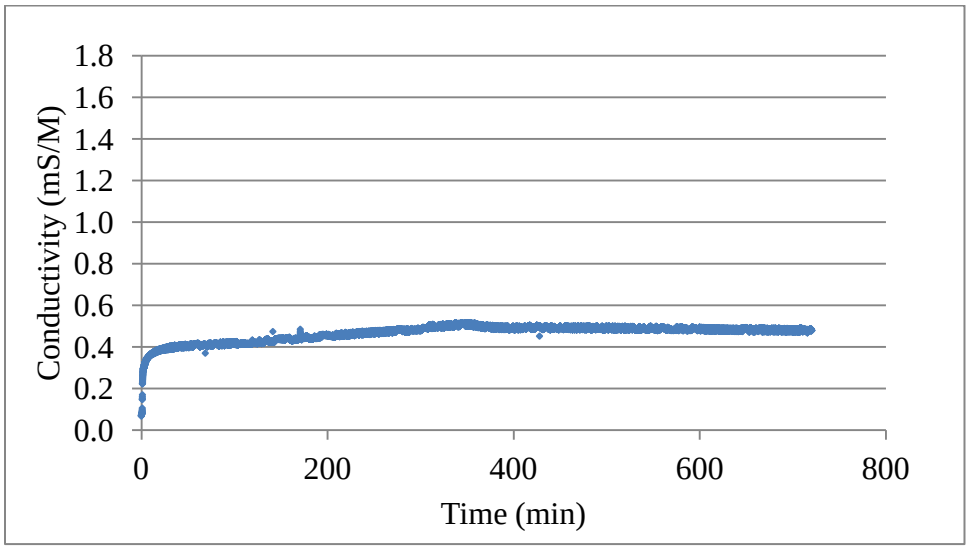

Figure A-52. Experiment 1 Desorption.

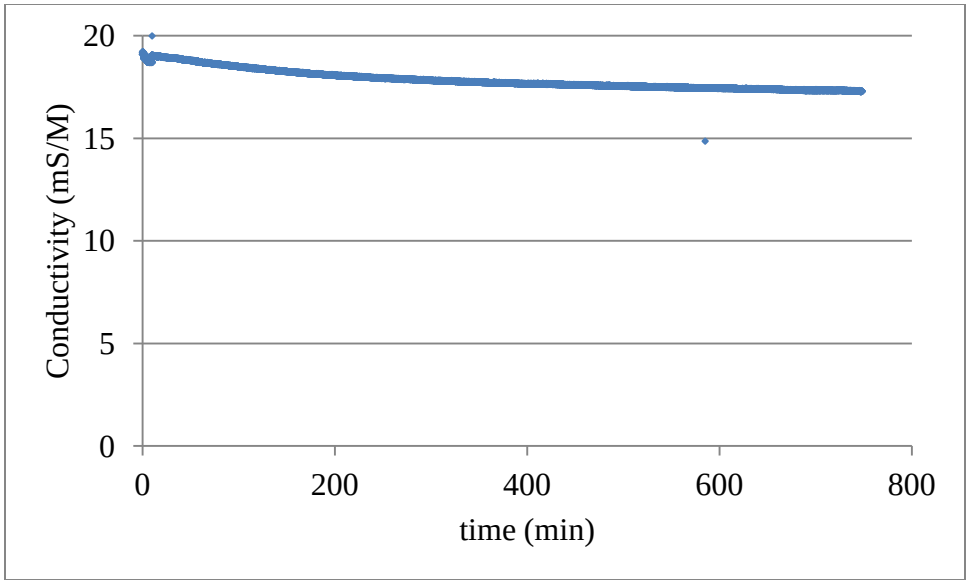

Figure A-53. Experiment 2 Adsorption.

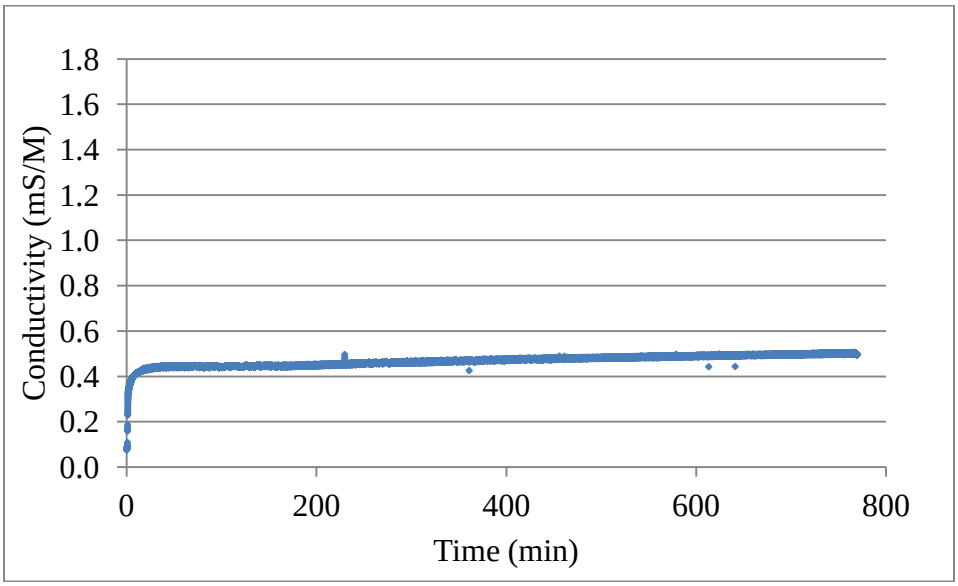

Figure A-54. Experiment 2 Desorption.

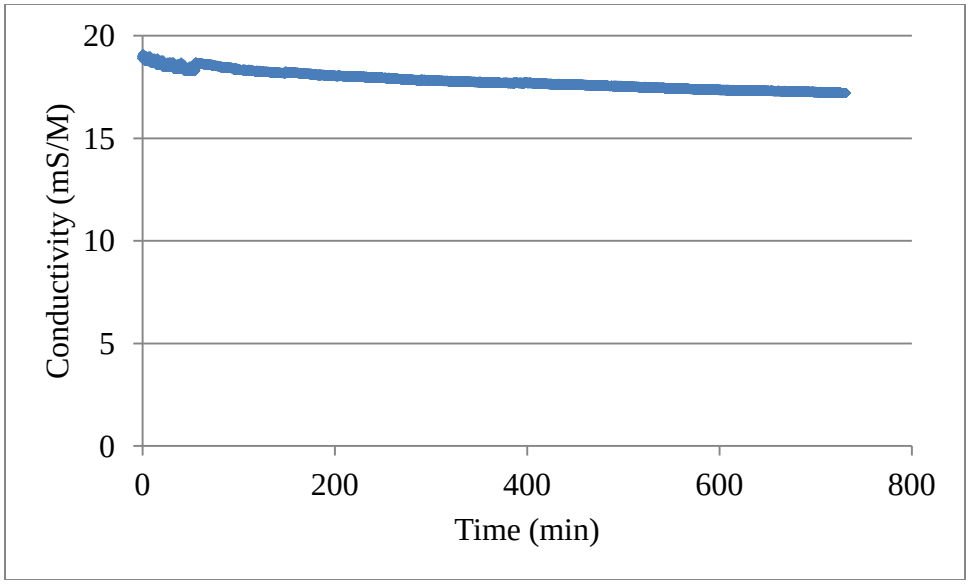

Figure A-55. Experiment 3-1 Adsorption.

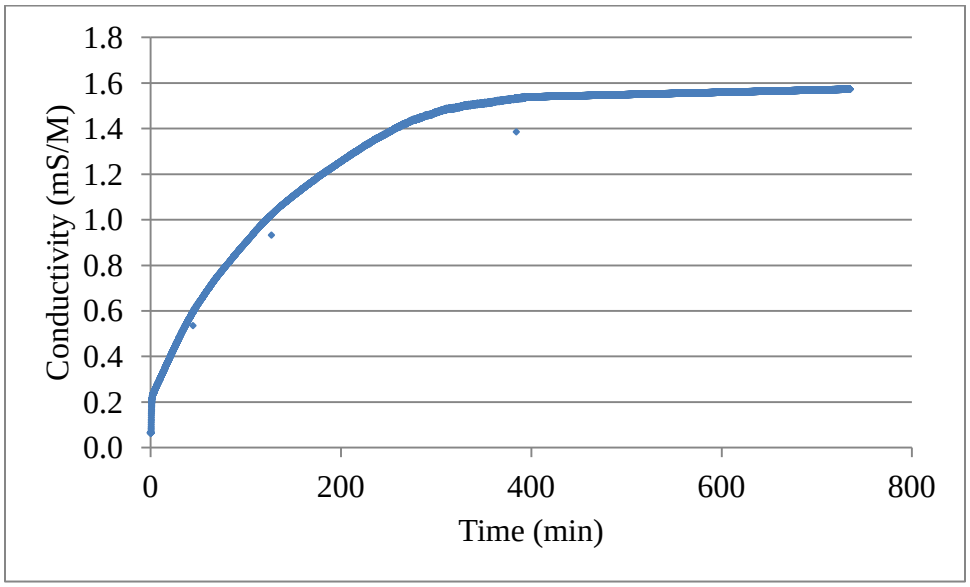

Figure A-56. Experiment 3-1 Desorption.

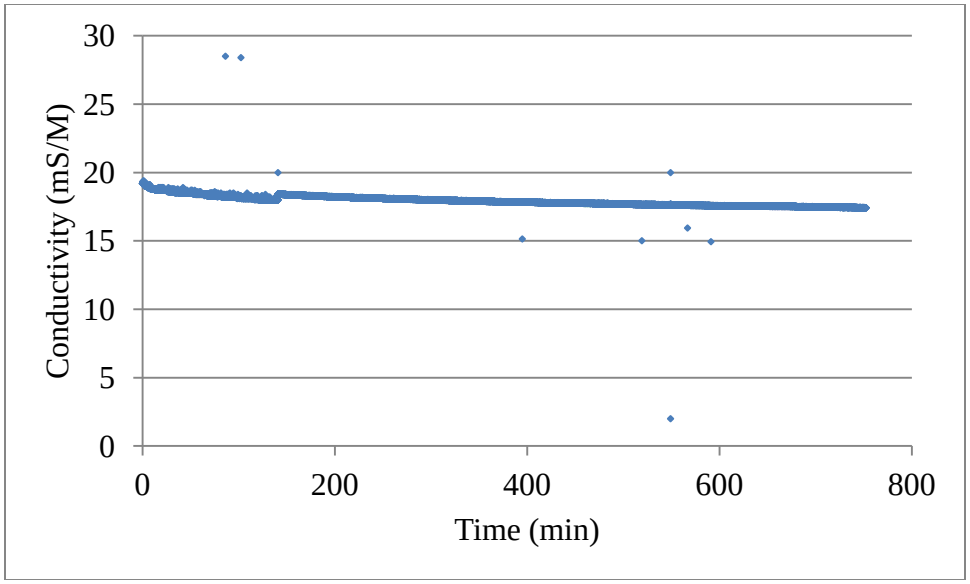

Figure A-57. Experiment 3-2 Adsorption.

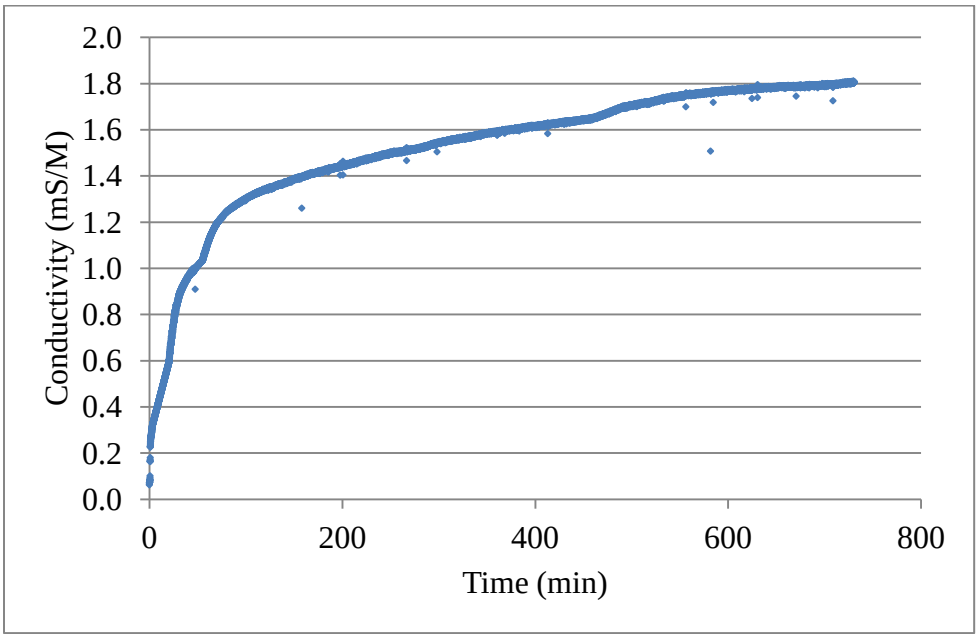

Figure A-58. Experiment 3-2 Desorption.

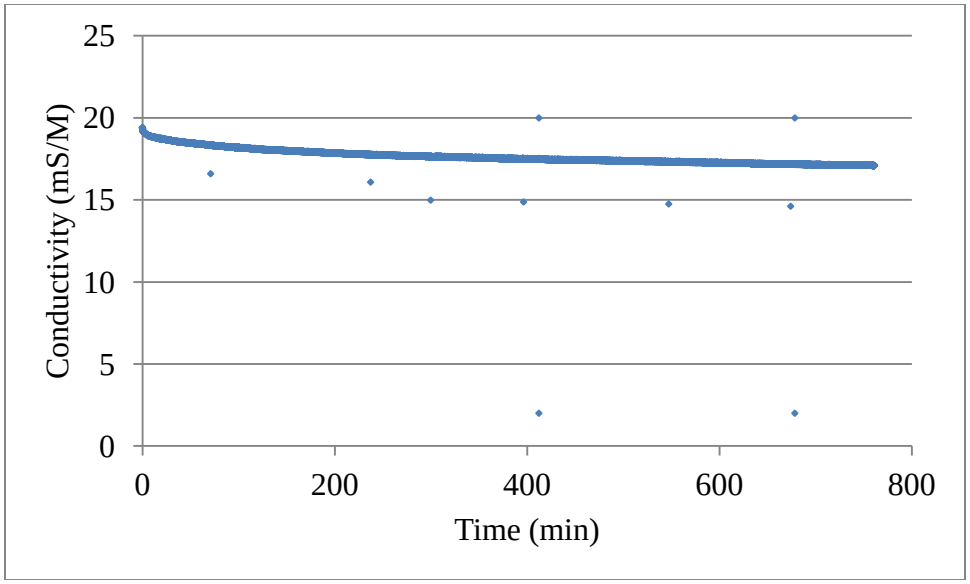

Figure A-59. Experiment 3-5 Adsorption.

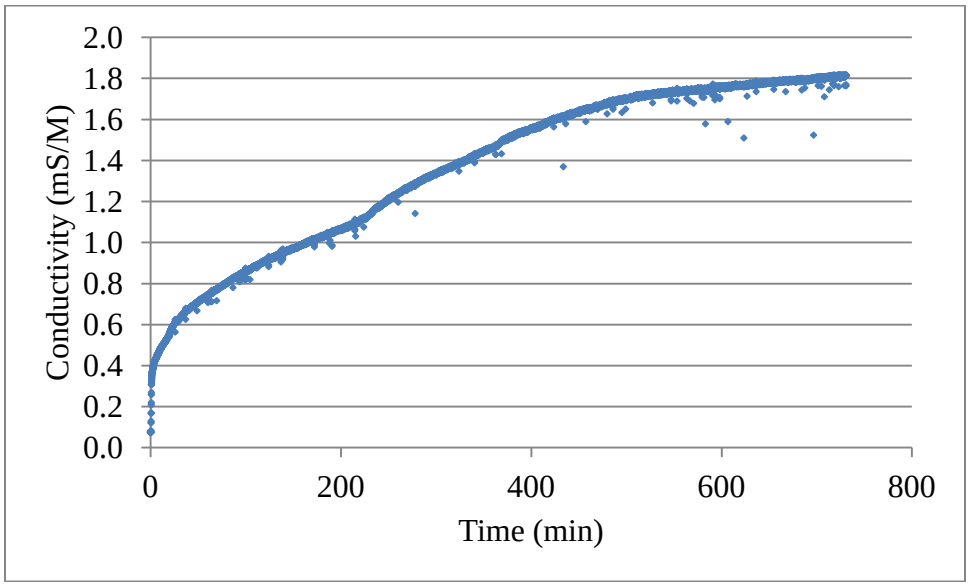

Figure A-60. Experiment 3-5 Desorption.

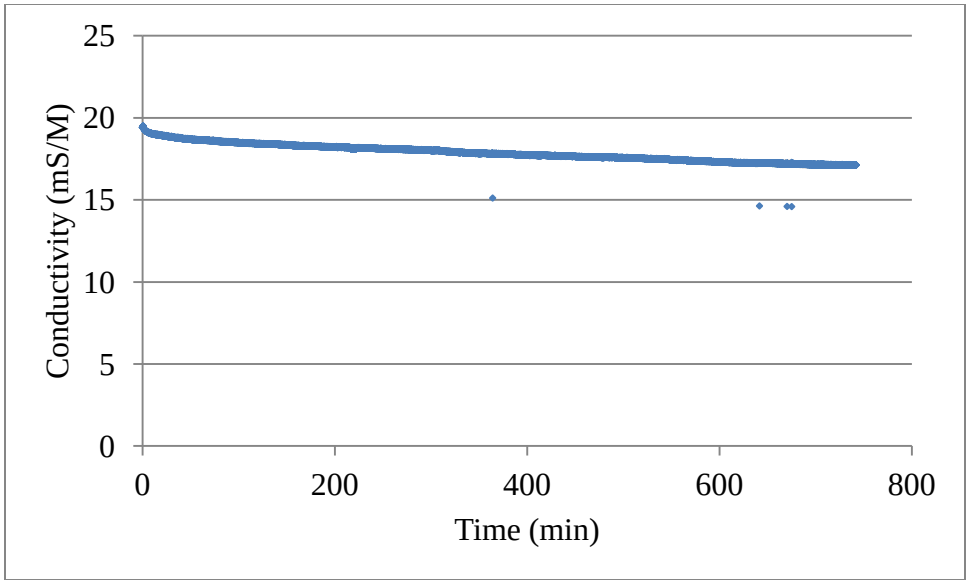

Figure A-61. Experiment 3-14 Adsorption.

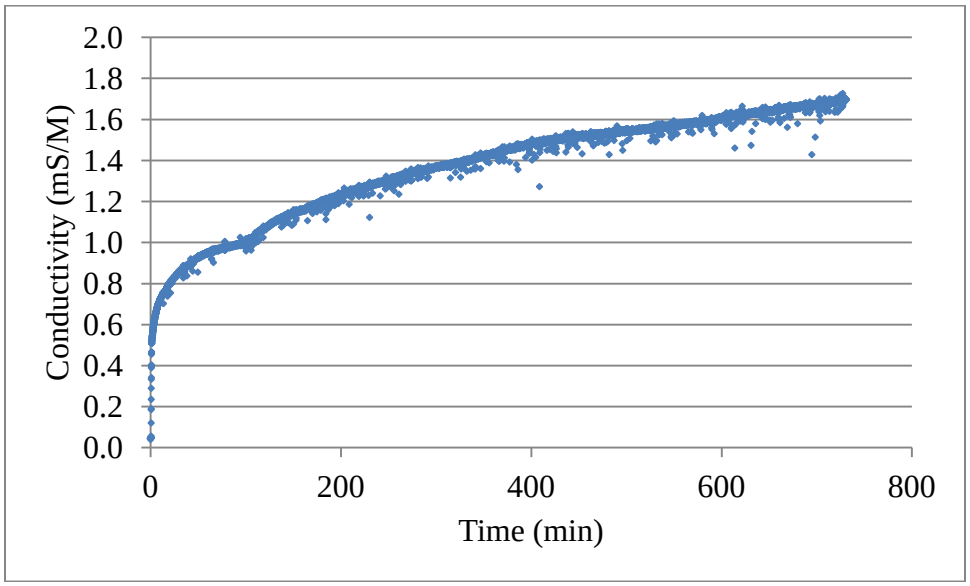

Figure A-62. Experiment 3-14 Desorption.

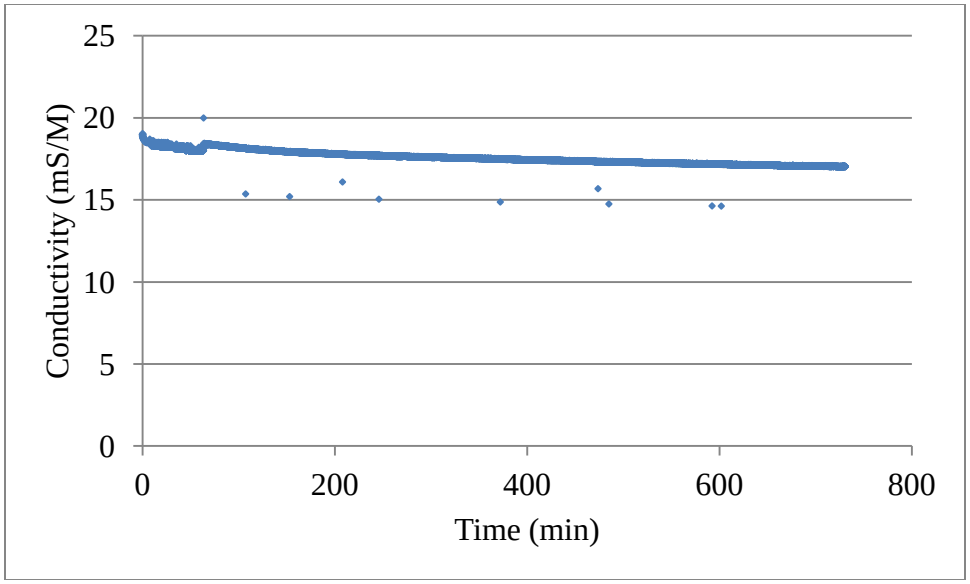

Figure A-63. Experiment 3-32 Adsorption.

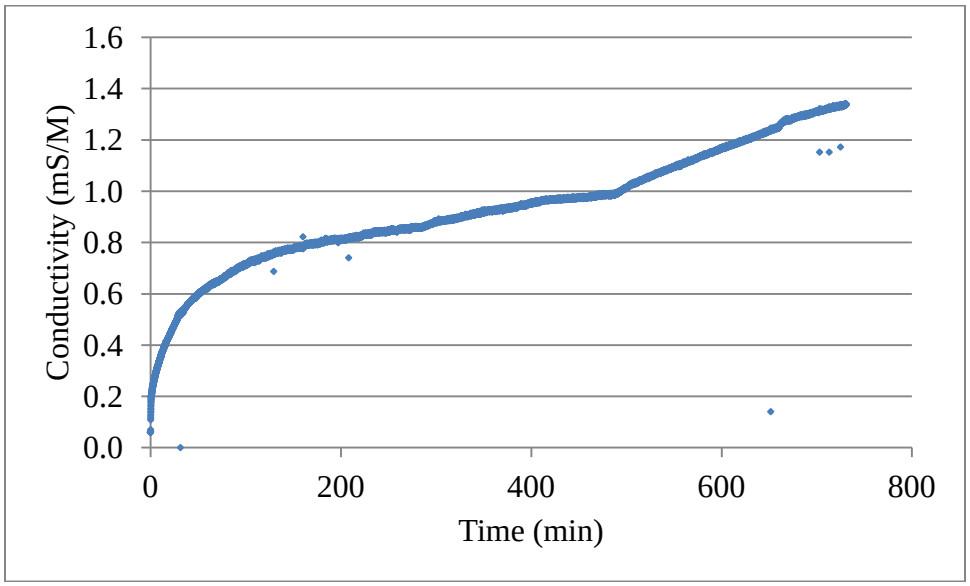

Figure A-64. Experiment 3-32 Desorption.

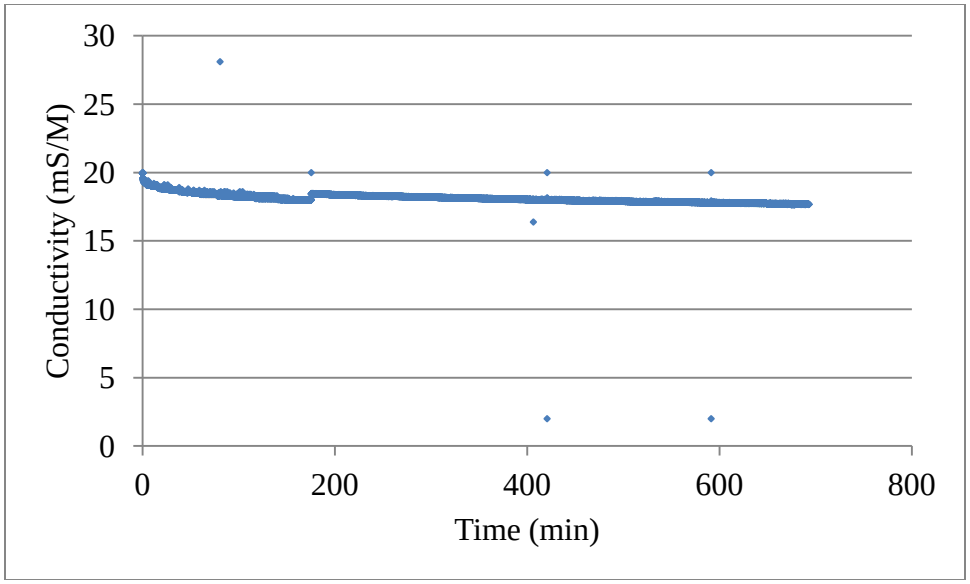

Figure A-65. Experiment 4-a Adsorption.

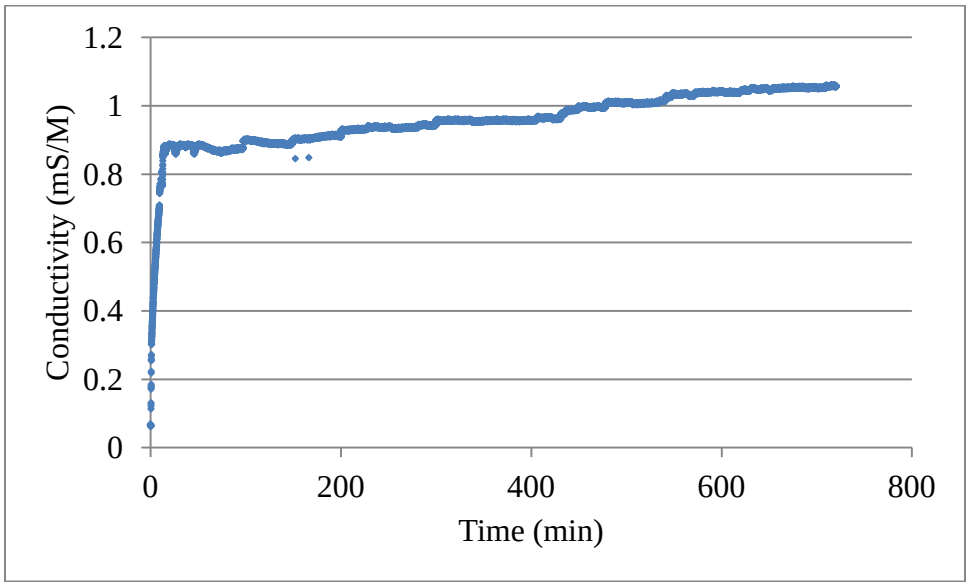

Figure A-66. Experiment 4-a Desorption.

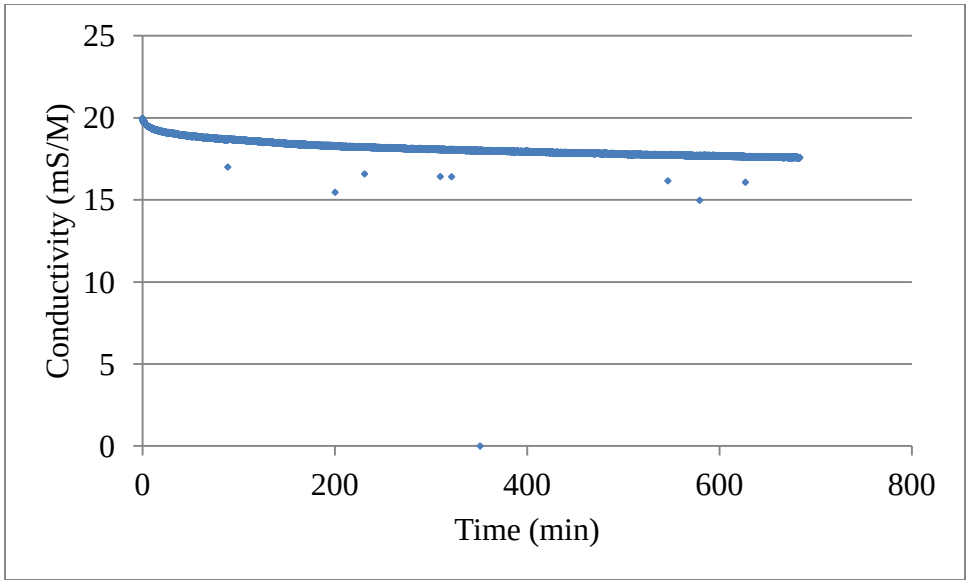

Figure A-67. Experiment 4-b Adsorption.

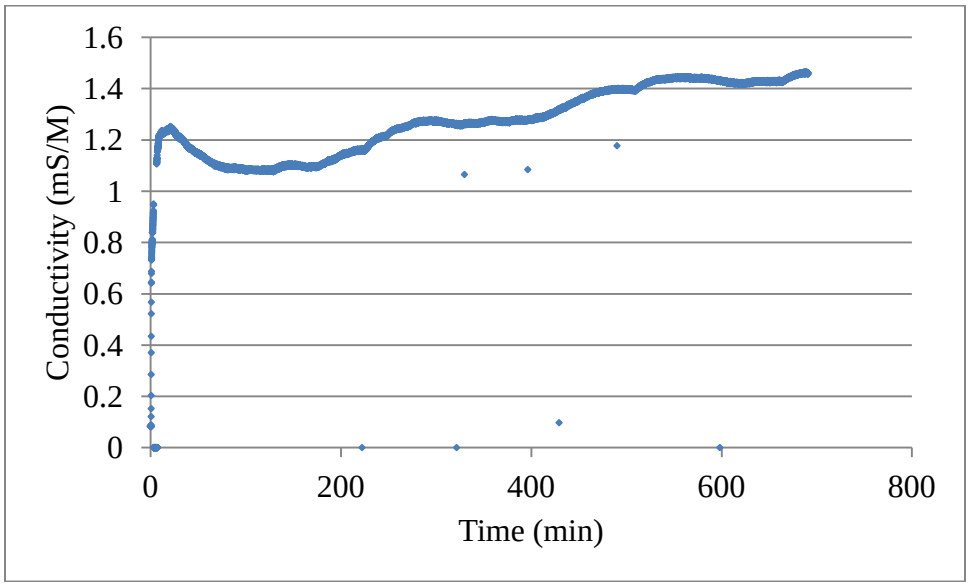

Figure A-68. Experiment 4-b Desorption.

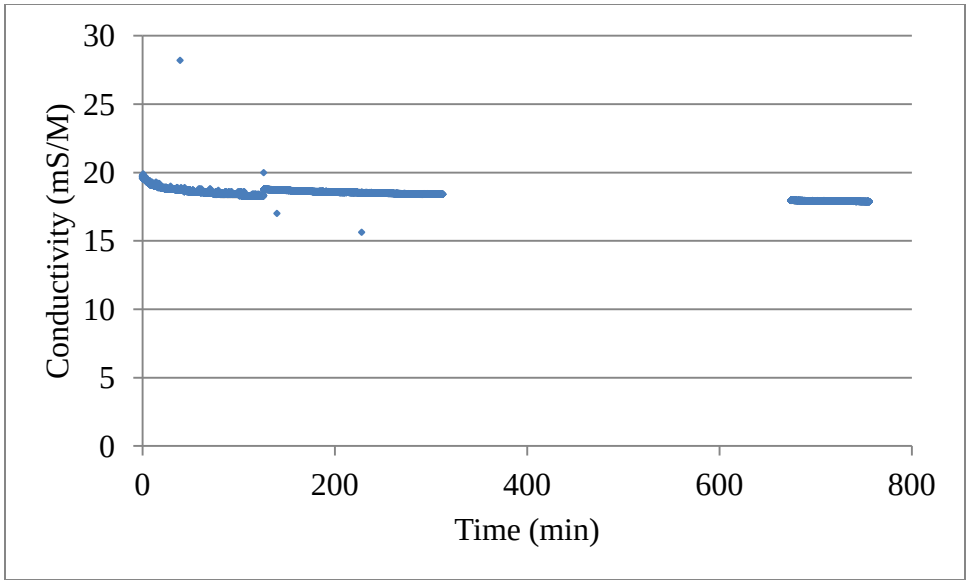

Figure A-69. Experiment 5-a Adsorption.

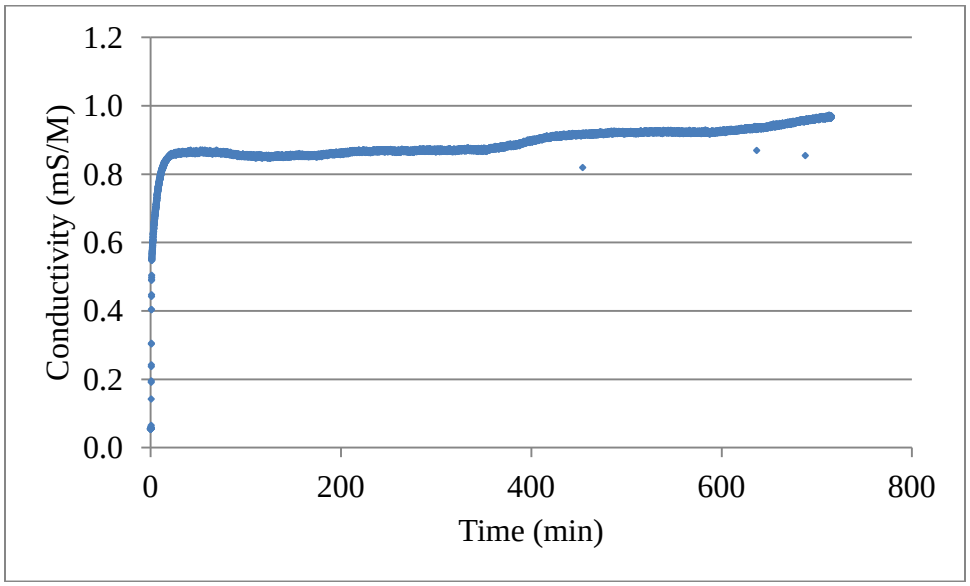

Figure A-70. Experiment 5-a Desorption.

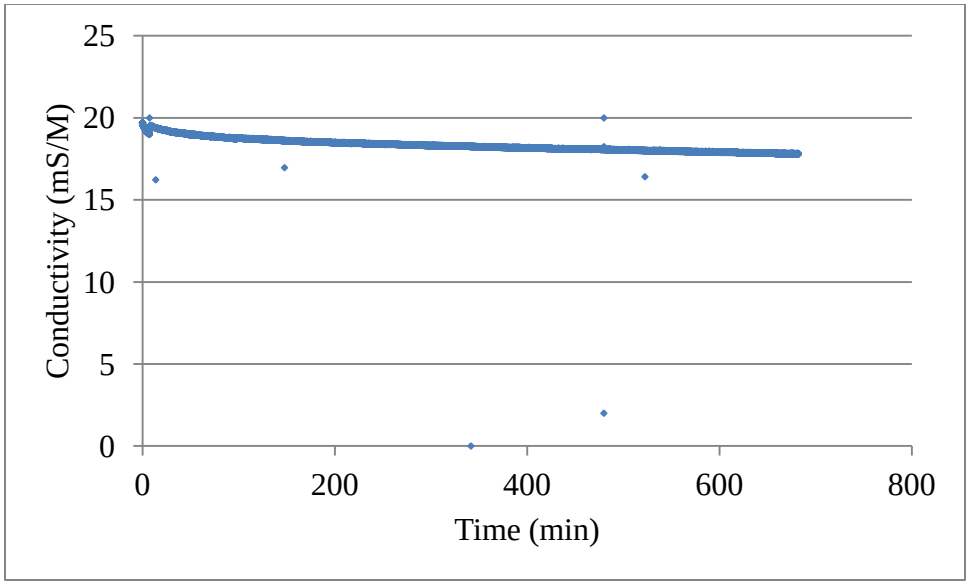

Figure A-71. Experiment 5-b Adsorption.

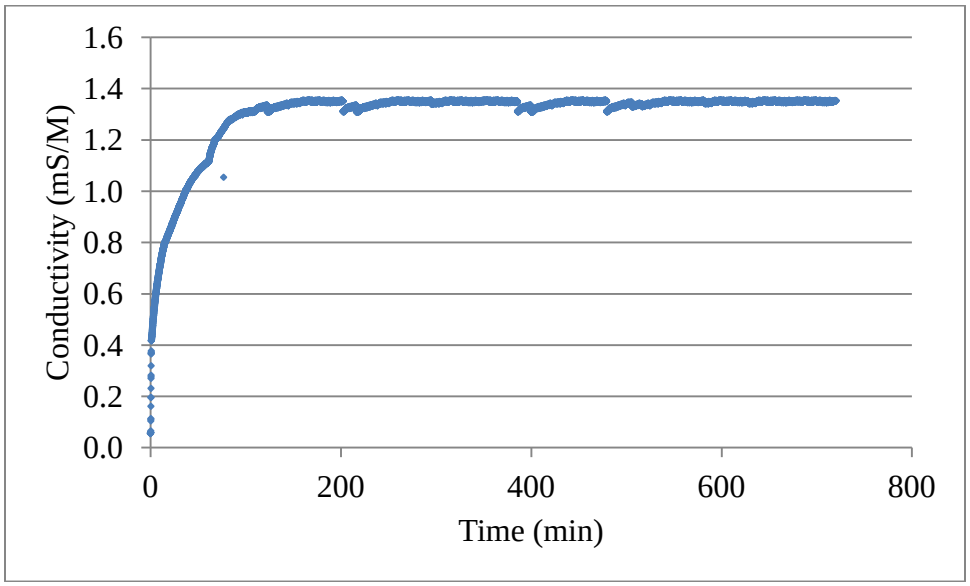

Figure A-72. Experiment 5-b Desorption.

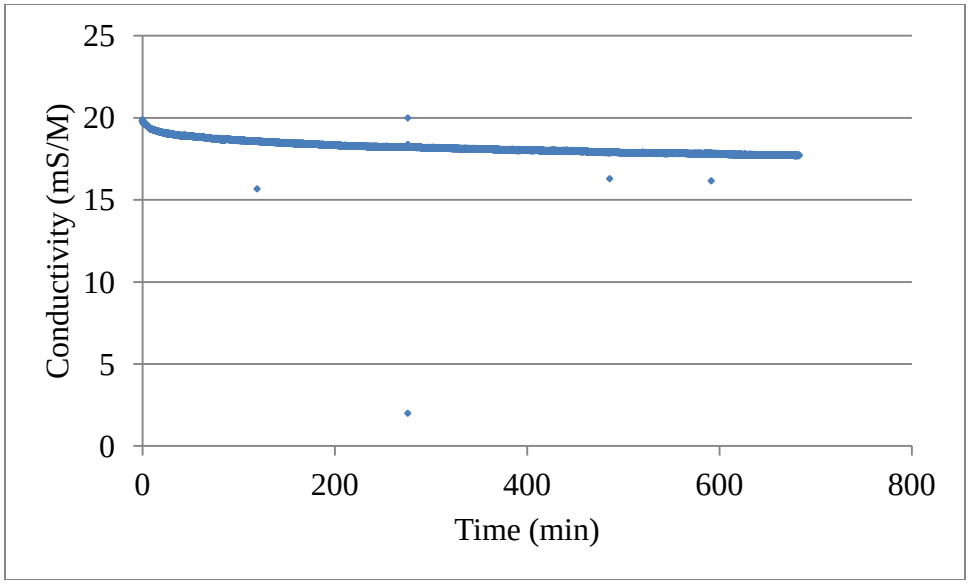

Figure A-73. Experiment 6-1-a Adsorption.

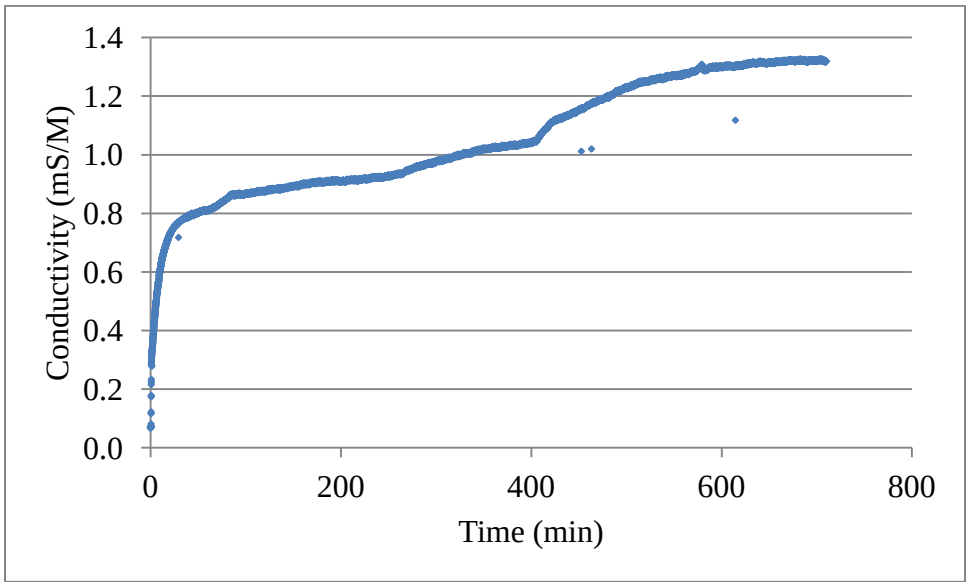

Figure A-74. Experiment 6-1-a Desorption.

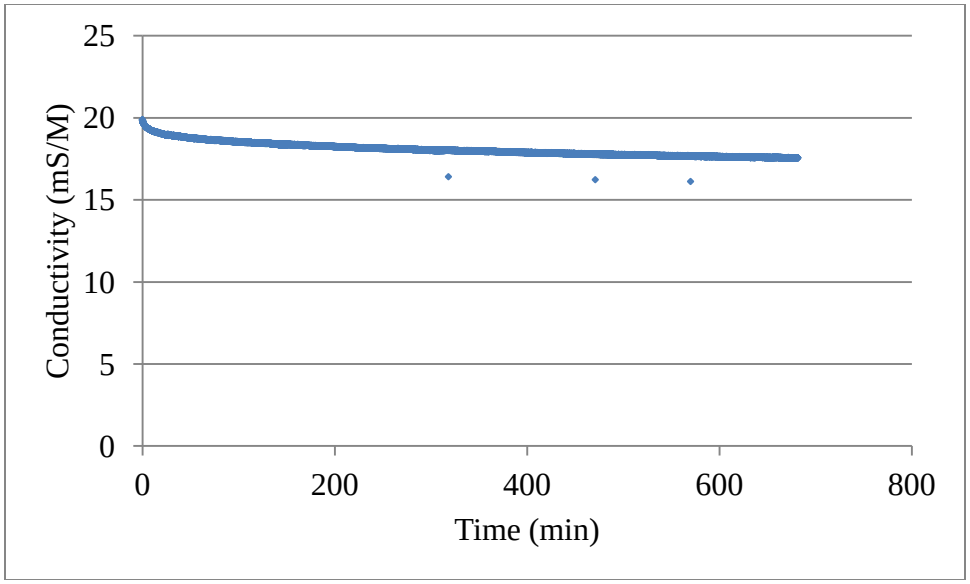

Figure A-75. Experiment 6-5-a Adsorption.

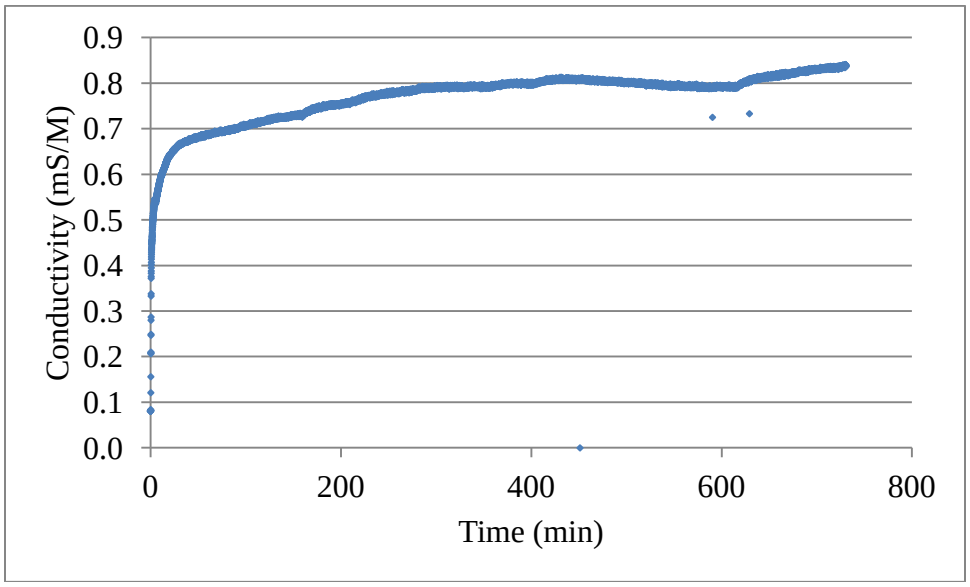

Figure A-76. Experiment 6-5-a Desorption.

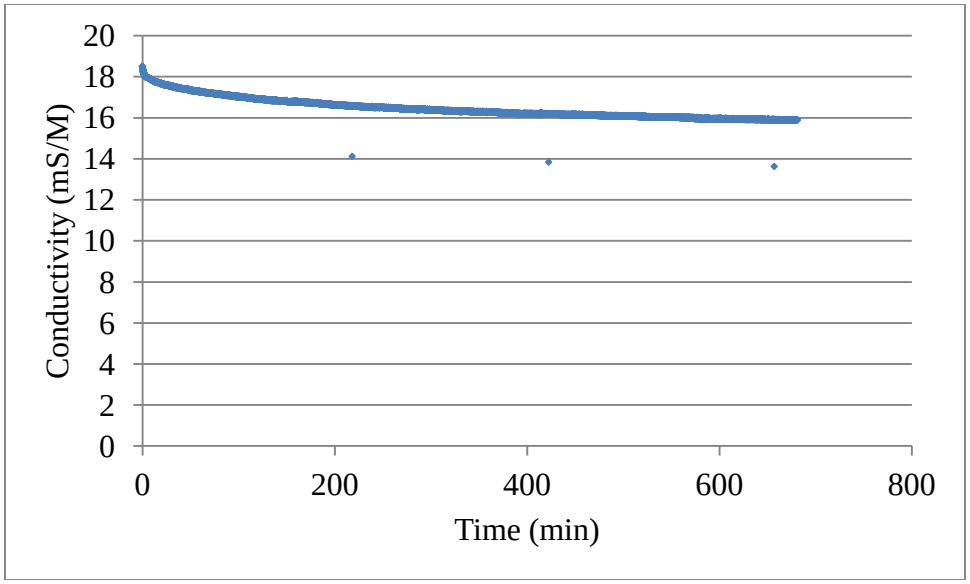

Figure A-77. Experiment 6-1-b Adsorption.

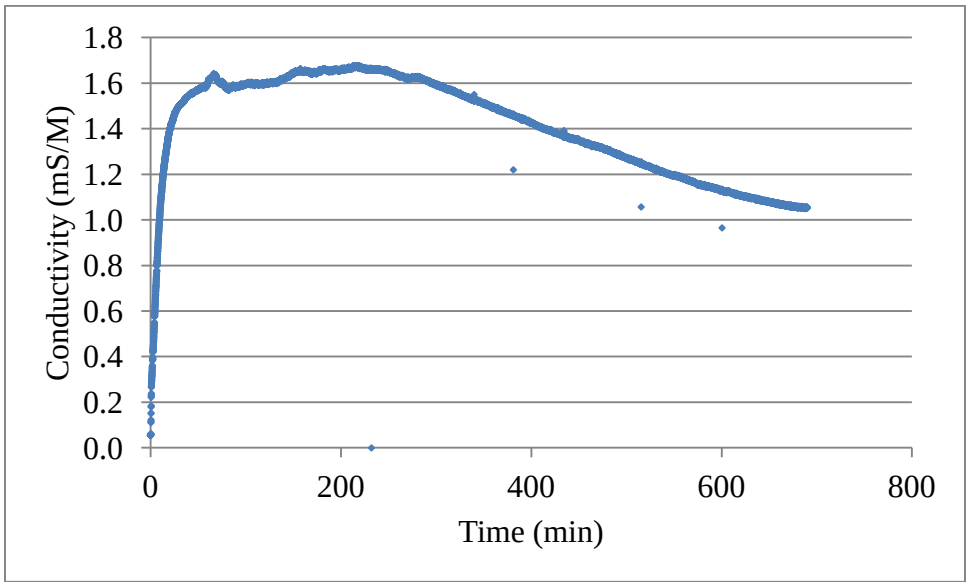

Figure A-78. Experiment 6-1-b Desorption.

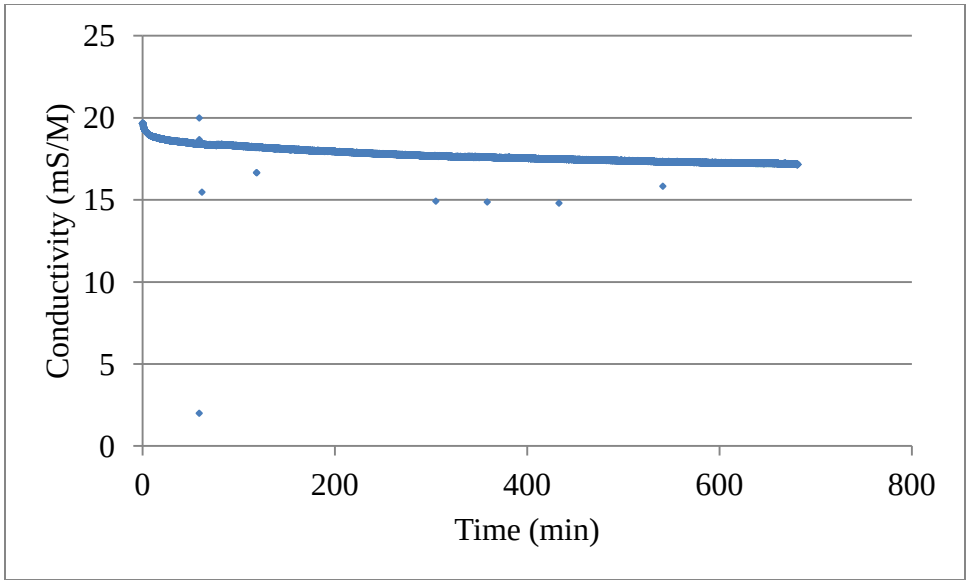

Figure A-79. Experiment 6-5-b Adsorption.

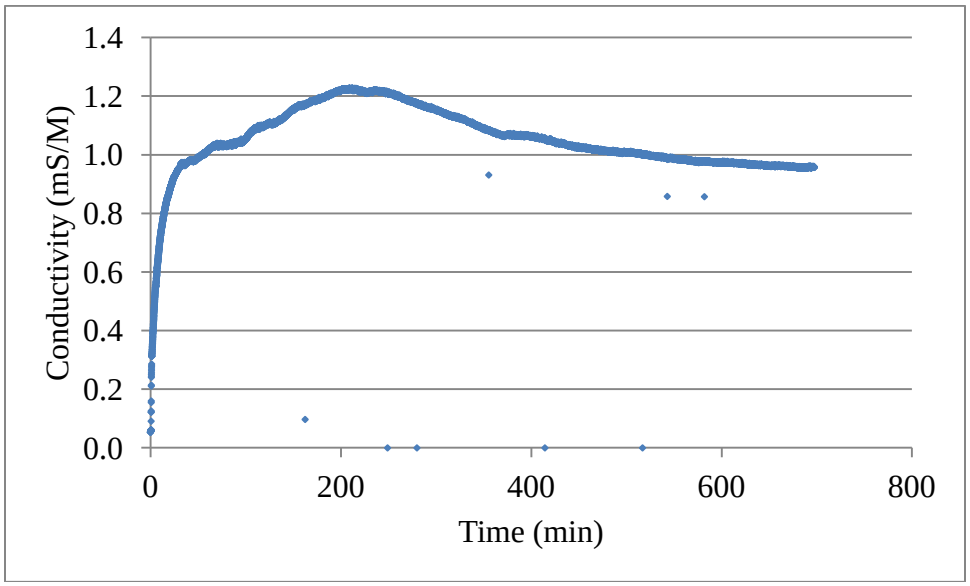

Figure A-80. Experiment 6-5-b Desorption.

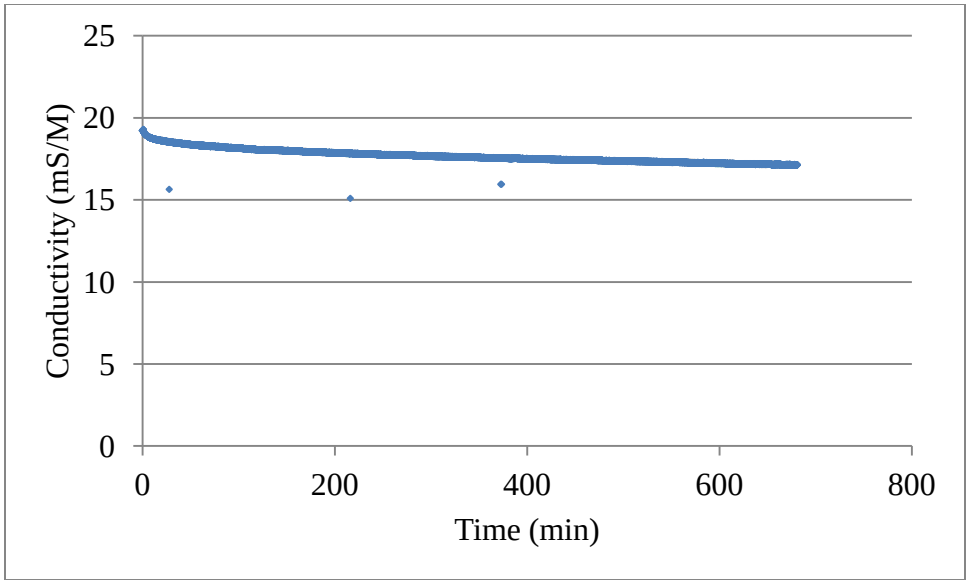

Figure A-81. Experiment 7-I Adsorption.

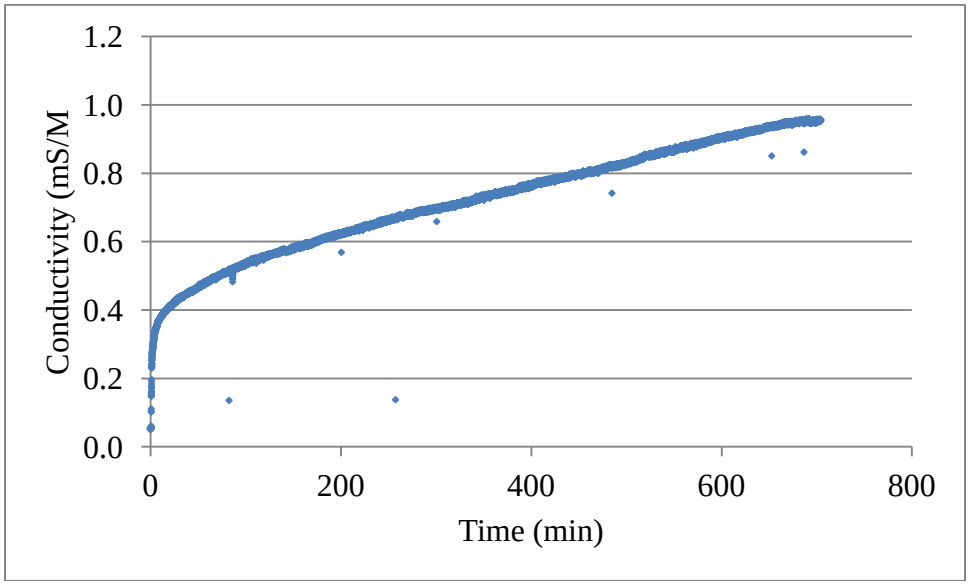

Figure A-82. Experiment 7-I Desorption.

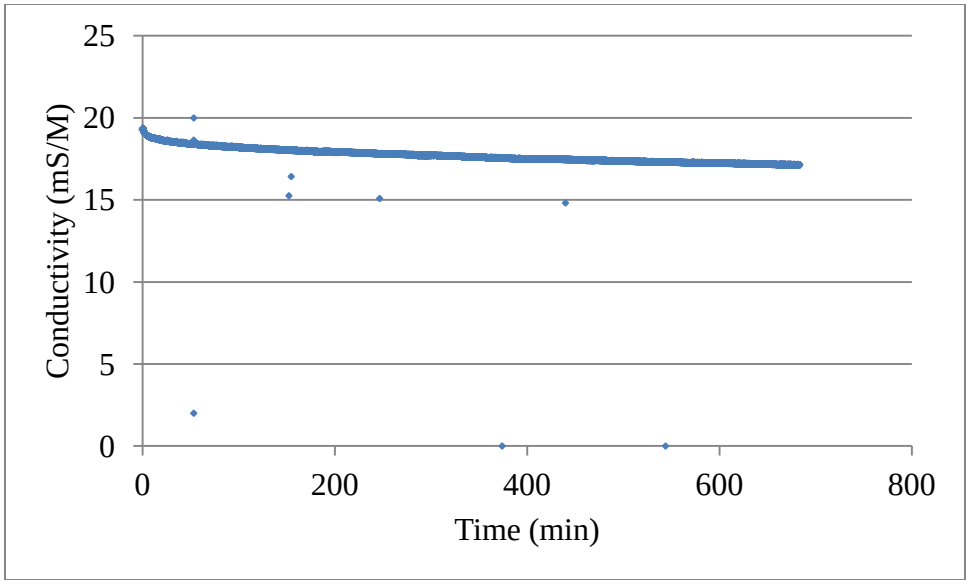

Figure A-83. Experiment 7-II Adsorption.

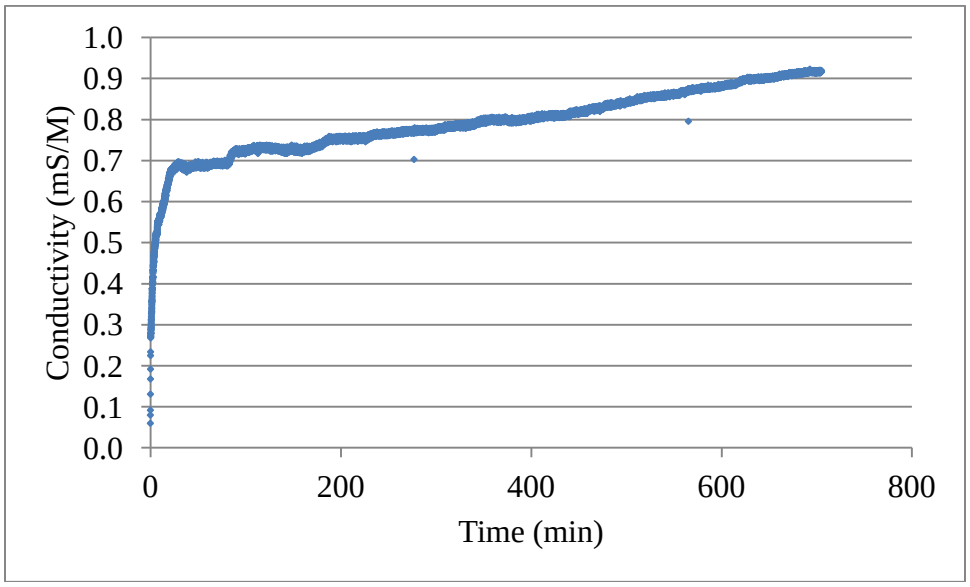

Figure A-84. Experiment 7-II Desorption.

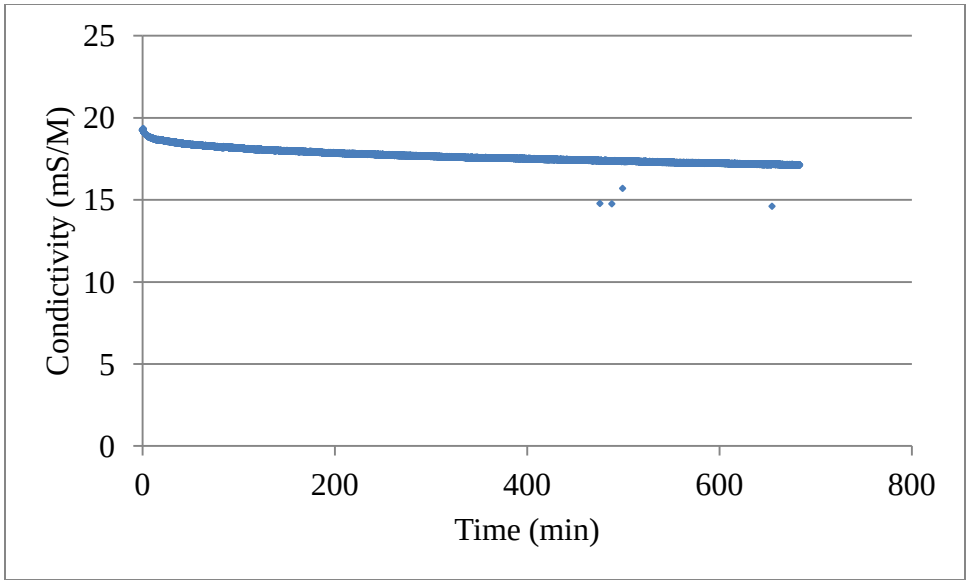

Figure A-85. Experiment 8-I Adsorption.

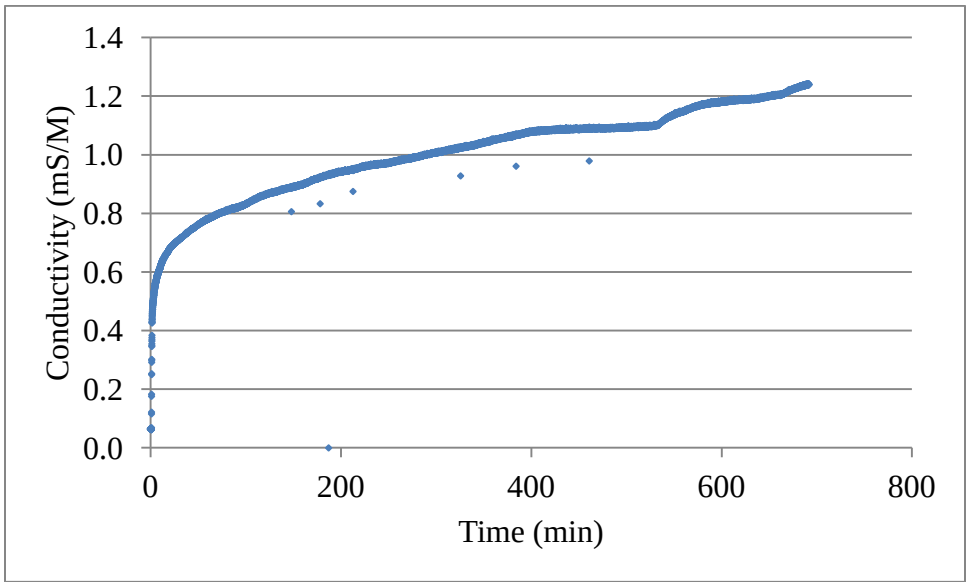

Figure A-86. Experiment 8-I Desorption.

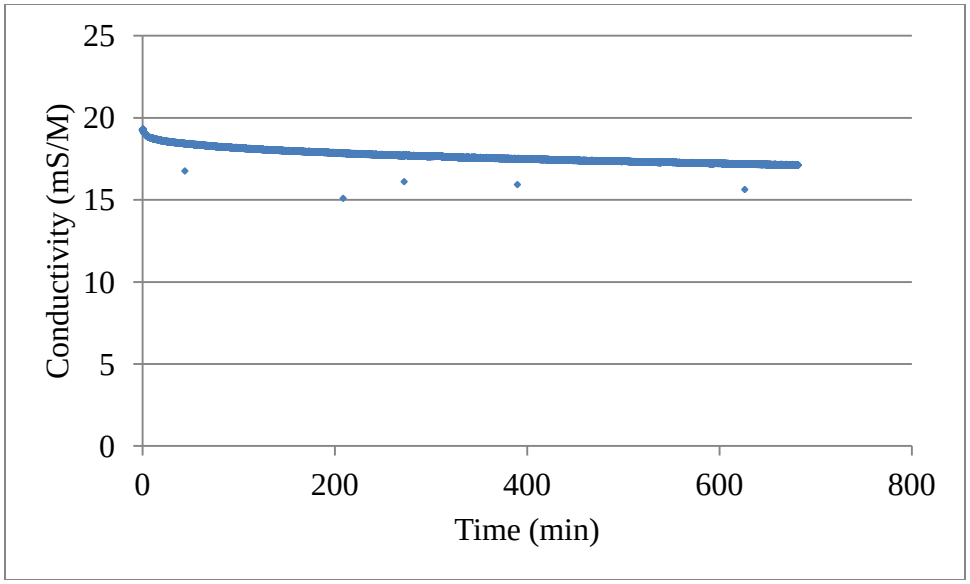

Figure A-87. Experiment 8-II Adsorption.

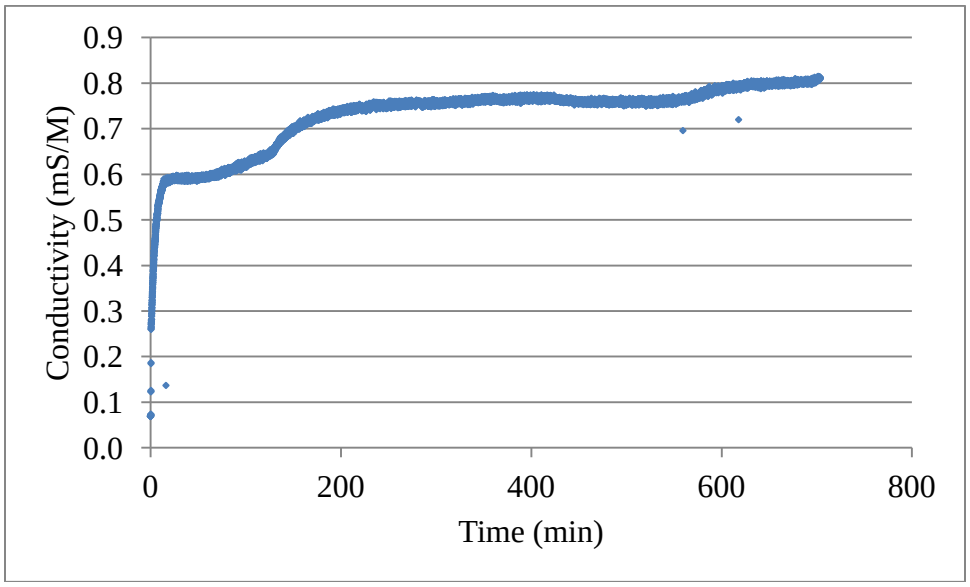

Figure A-88. Experiment 8-II Desorption.

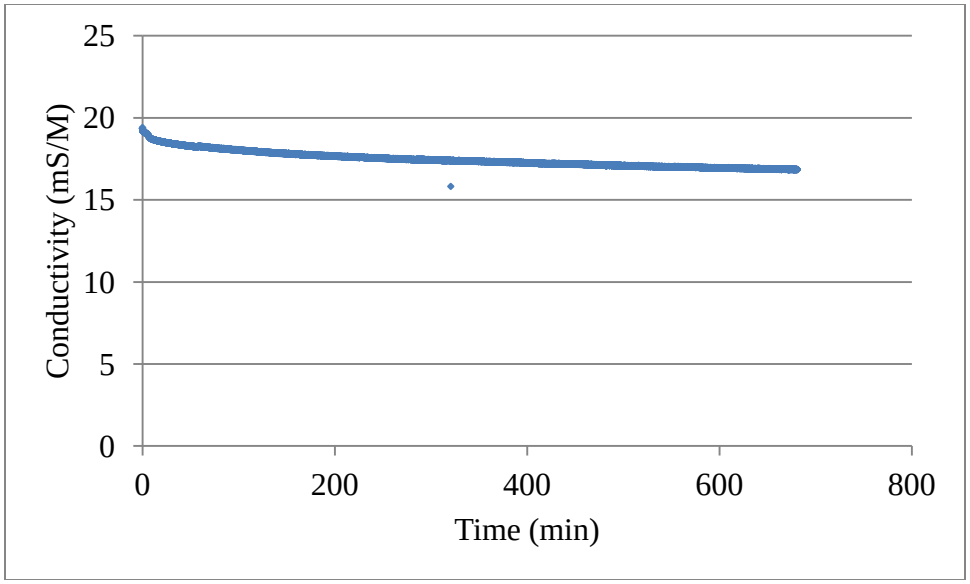

Figure A-89. Experiment 9-1-I Adsorption.

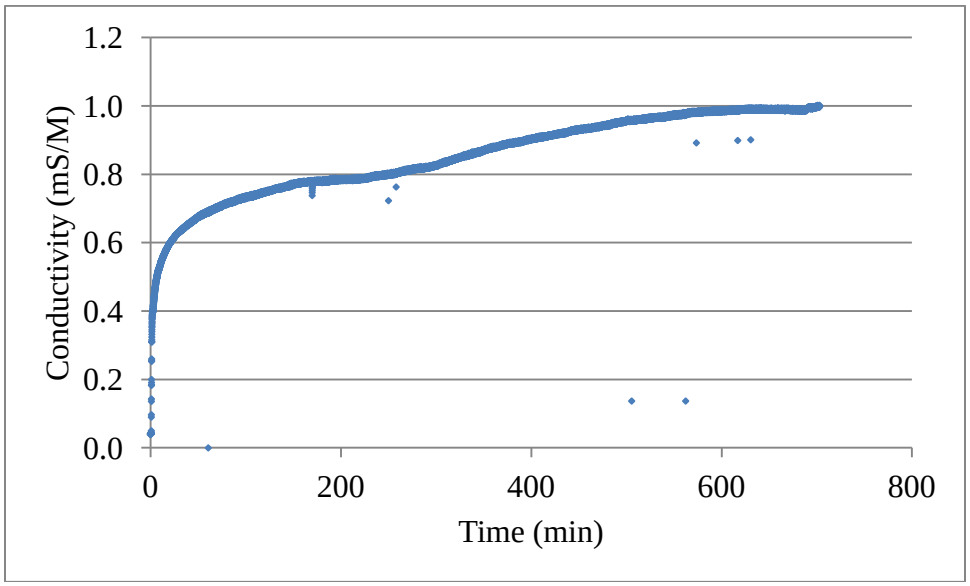

Figure A-90. Experiment 9-1-I Desorption.

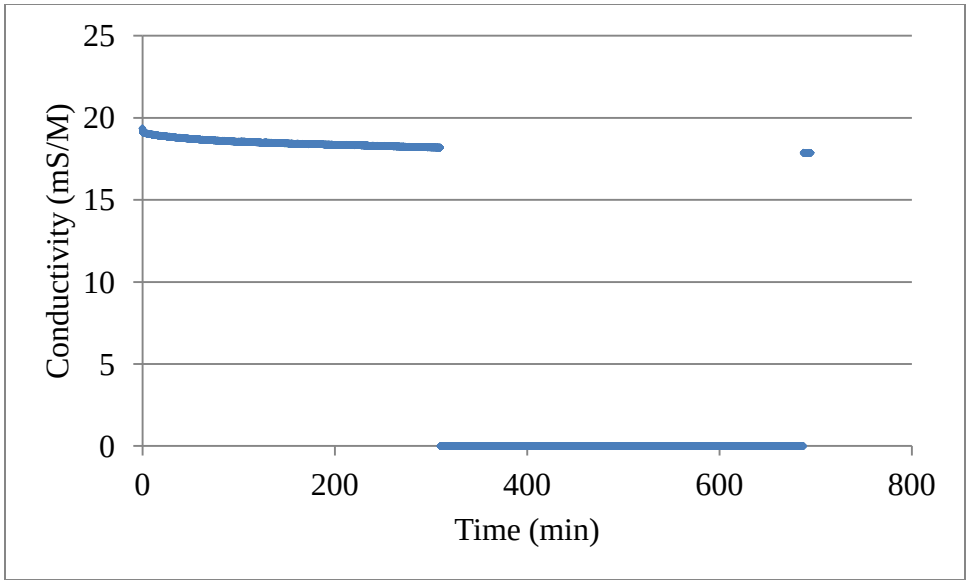

Figure A-91. Experiment 9-1-II Adsorption.

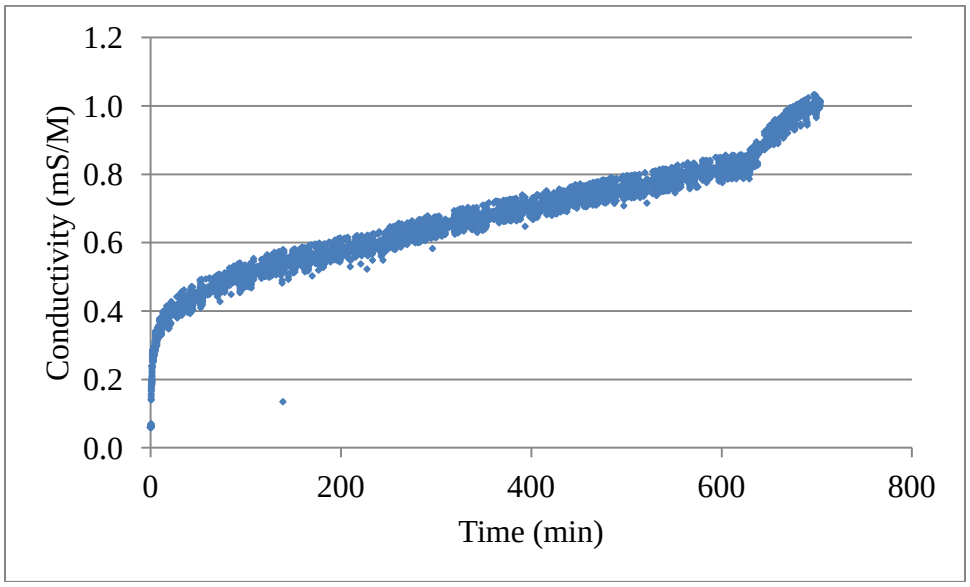

Figure A-92. Experiment 9-1-II Desorption.

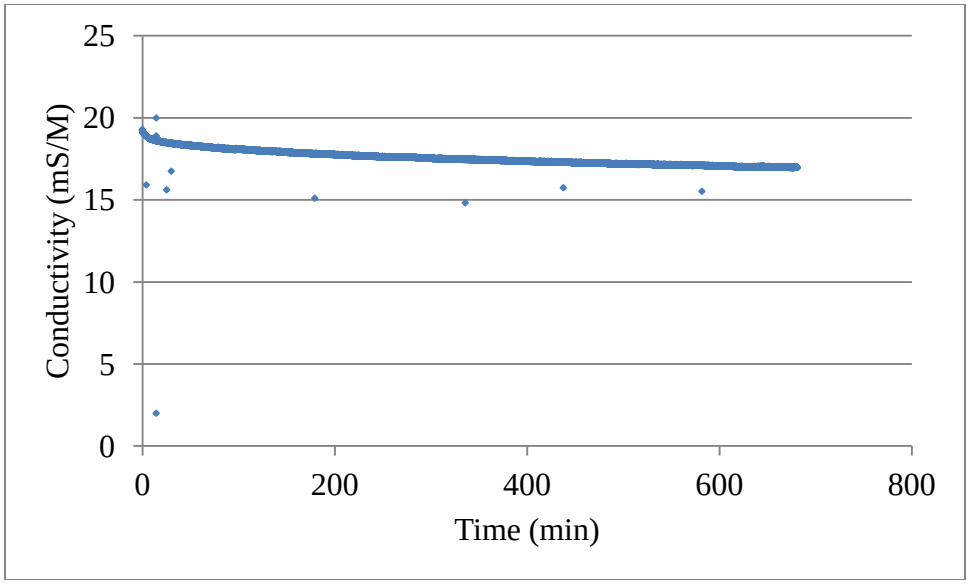

Figure A-93. Experiment 9-5-I Adsorption.

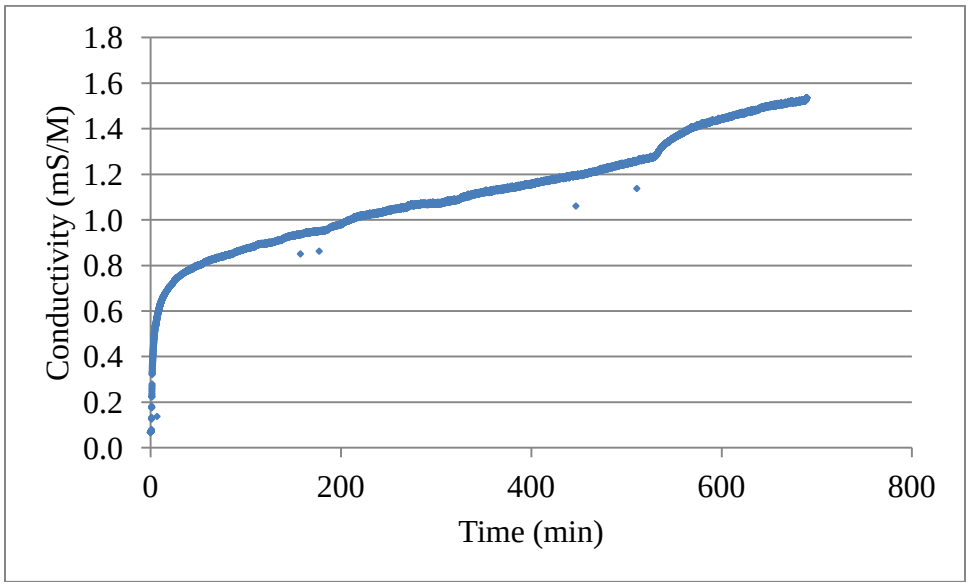

Figure A-94. Experiment 9-5-I Desorption.

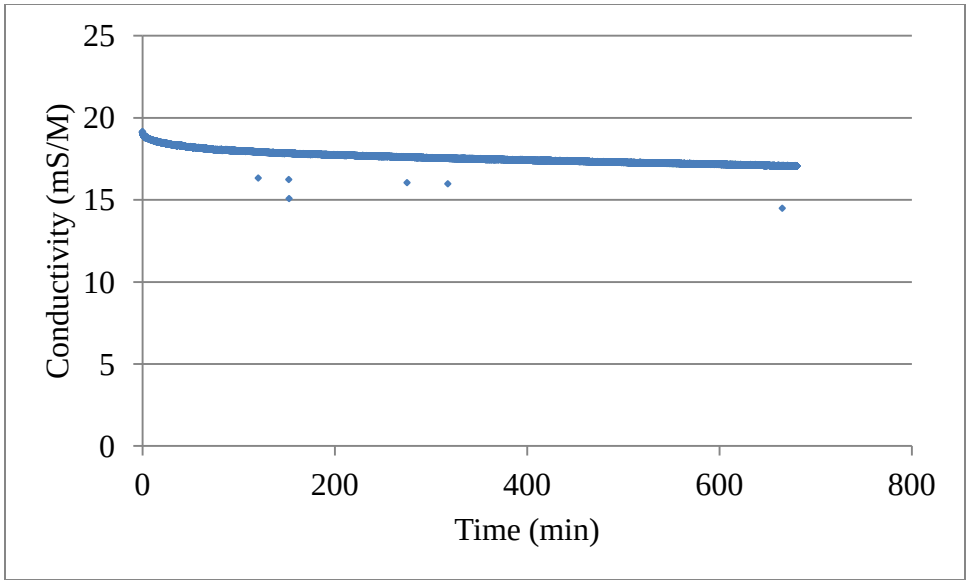

Figure A-95. Experiment 9-5-II Adsorption.

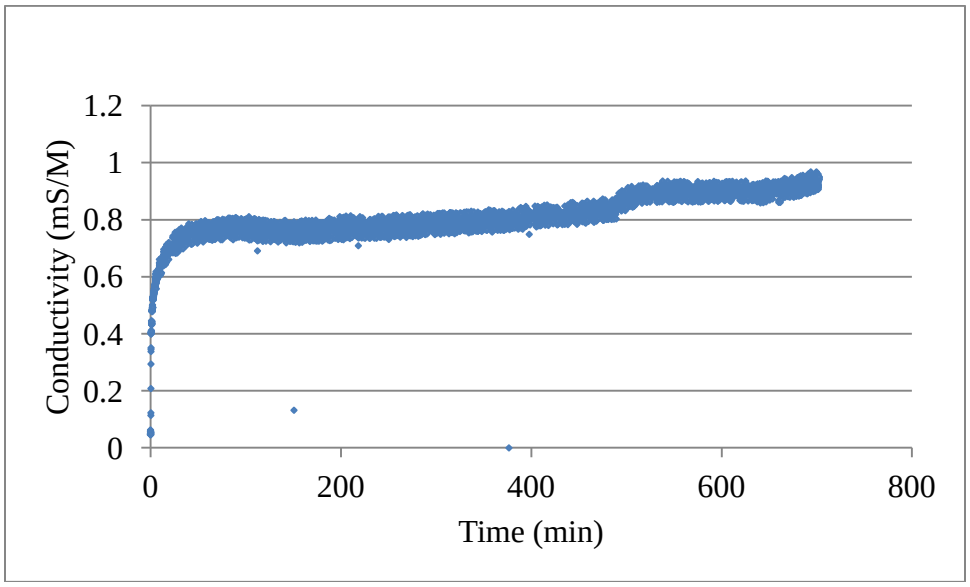

Figure A-96. Experiment 9-5-II Desorption.

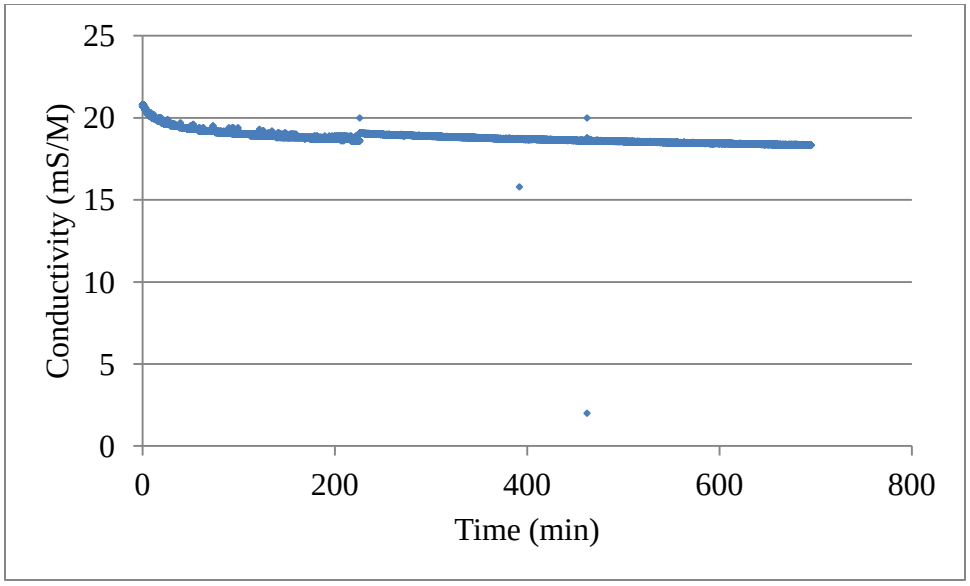

Figure A-97. Experiment 10 Adsorption.

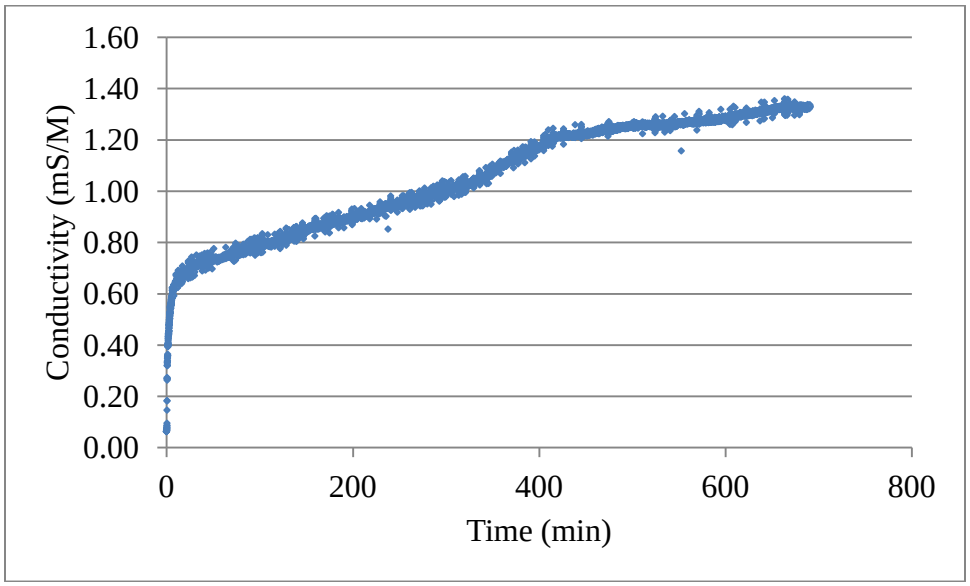

Figure A-98. Experiment 10 Desorption.

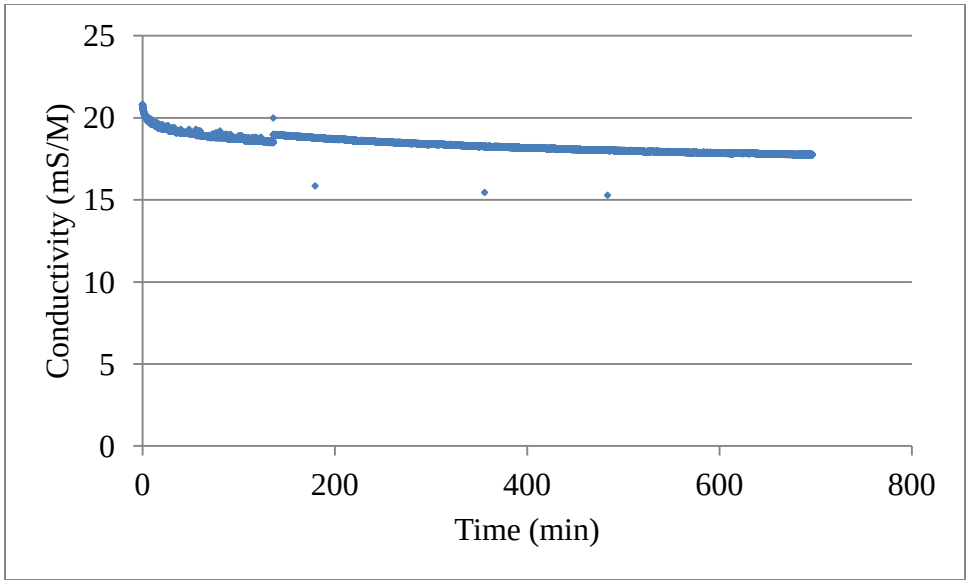

Figure A-99. Experiment 11 and 14 Adsorption.

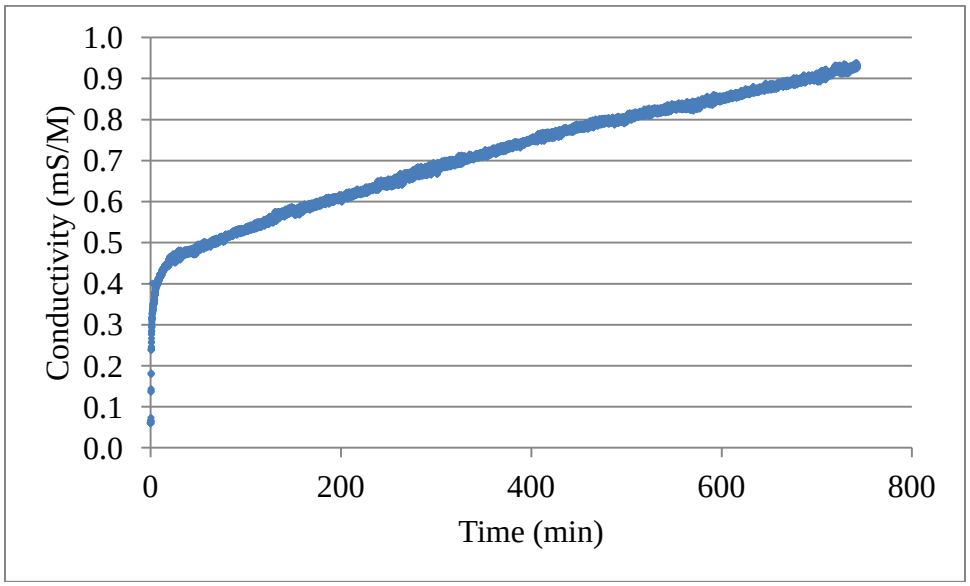

Figure A-100. Experiment 11 and 14 Desorption.

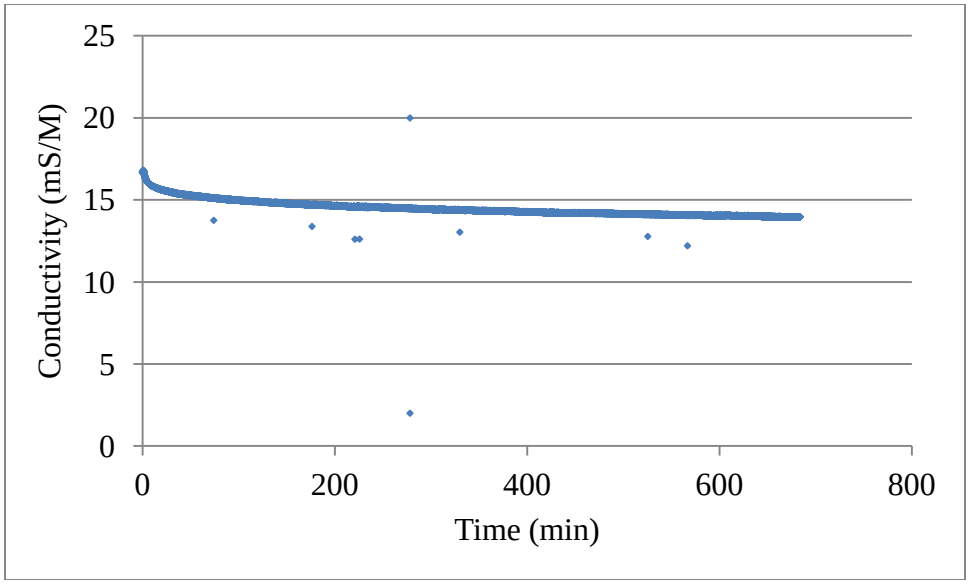

Figure A-101. Experiment 12 and 26 Adsorption.

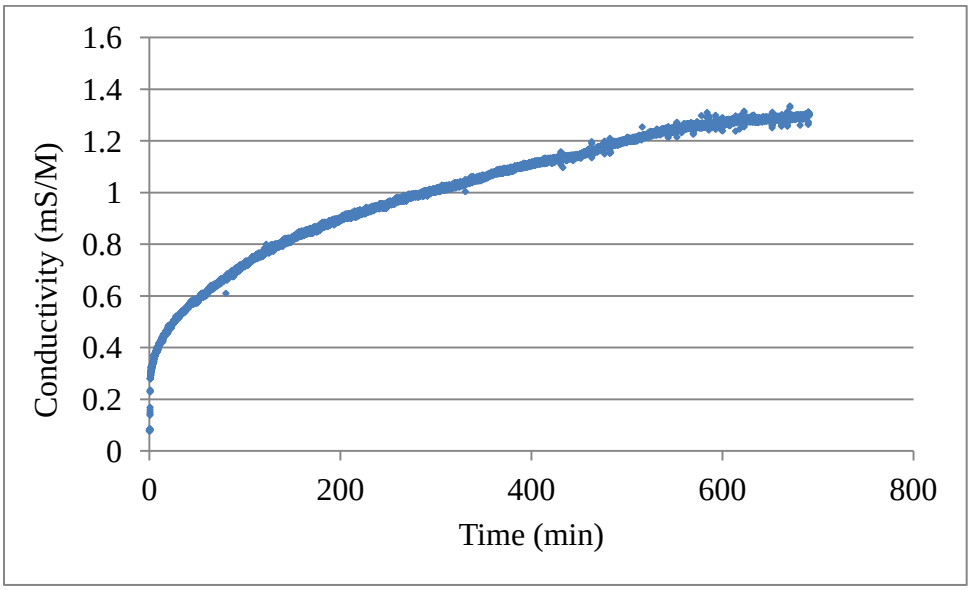

Figure A-102. Experiment 12 and 16 Desorption.

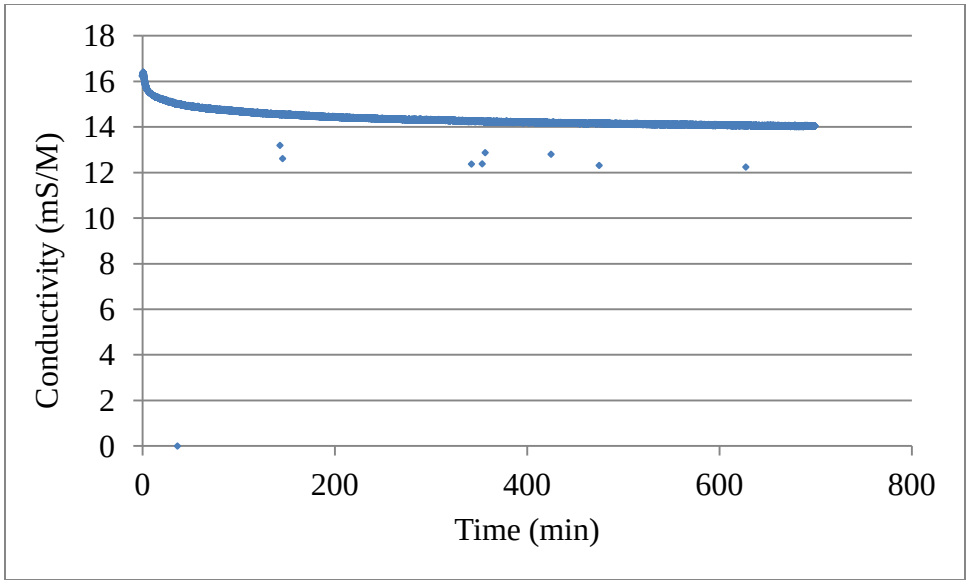

Figure A-103. Experiment 13 $NaNO_3$ Adsorption.

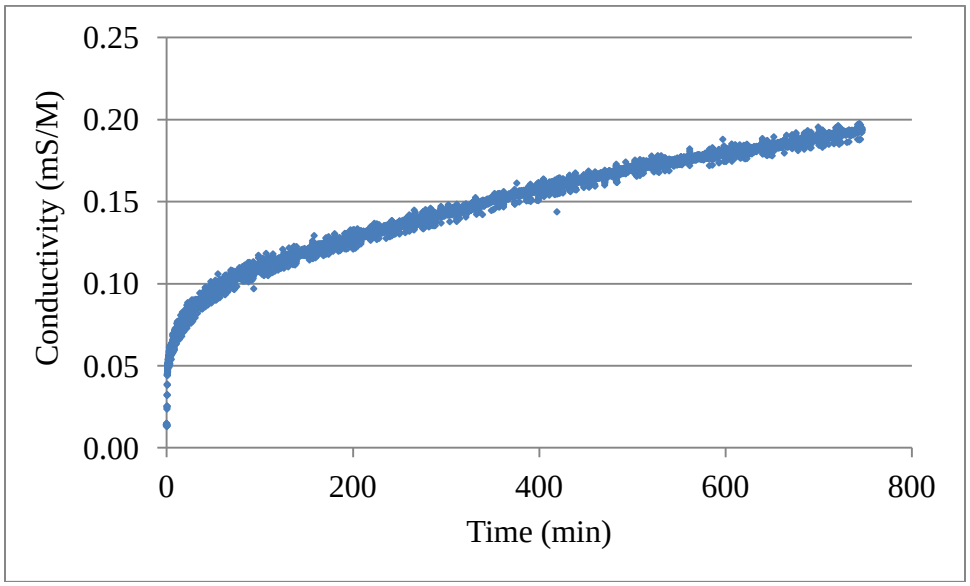

Figure A-104. Experiment 13 $NaNO_3$ Desorption.

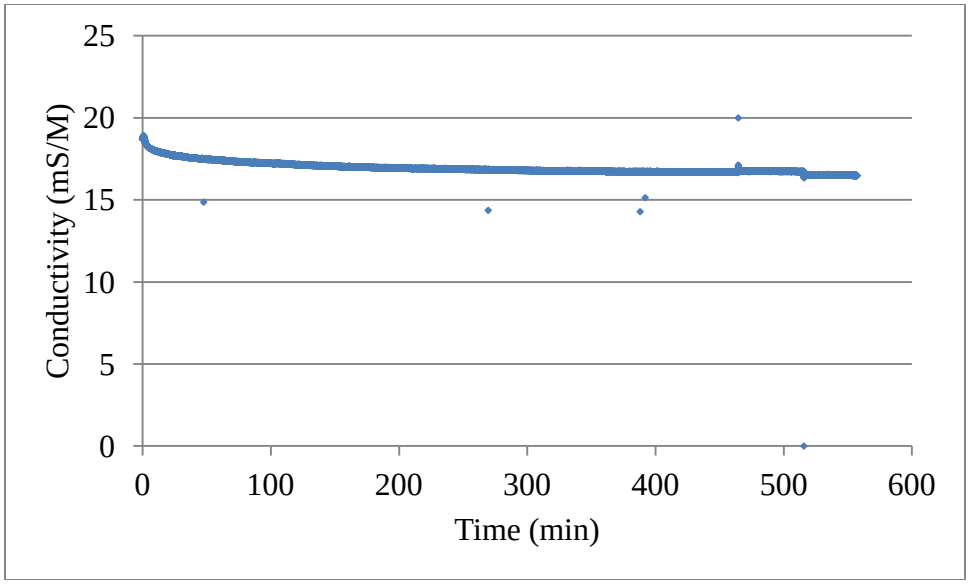

Figure A-105. Experiment 15 KNO_3 Adsorption.

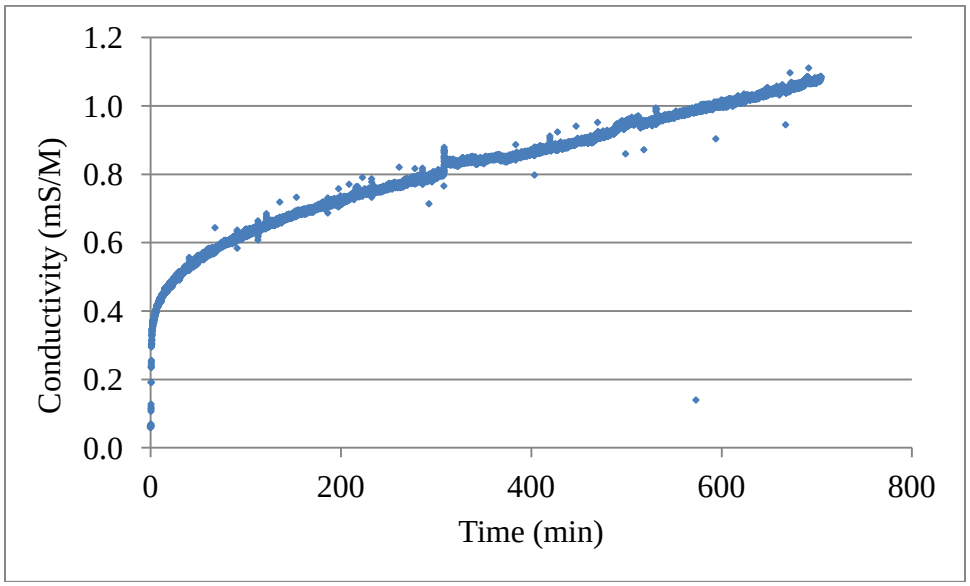

Figure A-106. Experiment 15 KNO_3 Desorption.

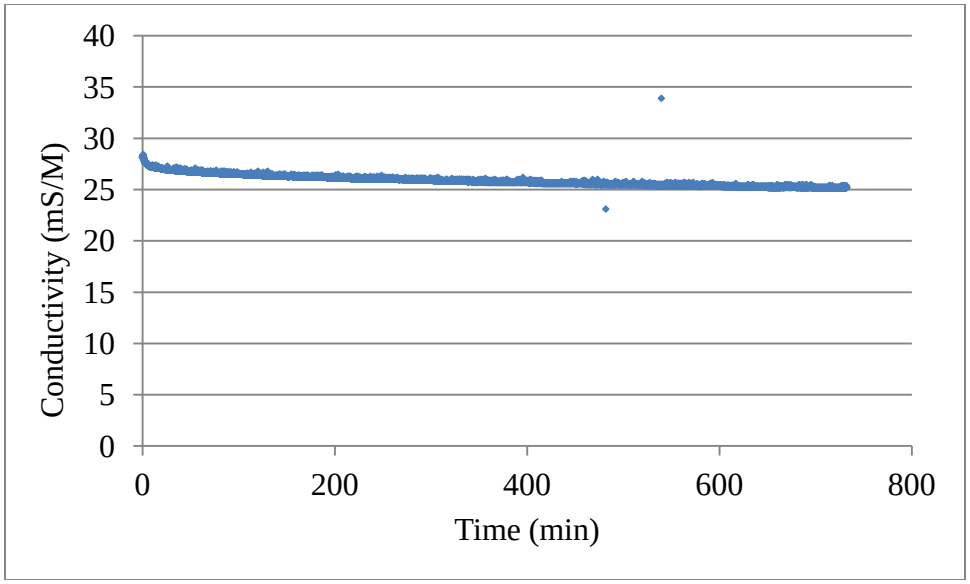

Figure A-107. Experiment 17 Na_2SO_4 Adsorption.

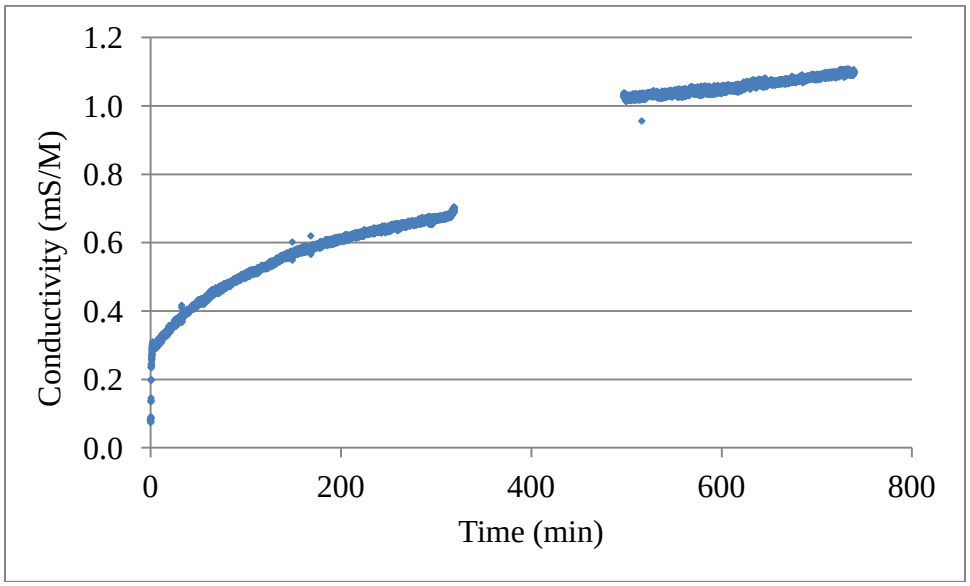

Figure A-108. Experiment 17 Na_2SO_4 Desorption.

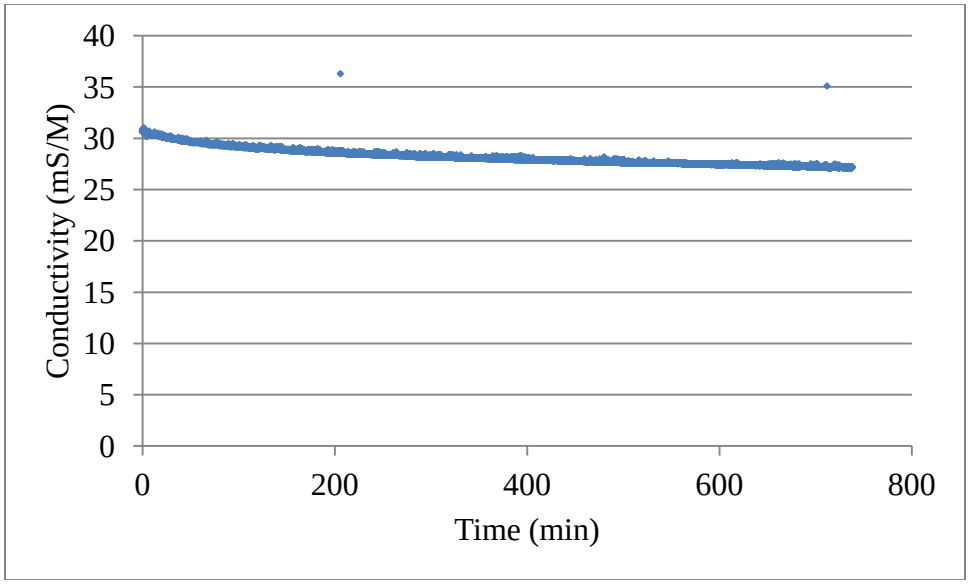

Figure A-109. Experiment 18 $MgBr_2$ Adsorption.

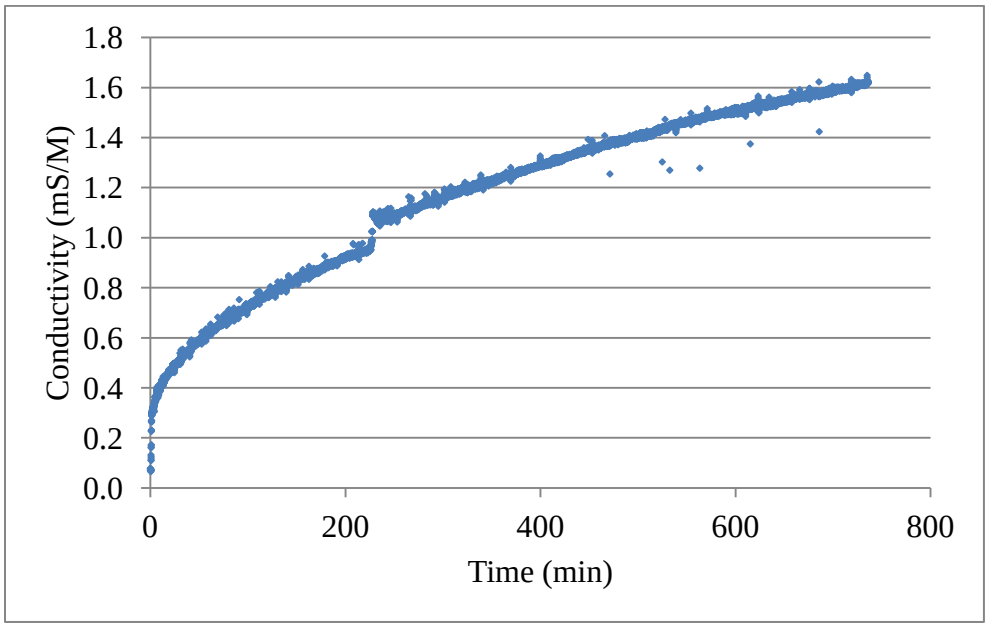

Figure A-110. Experiment 18 $MgBr_2$ Desorption.

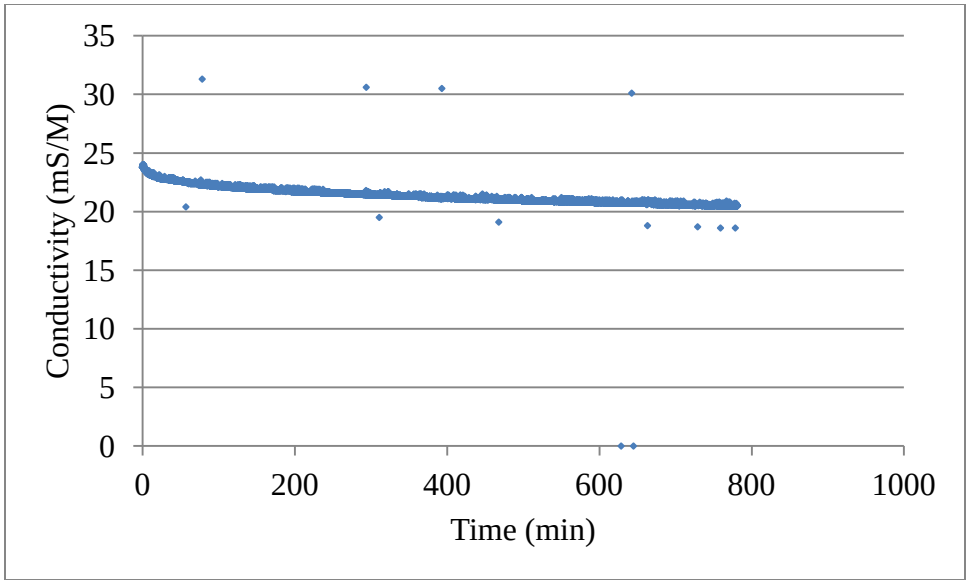

Figure A-111. Experiment 19 $MgSO_4$ Adsorption.

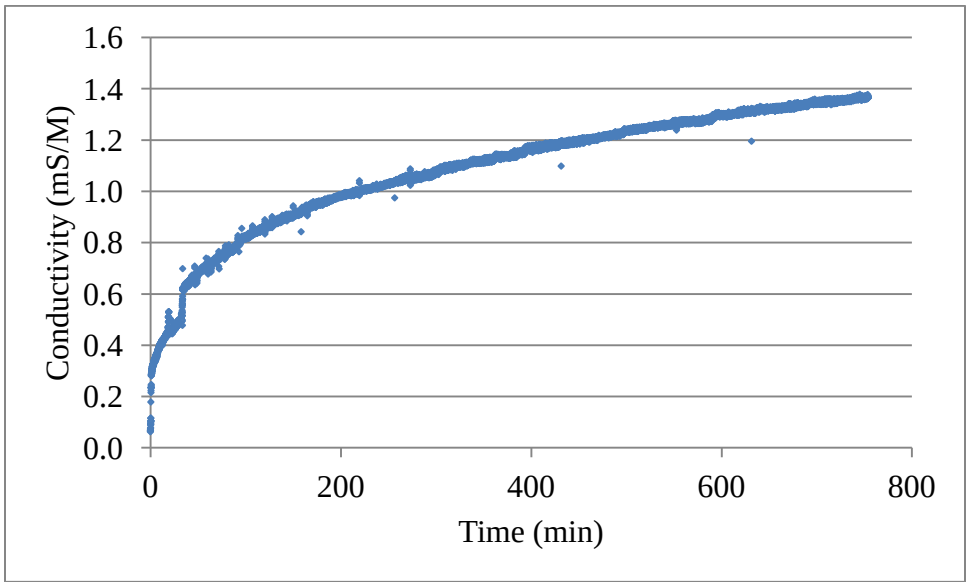

Figure A-112. Experiment 19 $MgSO_4$ Desorption.

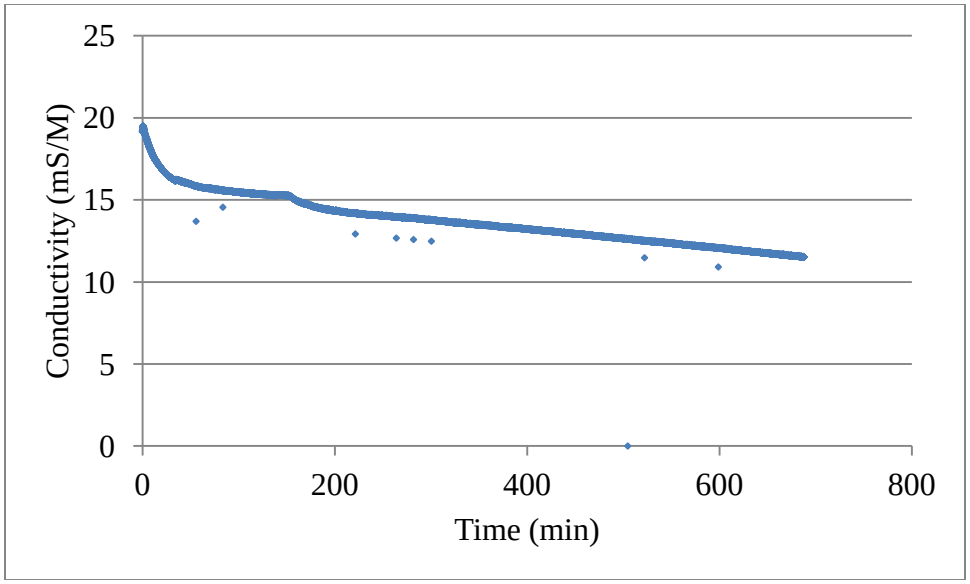

Figure A-113. Experiment 20 Adsorption Unit #2.

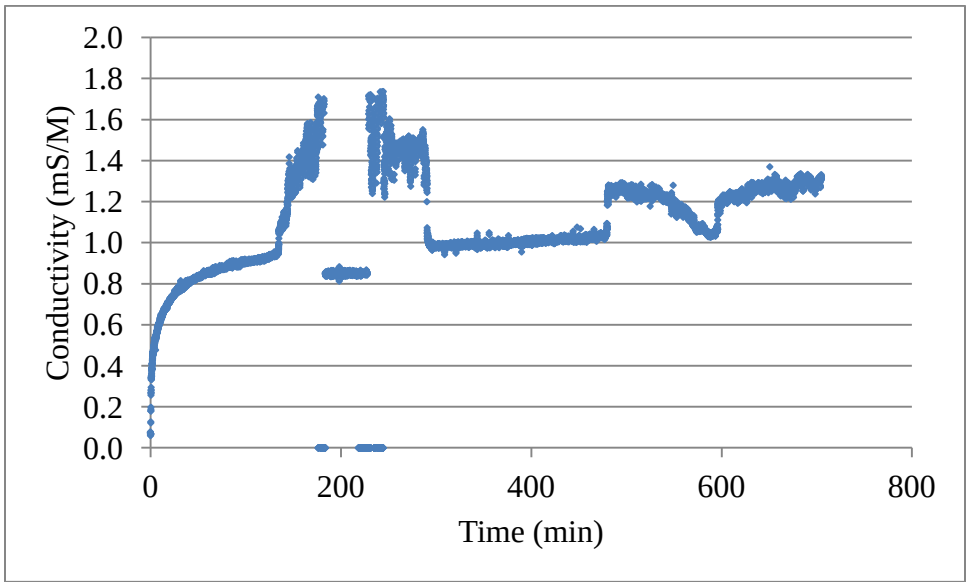

Figure A-114. Experiment 20 Desorption Unit #2.

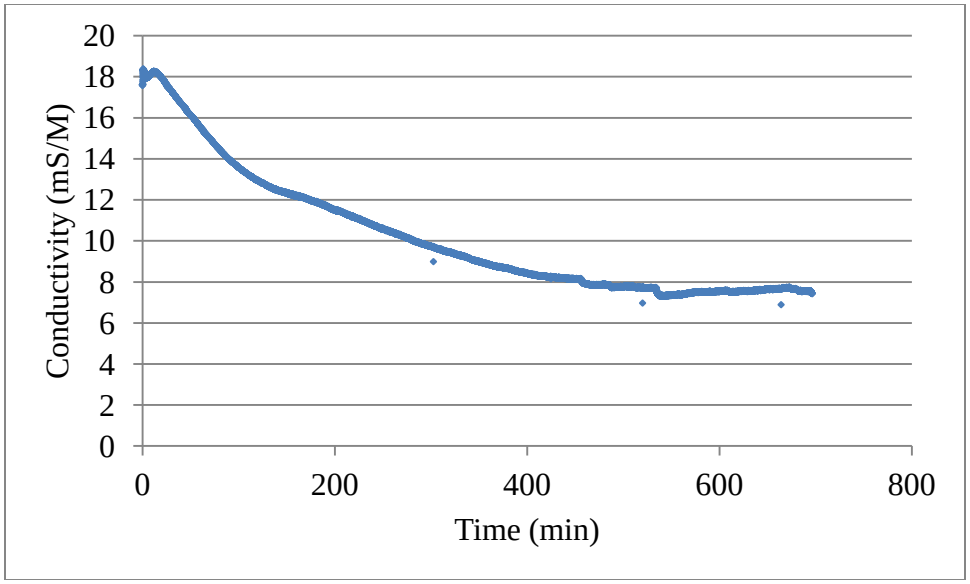

Figure A-115. Experiment 21 Adsorption Unit #3.

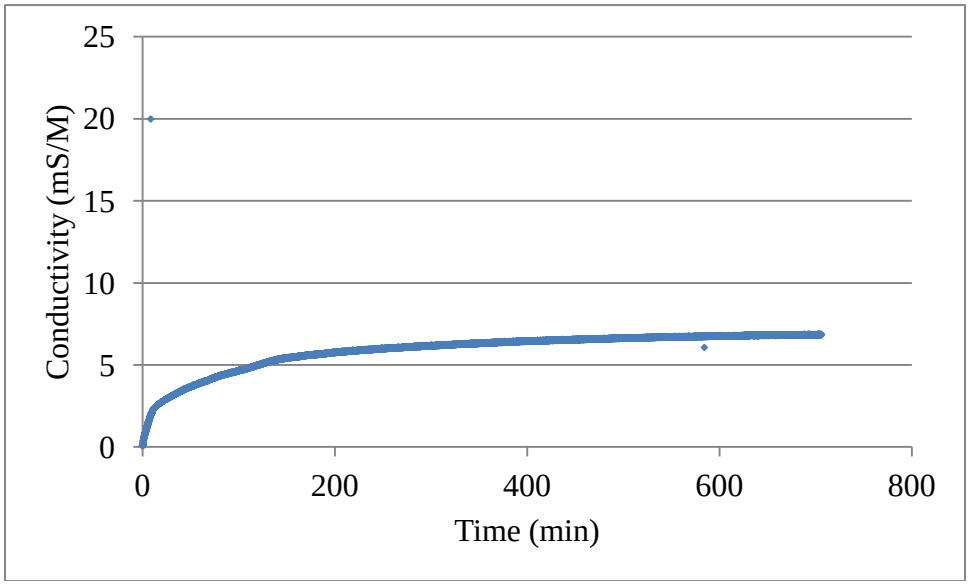

Figure A-116. Experiment 21 Desorption Unit #3.

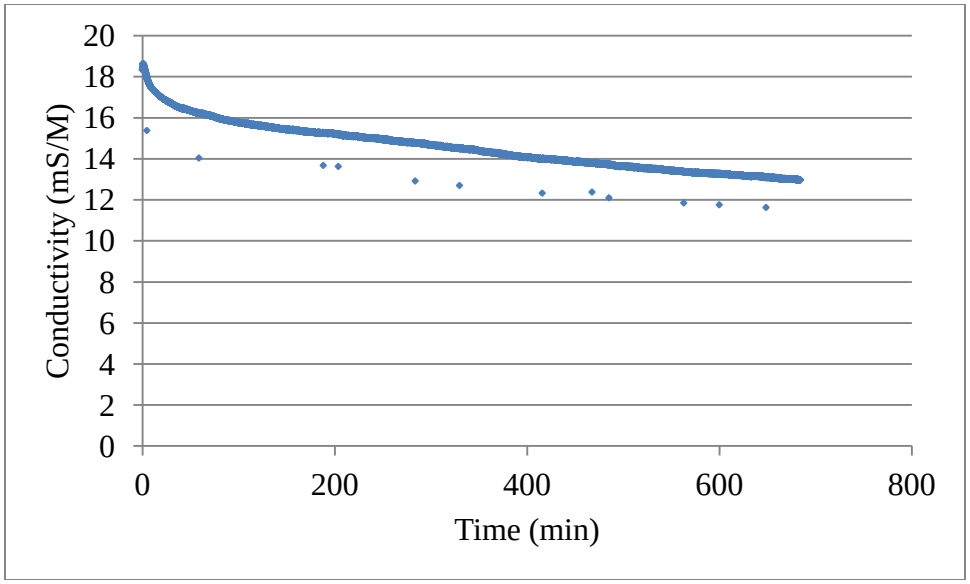

Figure A-117. Experiment 22 Adsorption Unit #4.

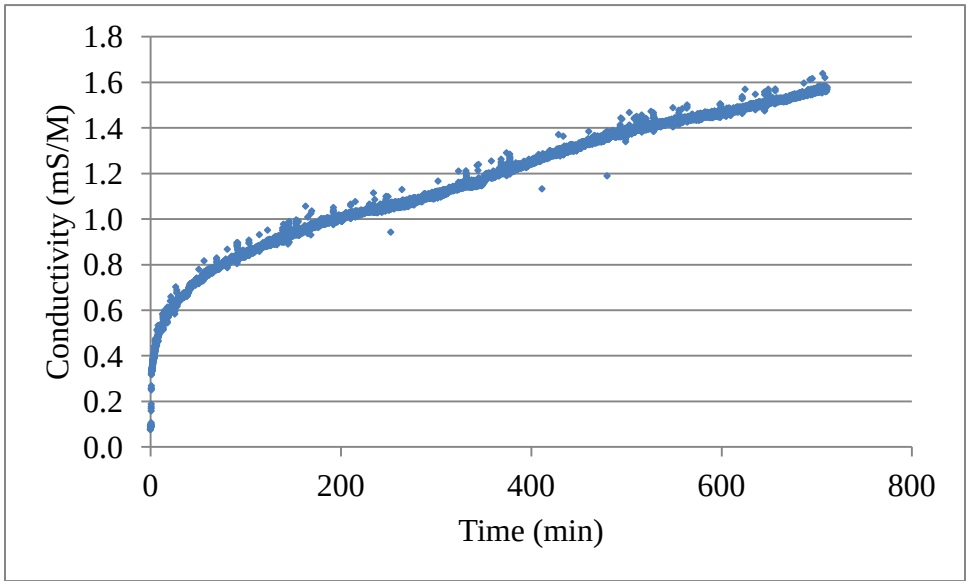

Figure A-118. Experiment 22 Desorption Unit #4.

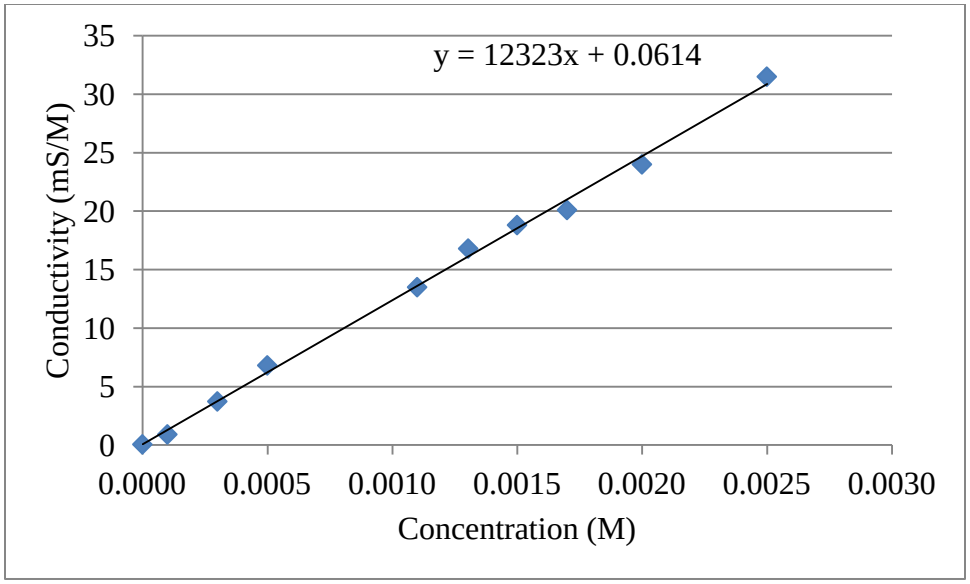

Figure A-119. Concentration versus conductivity of NaCl at 20 °C.

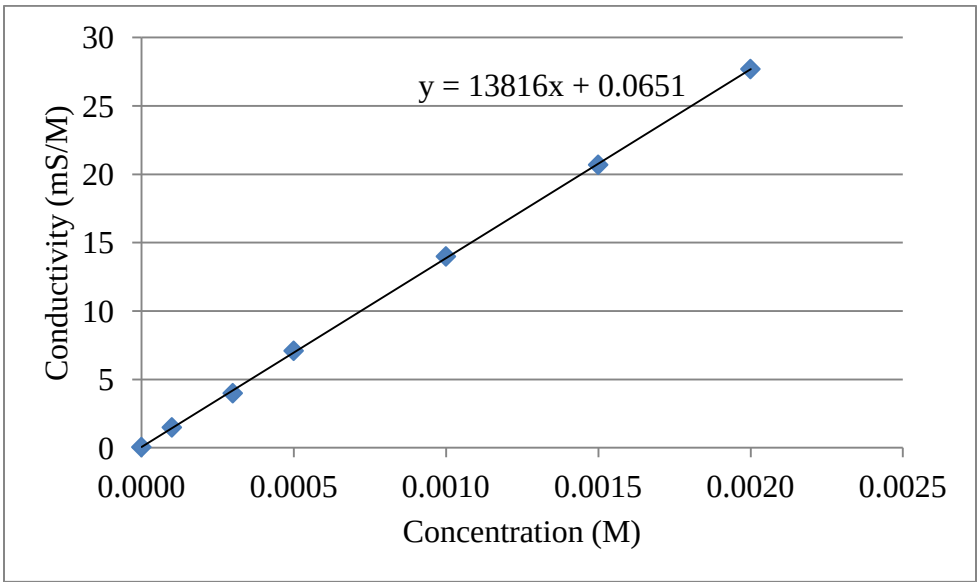

Figure A-120. Concentration versus conductivity of KCl at 20 °C.

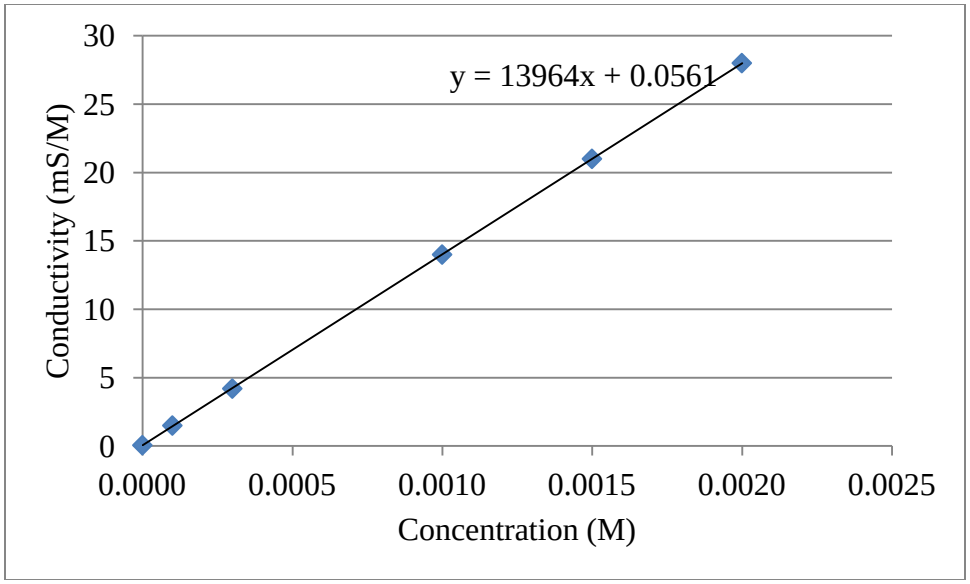

Figure A-121. Concentration versus conductivity of KBr at 20 °C.

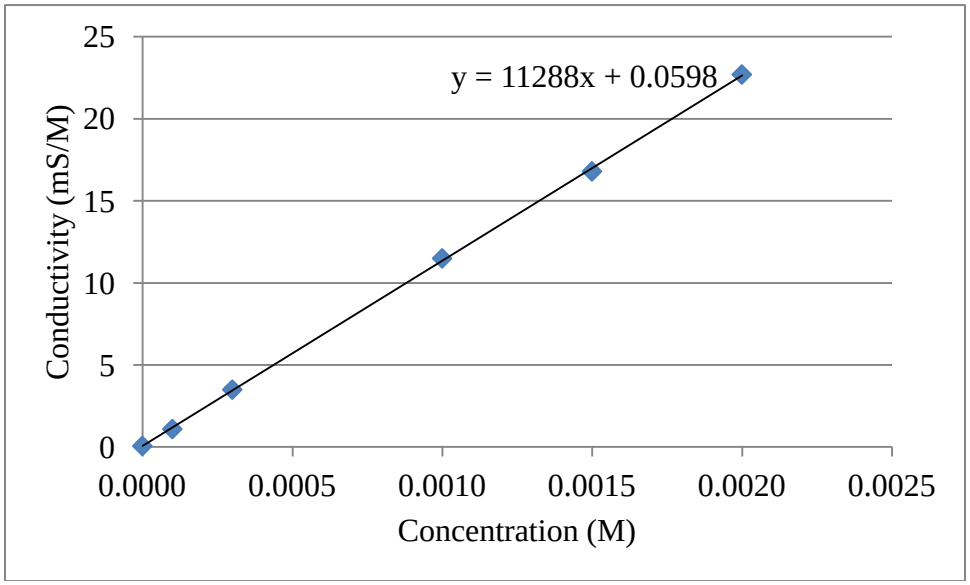

Figure A-122. Concentration versus conductivity of NaBr at 20 °C.

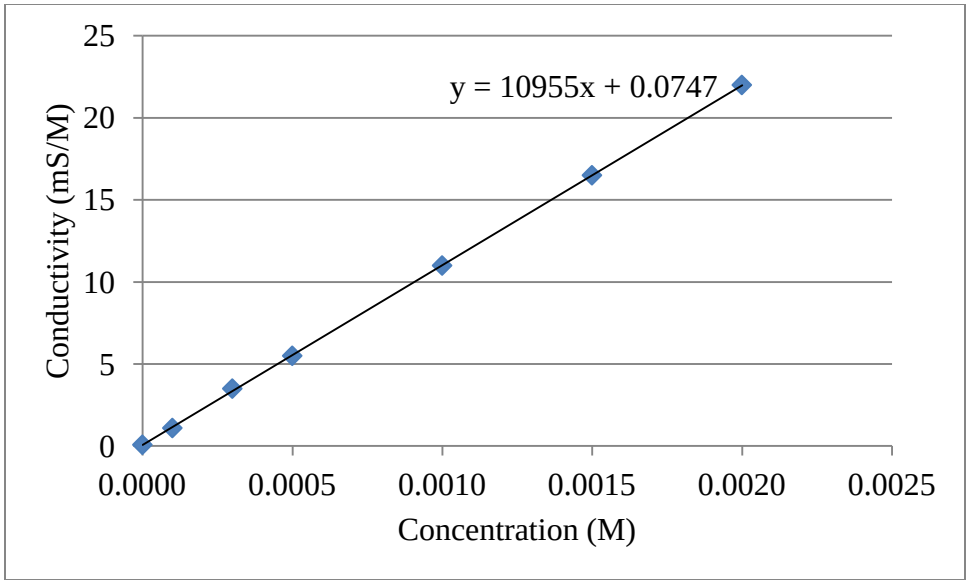

Figure A-123. Concentration versus conductivity of $NaNO_3$ at 20 °C.

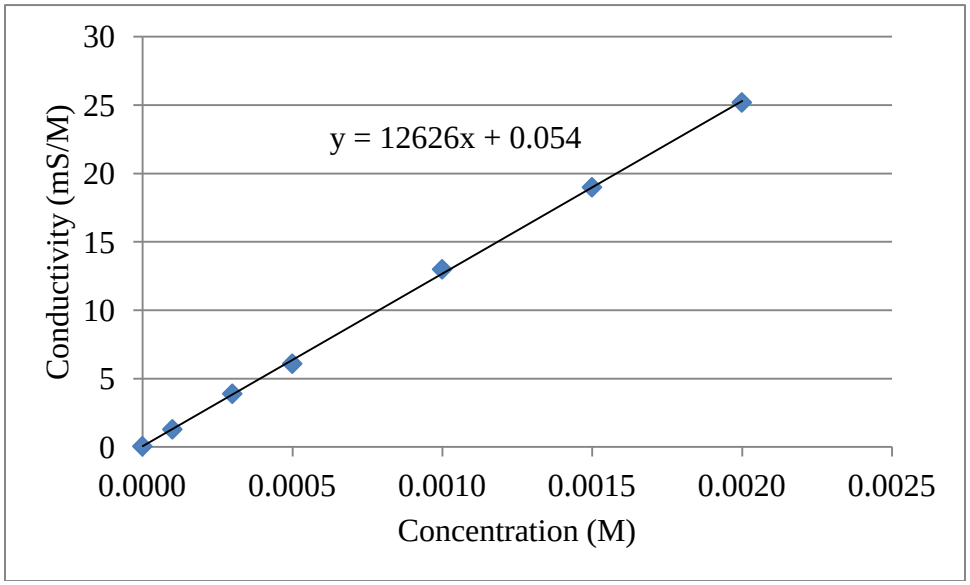

Figure A-124. Concentration versus conductivity of KNO_3 at 20 °C.

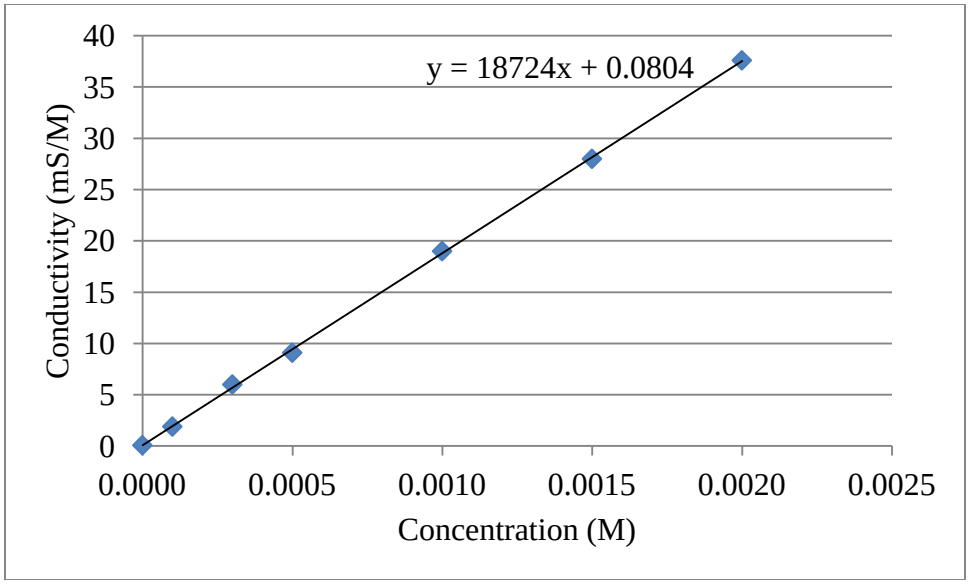

Figure A-125. Concentration versus conductivity of Na_2SO_4 at 20 °C.

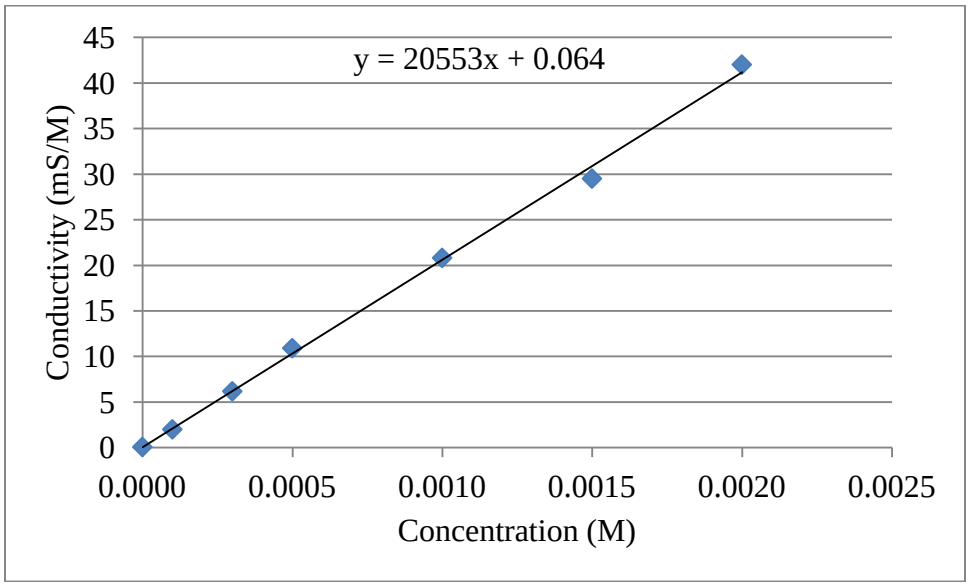

Figure A-126. Concentration versus conductivity of $MgBr_2$ at 20 °C.

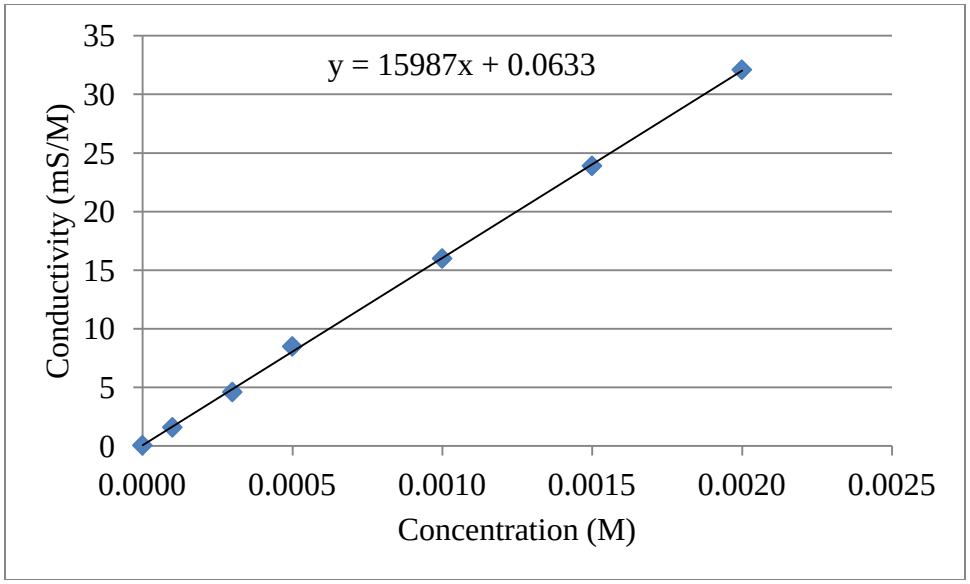

Figure A-127. Concentration versus conductivity of $MgSO_4$ at 20 °C.

VITA

Name: Sanjay Tewari

Address: Department of Civil Engineering,
Texas A&M University, 3136 TAMU
College Station, Texas 77843-3136
c/o Bill Batchelor

Email Address: sanjay.tewari@gmail.com

Education: B.E., Civil Engineering, 2000
S. V. National Institute of Technology, Surat, India

M.Tech., Chemical Engineering, 2002
Indian Institute of Technology, Roorkee, India

Ph.D., Civil Engineering, 2011
Texas A&M University, College Station, Texas